Energy Management of Li-Po Batteries in the Mobile Robotics Domain

Arezki Abderrahim Chellal

Supervisors

Prof. Dr. José Lima

Prof. Dr. José Gonçalves

Dr. Hicham Megnafi

Master in Renewable Energy and Energetic Efficiency

2020-2021

Energy Management of Li-Po Batteries in the Mobile Robotics Domain

Master in Renewable Energy and Energetic Efficiency

Escola Superior de Tecnologia e Gestão

Ecole Supérieure en Sciences Appliquées de Tlemcen

Arezki Abderrahim Chellal

2020-2021

Escola Superior de Tecnologia e de Gestão (EsTIG) and Ecole Supérieure en Sciences Appliquées de Tlemcen (ESSAT) are not responsible for the opinions expressed in this report.

To my dear father *Ziane* and my dear mother *Fatma*, for their love, sacrifices and support in the most difficult moments, which are at the origin of my success, may God keep and protect them.

To my dear brother *Mohamed El Amine*, for his continuous encouragement and support since my birth, I wish you a life full of happiness and success.

To all the people who, actively or not, participated and helped in the accomplishment of this work.

It is with great pleasure, I dedicate this modest work to you.

Acknowledgements

First of all, I would like to thank Allah, the Almighty and the Merciful, who has given me the strength and patience to accomplish this humble work.

With the most sincere gratitude, I would like to thank my supervisors ***Prof. Dr. José Lima***, ***Prof. Dr. José Gonçalves*** and ***Dr. Hicham Megnafi***, for all their efforts, their constant help and the trust they give me on a daily basis, without their active participation and encouragement this work would not have been done. You have been an undeniable source of motivation and working with you has been a real pleasure.

I would like to express my deepest gratitude to the members of the scientific committee for their kindness in reading this study and their interest in reviewing this document and enriching it with their proposals.

I would like to thank ***Dr. Fouad Boukli Hacene***, for all his efforts and for contributing to the success of the partnership between ESSAT and the IPB, which allowed us to carry out this work in the IPB premises. I also take this opportunity to thank all the staff and teaching team either at ESSAT, the IPB and the ESG2E.

And finally a big thank you to my friends, Merzoug Bouras, Abdeldjalil Benhanifia, Majd Chellal, Samir Hammideche, Mounir Sehad, Amine Benlakehal, Sofiane Benmohammed, Mehdi Ali and many others, for always being around.

Abstract

The importance of energy storage continues to grow, whether in power generation, consumer electronics, aviation, or other systems. Therefore, energy management in batteries is becoming an increasingly crucial aspect of optimizing the overall system and must be done properly. Very few works have been found in the literature proposing the implementation of algorithms such as EKF to predict the SOC in small systems such as mobile robots, where computational power in some application is severely lacking. To this end, this work proposes an implementation of two algorithms mainly reported in the literature for SOC estimation, in an ATMEGA328P microcontroller-based BMS, this embedded system is designed taking into consideration the criteria already defined for such a system and adding the aspect of flexibility and ease of implementation. One of the implemented algorithms performs the prediction, while the other will be responsible for the monitoring.

Keywords: Prediction Algorithm - Battery Management System - Extended Kalman Filter - Coulomb Counting Algorithm - Engineering applications.

Resumo

A importância do armazenamento de energia continua a crescer, seja na produção de energia, electrónica de consumo, aviação, ou outros sistemas. Por conseguinte, a gestão de energia em baterias está a tornar-se um aspecto cada vez mais crucial na optimização de todo o sistema e deve ser feita correctamente. Muito poucos trabalhos foram encontrados na literatura propondo a implementação de algoritmos como o EKF para prever o SOC em pequenos sistemas, tais como robôs móveis, onde a capacidade vezes é muitos aplicação escassa. Para este fim, este trabalho propõe uma implementação dos dois algoritmos principalmente relatados na literatura para a estimativa do SOC, num BMS baseado em microcontroladores ATMEGA328P, este sistema incorporado é concebido tendo em consideração os critérios já definidos para tal sistema e acrescentando o aspecto de flexibilidade e facilidade de implementação. Um dos algoritmos implementados realiza a previsão, enquanto que o outro será responsável pela monitorização.

Keywords: Algoritmo de Predição - Sistema de Gestão de Bateria - Filtro Kalman Estendido - Algoritmo de Contagem Coulomb - Aplicações de engenharia.

الملخص

تتزايد أهمية تخزين الطاقة، ليصبح الأن جانباً حاسماً لتحقيق المستوى الأمثل لأنظمة الطاقة، سواء في مجال توليد الطاقة، الإلكترونيات، الطيران او غيرها ، لذلك يجب أن تتم إدارة الطاقة في البطاريات بشكل صحيح. قد تم العثور على عدد القليل من الأعمال في الكتب و المؤلفات العلمية التي تقترح تنفيذ خوارزميات مثل تصفية كالمان الممتدة (EKF) للتنبؤ بحالة شحن البطاريات (SOC) في الأنظمة الصغيرة مثل الروبوتات المتنقلة، حيث تفتقر بشدة بعض الأنضمة إلى القوة الحاسوبية. لهذه الغاية، يقترح هذا العمل تنفيذ الخوارزميتين المشار إليهما أساسا في المؤلفات المتعلقة بتقدير حالة الشحن البطاريات في نظام للتحكم على البطاريات (BMS) على أساس الميكروكنترولر ATMEGA328P وقد صمم هذا النظام في لوحة التحكم مع مراعاة المعايير التي سبق تحديدها لهذا نوع من الأنظمة بإضافة جانب سهولة التنفيذ و الإستعمال. تقوم إحدى الخوارزميات المنفذة بالتنبؤ حالة شحن البطاريات، بينما الخوارزمية الأخرى ستكون مسؤولة عن تتبعها.

كلمات مفتاحية : خوارزمية التنبؤ ، نظام للتحكم على البطاريات ، تصفية كالمان الممتدة ، خوارزمية العد التيار كهربائي ، تطبيقات الهندسة.

Contents

1 INTRODUCTION **1**

1.1 Theoretical framework 1

1.2 Objectives 2

1.3 Document Structure 3

2 State of the Art **4**

2.1 Generality of Lithium-ion Batteries 4

2.1.1 The Electrode Pair 6

2.1.2 The Electrolyte 6

2.1.3 The Redox Effect 8

2.1.4 The Battery Characterization 9

2.1.5 Battery Assembly 11

2.2 Battery Management System 12

2.2.1 States of the Battery 13

2.2.2 Battery Modeling 15

2.2.3 States Determination Methods 19

2.3 Literature Review 23

2.4 Conclusion 25

3 System Design and Technical study **26**

3.1 Electronic Board Design 26

3.1.1 ATMEGA328P Microcontroller 28

3.1.2 Current sensor ACS712T - 5A . . . 32
3.1.3 0.91' Oled Display . . . 33
3.1.4 Temperature sensor LM35 . . . 33
3.1.5 Push Buttons . . . 34
3.1.6 LM324N Operational Amplifier . . . 34
3.1.7 MOSFETs . . . 35
3.2 Voltage Regulation . . . 35
3.2.1 Zener Diode . . . 36
3.2.2 Serie Voltage Regulator . . . 37
3.2.3 Buck Converter . . . 38
3.2.4 LM317 Integrated Regulator . . . 39
3.3 Power Consumption and Overall Efficiency . . . 40
3.3.1 Battery Dimensioning . . . 40
3.3.2 Bbox Power Consumption . . . 40
3.3.3 Robot Power Consumption . . . 41
3.3.4 Product Efficiency . . . 41
3.4 Cell balancing . . . 42
3.5 Financial Study . . . 42
3.6 Software and Programming Tools . . . 43
3.6.1 MATLAB . . . 44
3.6.2 ARDUINO IDE . . . 44
3.6.3 Schematic and PCB Design Software . . . 44
3.7 Conclusion . . . 45

4 State Determination **46**

4.1 Cell Parameter Extraction . . . 46
4.1.1 Experimental Data Collect . . . 47
4.1.2 Parameter Estimation Technique . . . 48
4.1.3 Parameter Estimation Circuit . . . 50

4.2 Proposed Algorithm 52
4.2.1 Extended Kalman Filter Algorithm 52
4.2.2 Coulomb Counting Algorithm 53
4.3 Operating Principle 55
4.3.1 Initialisation Mode 55
4.3.2 On Mode 56
4.3.3 I2C Communication Protocol 57
4.4 Conclusion 60

5 Results and Discussion **61**
5.1 Simulation Results 61
5.1.1 Simulink Battery Model 62
5.1.2 Simulation Results 63
5.2 Hardware Validation 68
5.2.1 Correct Cell Parameters Implementation 68
5.2.2 Incorrect Cell Parameters Implementation 71
5.3 Electronic Circuit 72
5.3.1 Circuit Diagram 73
5.3.2 Breadboard Circuit 73
5.3.3 Printed Circuit Design 77
5.4 Product Incorporation Principal 78
5.5 Conclusion 80

6 Conclusion and Future Work **81**

A Least Square Curve-fitting results **A1**

B Wiring Scheme **B1**

List of Tables

3.1 Operating and performance characteristics for the ATMEGA328P device . 32
3.2 Operating and performance characteristics for the ACS712 5A device . . . 33
3.3 Electronic components costs 43

4.1 Summary of the result obtained by applying a Least Square curve-fitting algorithm 49

A.1 Least Square curve-fitting algorithm results A1

List of Figures

1.1 General representation of Bbox prototype 3

2.1 Ragonne diagram for different electrochemical storage device [1] 5
2.2 A typical Lithium-ion battery scheme [5] 6
2.3 Schematic representation of the cell for discharging process [4] 8
2.4 Schematic representation of the cell for charging process [4] 9
2.5 Simplified battery management system diagram 12
2.6 First order equivalent Lithium battery model 16
2.7 RC complex equivalent electrical model for lithium batteries 17

3.1 Block diagram of the system 27
3.2 ATMEL ATMEGA328P - 28P3 Package Format 28
3.3 Reset pin wiring diagram 30
3.4 0.91' Oled Display 33
3.5 LM35 Temperature device [37] 34
3.6 LM324N operational amplifier device 34
3.7 Zener based regulator 36
3.8 Serie voltage regulator scheme 37
3.9 Buck converter scheme 38
3.10 LM317 regulator scheme 39
3.11 Bbox discharge characteristics 42

4.1 Voltage and Current for a constant current pulse discharge 47

4.2 Open circuit voltage and State of Charge relation, for comparison between measured data and 7^{th} order polynomial approximation 48
4.3 Open circuit voltage and state of charge relation, for comparison between measured data and 10 points linearization 49
4.4 Electronic circuit for current and voltage measurements 51
4.5 Schematic diagram of the electronic circuit for current and voltage measurements 51
4.6 Flow chart of the EKF algorithm implemented in the Arduino 53
4.7 Flow chart of the system algorithm. (a) Initialisation mode flow chart. (b) On-mode flow chart with EKF algorithm activated. 56
4.8 I2C bus connection principle 57
4.9 Master to slave microcontrollers bus signal 58
4.10 Slave to master microcontroller bus signal 59

5.1 (a) overall Simulink model highlighting the Input/Output of the simulation (b) Battery sub-system model 62
5.2 Voltage & Current for a constant current pulse discharge simulation 63
5.3 (a) overall Simulink model highlighting the Input/Output of the battery model simulation and Link with the Luenberger Observer (b) Luenberger observer sub-system model 64
5.4 Estimated and reference SOC comparison with the absolute error of the SOC for Luenberger Observer 64
5.5 Estimated and reference SOC comparison for Kalman Filter 65
5.6 Estimated and reference SOC comparison with the absolute error of the SOC for Extended Kalman Filter with a constant discharge test and a rest period. 66
5.7 Estimated and reference SOC comparison with the absolute error of the SOC for Extended Kalman Filter with a constant discharge test. 67

5.8 The measured battery terminal voltage compared with the estimated voltage by the proposed Extended Kalman Filter algorithm 68
5.9 The reference SOC compared with the SOC estimated by the Extended Kalman Filter and the current measured 69
5.10 Absolute Error 70
5.11 The reference SOC compared with the SOC estimated within the first 3 minutes of estimation 71
5.12 Results of the EKF prediction with wrong parameters 72
5.13 Breadboard circuit 74
5.14 Logo display. (a) ESSAT. (b) IPB 74
5.15 Menu display 75
5.16 On-mode display of cells 1, 2, 3 and 4 with a SOC value of 9.51 %, 77.25 %, 71.10 % and 55.02 % respectively. (a) Average SOC of the first 50 iteration. (b) Few seconds after. (c) approximately 1 minute after. 76
5.17 Printed Circuit Board. (a) components view. (b) top view 77
5.18 Printed Circuit Board with soldered components 78
5.19 Bbox incorportation principale 79

B.1 Schematic diagram of the electronic circuit B2
B.2 PCB Design Diagram - Top Layer B3
B.3 PCB Design Diagram - Bottom Layer B4

List of Publication

Peer-Reviewed Scopus/ISI Indexed Conference Contribution

Chellal, A. A., Lima, J., Gonçalves, J., & Megnafi, H.: Battery Management System For Mobile Robots based on an Extended Kalman Filter Approch, In 2021 Mediterranean Conference on Control and Automation. IEEE (2021).

Chellal, A. A., Lima, J., Gonçalves, J., & Megnafi, H.: Dual Coulomb Countring Extended Kalman Filter for Battery SOC Determination, In 2021 International Conference on Optimization, Learning Algorithms and Applications. Springer (2021).

Acronyms

This document contains some abbreviations which are defined here.

A/DC	Analogic to Digital Converter
BMS	Battery Management System
CC	Coulomb Counting
DEC	Diethyl Carbonate
DCC-EKF	Dual Coulomb Counting Extended Kalman Filter
DEKF	Dual Extended Kalman Filter
DKF	Dual Kalman Filter
DMC	Either Dimethyl Carbonate
DOD	Depth of Discharge
EC	Ethylene Carbonate
EEPROM	Electrically Erasable Programmable Read Only Memory
EKF	Extended Kalman Filter
FFRLS	Forgetting Factor Recursive Least Squares
I2C	Inter-Integrated Circuit
MOSFET	Metal-Oxide-Semiconductor-Field-Effect-Transistor
OCV	Open Circuit Voltage
PCB	Printed Circuit Board
POR	Power on Reset

SCL	Serial Clock Line
SDA	Serial Data Line
SOC	State of Charge
SOE	State of Energy
SOF	State of Function
SOH	State of Health

Chapter 1

INTRODUCTION

1.1 Theoretical framework

Embedded systems are ubiquitous today, but because these systems are barely perceptible, their importance and impact are often underestimated. They are used as sub-systems in a wide variety of applications for an ever-increasing diversity of functions. Whether it is a hybrid vehicle, a solar power plant, or any other everyday electrical device (laptops, smartphone, drone...), the key element remains the ability to monitor, control and optimise the performance of one or more modules of these batteries, this type of device is often referred to as a Battery Management System (BMS). A BMS is one of the basic units of electrical energy storage systems, a variety of already developed algorithms can be applied to define the main states of the battery, among others: state of charge (SOC), state of health (SOH) and state of functions (SOF) that allow real-time management of the batteries.

For the BMS to provide optimal monitoring, it must operate in a noisy environment, it must be able to electrically disconnect the battery at any time, it must be cell-based and perform uniform charging and discharging across all cells in the battery, and the components used must be able to withstand at least the total current drawn by the load. In addition, it must continuously monitor various parameters that can greatly influence the

battery, such as cell temperature, cell terminal voltage and cell current. This embedded system must be able to notify the robot using the battery to either stop drawing energy from it, or to go to the nearest charging station.

However, in the field of mobile robotics and small consumer devices, such as Smartphones or Laptops, as there are no requirements regarding the accuracy to which a BMS must be held, the standard approach such as Open Circuit Voltage (OCV) and Coulomb Counting (CC) methods are generally applied, this is mainly due to the fact that the use of more complicated estimation algorithms such as Extended Kalman Filter (EKF), Sliding Mode and Machine Learning requires higher computational power, thus, the most advanced battery management system algorithms reported in the literature are developed and verified by laboratory experiments using PC-based software. As an additional information, the most widely used battery systems in robotics today are based on electrochemical batteries, particularly lithium-ion technologies with polymer as an Electrolyte.

1.2 Objectives

All research in the field of EKF-based BMS is based on bench-scale experiments using powerful softwares, such as MATLAB, for data processing and controllers such as dSPACE. So far, the constraint of computational power limitation is not really addressed in the majority of scientific papers dealing with this subject. This thesis first validates the possibility of applying an extended Kalman filter in an ATMEGA328P, and then focuses on the implementation of such a filter assisted with a Coulomb Counting technique, as a SOC and SOH estimator in ATMEGA328P Microcontrollers. This approach, called DCC-EKF, consists of performing an SOC prediction with an EKF function, and then sending the result to a Coulomb counting function for monitoring. The approach is implemented in a Battery Managment System designed from scratch, The BMS called *Bbox* is self-powered, polyvalent for all types of Lithium cells, easy to connect with other systems and takes into account most of the BMS criteria reported in the literature. The general idea of the designed product can be expressed by the following figure :

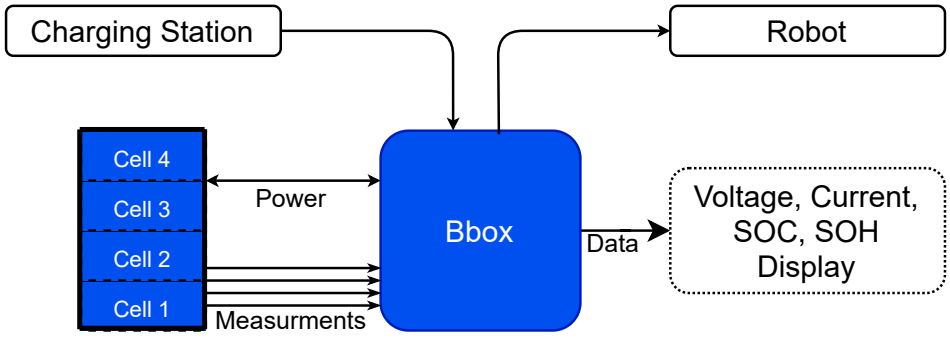

Figure 1.1: General representation of Bbox prototype

1.3 Document Structure

This document is devided into 5 sections, the rest of the paper is structured as follow. Section 2 promotes the work already done in this field and highlights the objectives intended throught this work. Section 3 describes the proposed system solution, where a block diagram and a financial study are proposed, as well as a description of each electronic component used. Section 4 highlights the importance of parameter identification and describes the proposed DCC-EKF approach and algorithm. Section 5 provides the results and offer some discussion. Finally, Section 6 draws together the main ideas described in this document and outlines future work to further improve this prototype.

Chapter 2

State of the Art

Robots are developing rapidly due to technological advances and the increased need for their mobility, they are taking an ever more complex form, moving from huge stationary robots a few years ago to small devices capable of moving around and performing many difficult tasks, now robots move freely around factories, offices or even homes, but are forced to carry their own energy with them; usually the battery is the only source of energy they can access, this is why the energy management of these batteries is so crucial and must be done correctly. There are therefore many different methods in the literature, which could give an accurate representation of the actual battery charge, also referred as State of Charge (SOC) and help to assess the main energy loss. In this chapter, the focus is on a description of the state of the art in this field, defining the architecture of the batteries, as well as the different methods used to determine the state of charge of the batteries both in laboratories based devices developed in research centers around the world or devices that are already commercialised.

2.1 Generality of Lithium-ion Batteries

Energy storage is one of the most important aspects to consider when designing a robot, especially with the miniaturisation of robots and the diversification of their activity; many different types of batteries can be used in the field of robotics [1], the Ragone diagram,

that can be seen in Figure 2.1, makes possible to determine the most suitable battery type according to the use. This diagram offers a performance comparison between the main types of batteries that can be used and easily found on the market, it shows the Energy density ($^{Wh}/_{Kg}$) plotted versus the Power density ($^{W}/_{Kg}$).

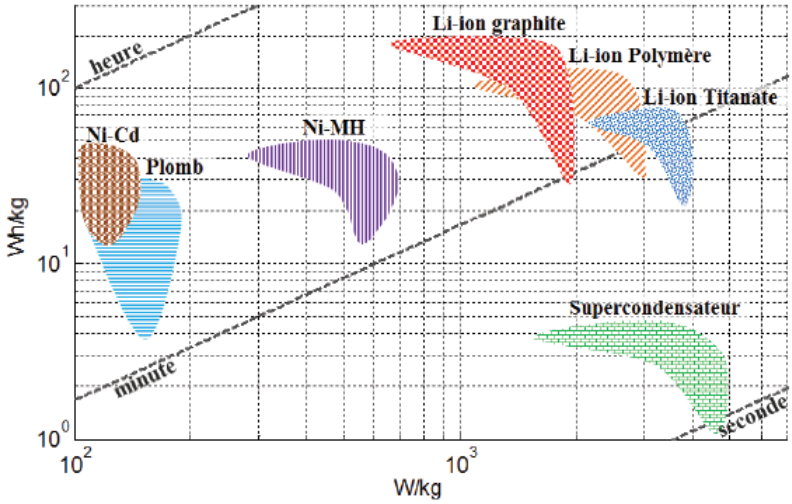

Figure 2.1: Ragonne diagram for different electrochemical storage device [1]

The most widely used battery systems in robotics today are based on electrochemical batteries, particularly lithium-ion technologies. In an electrochemical battery, chemical energy is directly converted into electrical energy, this process can be reversed in rechargeable system. This type of reaction involves the transfer of electrons from one material to another through an external electrical circuit [2]. As it can be seen in the previous figure (Figure 2.1), the use of Lithium batteries is mainly due to their high energy density, power density and their great efficiency. Also, the traditional batteries such as nickel or lead batteries contain toxic and harmful metals and resources that are found in politically unstable region [3]. Lithium-ion batteries have a very good reputation and become indispensable in many consumer devices (smartphones, watches, laptops...), in the automotive sector (mild or full hybrid vehicles), or in space applications.

This technology was first proposed by M.S. Witthingham in 1976 and commercialised by Sonny in 1990 [4], it was first based on a LiCoO2/Graphite electrode and LiPF6 electrolyte. The cell is the basic unit of a battery, thus the battery is composed of one

or more of these cells electrically connected in series and/or parallel to give a specific operating voltage and current levels. One conventional lithium-ion cell is composed of some crucial components, that are further discussed in this section.

2.1.1 The Electrode Pair

The electrodes pair making up the cell, called the anode and cathode, are usually isolated by a "separator" that prevents physical contact to be made between them. Nevertheless, it is essential to maintain a charge balance in the Red/Ox components, which is accomplished through the use of an electrolyte that indirectly connects them, and allows ion transport [5]. Figure 2.2 is a typical representation of a lithium-ion battery.

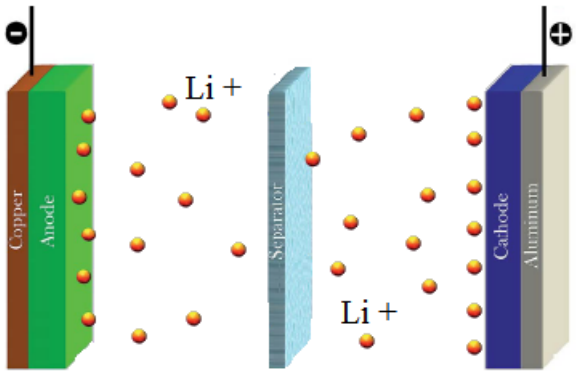

Figure 2.2: A typical Lithium-ion battery scheme [5]

2.1.2 The Electrolyte

It is the key component in the battery system; it influences the total capacity, the lifetime and also the operating temperature range. They are generally classified into two categories, liquid and solid electrolyte.

Liquid electrolyte are widely used in Lithium-ion batteries due to their high ionic conductivity. About twenty years before, Alkyl carbonate were found to be the best for use in Lithium-ion batteries [6]. Binary solvent mixture like Ethylene Carbonate (EC), Either Dimethyl Carbonate (DMC) and Diethyl Carbonate (DEC) mixed with lithium

salt (such as LiPF6, LiCIO4) are mostly used as electrolyte, but due to the high risk of electrolyte leakage leading to safety problems, their marketing and use in mobile devices has been hampered [5].

Recent advance in battery technology involved the development of *solid electrolyte* material, such as inorganic one (ceramics and glasses), or others like polymer electrolyte. Polymer-based electrolytes have been the subject of much research in the field of batteries and are the focus of increasing interest in this area. The use of this component allows for greater resistance to volume changes during charge/discharge and offers excellent flexibility. In fact, redox active polymers are synthesised from fossil fuels, but there are many attempts to use renewable resources to achieve it, the elimination of all the heavy metals used in these batteries, including cobalt, lead and nickel, allows for a more environmentally friendly battery [5], [6].

In a lithium polymer battery, the polymer is sandwiched between the two pairs of electrodes and serves as both separator and electrolyte. A good polymer electrolyte should have the following characteristics:

- High ionic conductivity and a good electronic isolation;
- Close to unity Li+ transference number, also called ion transport number, representing the fraction of the total electrical current carried in the electrolyte by a given ion species;
- Good mechanical strength, it must be robust and stretchable to avoid any problems during the manufacturing process or in operation;
- Excellent chemical and thermal stability;
- Low toxicity.

The Lithium-ion polymer batteries usually called Li-Po battery are battery that use this type of polymer electrolyte technologies, there are many advantages for this design, they are lighter and more condensed, thus Li-Po batteries offer 20% more energy density

then a classical lithium-ion battery and are approximately three time better than NiCd or NiMH batteries [7], they are also safer, as they are less likely to catch fire and are less dangerous if mistreated.

2.1.3 The Redox Effect

As with all rechargeable batteries, Li-po batteries make use of the redox phenomena that occur in their electrode. The equation 2.1 represents a typical red-ox equation.

$$Red_1 + Ox_2 \Longleftrightarrow Red_2 + Ox_1 \tag{2.1}$$

During discharge, the negative electrode, called the anode, is oxidised and releases Li+ into the electrolyte [1]; while the electrons are transferred to the cathode via an external circuit, the positive electrode, called the cathode, is reducing and receives the ions previously released by the anode into the electrolyte, as well as electrons from the external circuit; Li+ is thus intercalated into the positive electrode. Figure 2.3 represent the discharge process.

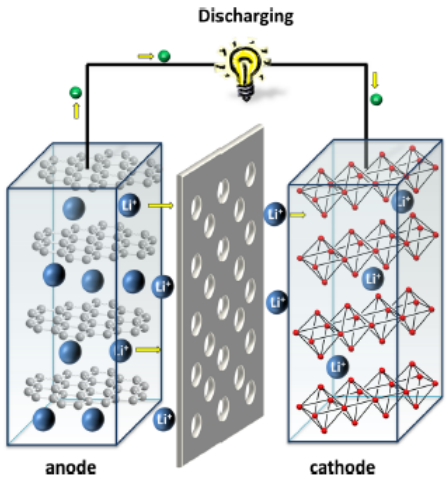

Figure 2.3: Schematic representation of the cell for discharging process [4]

During the charge of the battery, the previous phenomena is reversed, the positive electrode is oxidized, thus releasing Li+ ions in the electrolyte and electrons in the external conductor, the electrons are forced to move from the positive electrode to the negative one, while the negative electrode is reduced and Li+ are intercalated. Figure 2.4 represent the charge process.

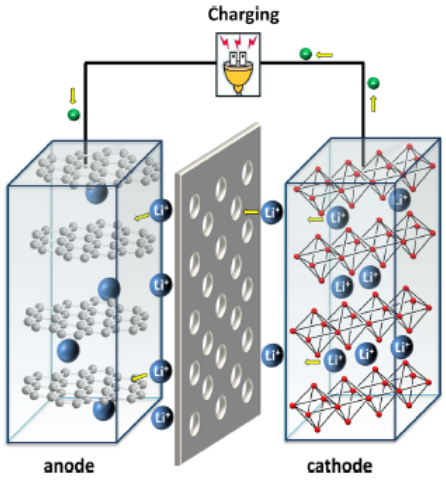

Figure 2.4: Schematic representation of the cell for charging process [4]

2.1.4 The Battery Characterization

Various characteristics must be considered before using any type of battery, especially lithium-ion batteries. In this section, a description of the main quantities governing the battery is given.

Charge/Discharge curve, each battery follow a specific behaviour, this behaviour can be extracted from an experimental discharge test by applying a constant current method, under constant power. As the voltage will drop progressively, the current supplied by the battery will also drop, It is therefore essential to control the current delivered by the battery, this can be achieved by controlling the power consumed by the load and taking advantage of Ohm's law $Z = \frac{V}{I}$, and setting the impedance or voltage of the load to a constant value [4].

Theoretical capacity, defined in ampere-hours (Ah) or coulombs (C), is an essential value to know for the determination of the states, it represents the total amount of charge involved in the reaction [2] and the amount the battery is able to store. This parameter can change from one battery to another, and can deteriorate after exceeding a specific temperature or due to ageing [1]. For example a 3 Ah battery is a battery that allows the drain of a 03 A current continuously from it during one (01) hour, or 06 A current for half an hour (30min).

Theoretical energy, represent the maximum energy value that can be delivered by a battery cell [2], it take both of the theoretical capacity and voltage into consideration (see Equation 2.2). As the previous quantity, it may change with the variation of temperature, level of current and the ageing of the cells, and is represented in watt-hour (Wh).

$$Watthours\ (Wh)\ =\ Voltage\ (V) \times AmpereHour\ (Ah) \tag{2.2}$$

In practice, the *theoretical energy* cannot be achieved by the battery due to the voltage drop (loss of energy) in the various battery components.

Internal impedance, is the parameter that defines the behaviour of the battery when current flows through it, it is useful for output voltage (power) estimation. This parameter is closely related to temperature, state of charge, state of health (ageing) of the battery, and is used as a representation tool in the electrical model.

Faradic efficiency, is a ratio of the amount of electricity involved in the discharging and charging phases, the closer the faradic efficiency is to unity, the higher the efficiency of the battery. Thus, representing an important parameter for indicating the efficiency of any battery.

Energy efficiency, is the same as the faradic efficiency but for energy, it represents the ratio of energy discharged to energy charged in the battery and corresponds to the energy loss that occurs in the cells.

Capacity Retention and Self discharge, the battery loses gradually its capacity and becomes more evident when the battery remains unused for a long time, this phenomena is due to internal reaction, and depends highly on the SOC and the temperature, for example after 28 days with a constant temperature at 25°C, if fully charged the LIR18650 2600mAh battery loses 20% of its total charge, letting the remaining capacity of the battery at 2080mAh [8], [9].

Life span and ageing effect, is attached with the temperature, the external environment, the condition of charging and discharging, the utilization of the battery and deep discharging. There are many causes of ageing that change the behaviour of the batteries and affect there parameters, two distinct types of ageing mode exist, calendar ageing and cyclic ageing.

After 299 cycle at 100% Depth of Discharge (DOD), with a 1.3 A charge and discharge performed, the residual discharge capacity for the LIR16850 Battery reach a value of 80% (2050mAh) of the initial capacity (2600mAh) [8].

2.1.5 Battery Assembly

The cells in a battery pack can be connected in series, parallel or series-parallel, with the configuration depending on the output voltage and current required for the application. For example, the 85 kWh battery pack in the Tesla Model S uses 74 cylindrical 3100 mAh cells connected in serie to create a parallel unit; each of these unit is repeated 96 times and connected in parallel [10]. In general, a battery system can provide a higher voltage with cells connected in series, and a higher current when connected in parallel.

The number of cells that can be connected in a module is dependent mainly on the desired capacity and is limited by the monitoring capability of the Battery Management System (BMS). Each battery module has its own monitoring, electrical and thermal control components, which are closely grouped together in the electronic board [11].

2.2 Battery Management System

The battery management system is an electronic device that continuously monitors and controls various harmful parameters, and can at any time electrically isolate the Lithium cells, while indicating to the system that a cell is out of order and should not be used. Figure 2.5 represent a graphical representation for a serie configuration battery management system.

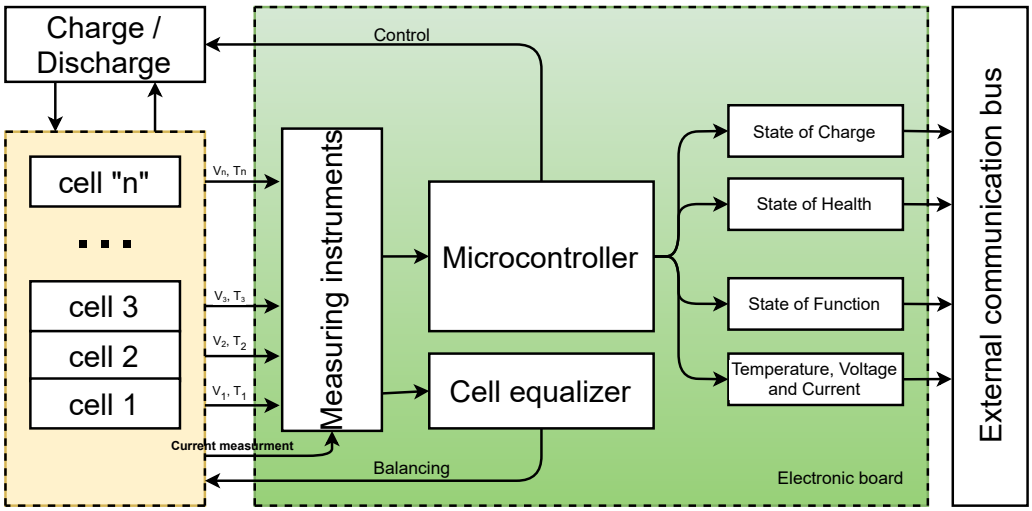

Figure 2.5: Simplified battery management system diagram

The main parameters that need to be taken into account by the BMS are:

- Temperature, as described in the previous section, has a significant impact on cell performance and could severely increase the internal impedance of the battery, decreasing the capacity and life of the battery, Temperature increases performance in the short term by increasing capacity, but above $55°C$, performance begins to decline. At much higher temperatures, an internal chemical reaction can be triggered and could quickly lead to fire and explosion [12].

- The voltage also has a major impact, too low or high cell voltage can damage the battery almost immediately.

- The current, a specific value of the current should not be exceeded as for the 18650 Battery the maximum discharge current should not go beyond 2.6 A [8].

- The state of charge is also a crucial parameter, to extend the life of the battery and its availability it is recommended to not go under 60% of SOC.

2.2.1 States of the Battery

The BMS is one of the basic unit of electrical energy storage systems, a variety of already developed algorithms can be applied to define the main states of the battery, among others: SOC, State of Health (SOH) and State of Function (SOF) that allow real-time management of the batteries.

State of Charge

The management of a Lithium battery in mobile robots requires mainly the knowledge of the SOC, which represents the ratio between the energy stored in (Ah) at a specific time "t" (C_{used}) and the total energy storable in the battery also in (Ah) in a reference time "t_{ref}" (C_{actual}) [1], in other words, it represents the quantity of charge that still remain in the battery and could be discharged and can be expressed as given in Equation 2.3 [13].

$$SOC \;=\; 1 - DOD \;=\; \frac{C_{actual} - C_{used}}{C_{actual}} \tag{2.3}$$

It is also common in the literature to find the notion of DOD, it's the complementary of the SOC, which refers to the quantity of charge that has been used (discharged) or the quantity of charge that could be charged in the battery. The notion of State of Energy (SOE) is unusual but can be found, it has the same definition as SOC but for power, so it is the ratio of the energy remaining in the battery at time "t" to the actual total energy in the battery [1], [14], [15].

The State of Charge determination is a challenging task, due to the lack of any type of sensor that could directly give the SOC, thus it cannot be measured directly, some

basical approaches such as the Open Circuit Voltage (OCV) measure and the Coulomb Counting (CC) technique, are used to help monitor's the charge and discharge process, these methods are inexpensive and requires only an accurate current sensor and a good voltage measurement. But, the SOC is the main state and it's calculation is a key factor that must be accurately determined, a reliable SOC measurement is essential for ensuring safety and maximizing battery life. This is why, other methods, slightly more complicated, such as Sliding mode, Artificial Intelligence and Kalman Filtering were developed, these method try to estimate or predict the SOC of the battery [1]. The characteristics of each methods will be further discussed in the thesis.

State of Health

State of Health is an important factor for all types of batteries, it takes into account the ageing of the cells and predicts future malfunctions, thus avoiding future accidents if calculated correctly. It shows the decrease in battery capacity, or the increase in internal resistance over time, depending on the estimation method. The determination of the SOH is as challenging as the SOC and can be done with approximate methods such as the Dual Kalman Filter (DKF) the Dual Extended Kalman Filter (DEKF) and the Forgetting Factor Recursive Least Squares (FFRLS), which are commonly found in the literature for SOH estimation [1], [16]–[18]. More basic approaches, such as the application of a simple algebraic method, can also be found in the scientific literature [19], [20]. The following equation represent the mathematical definition of the SOH [13]:

$$SOH = \frac{C_{actual}}{C_{start}} \tag{2.4}$$

where, C_{actual} is the measured cell capacity at instant "t_{ref}" and C_{start} is the capacity of the cell when first used.

State of Function

The notion of SOF is present in the literature, it is very little developed compared to the other states described above because its determination in some fields, such as photovoltaics, is unnecessary [13]. However, it can be of great use in the fields of robotics and it is therefore important to describe it in this report. SOF is a Boolean yes/no parameter that indicates whether the battery has sufficient energy capacity to perform a specified function [21], or whether it should return to the nearest charging station as soon as possible. This parameter can be derived from the SOC and SOH described above, hence the interest in providing an accurate representation of the latter.

It is necessary to enter a battery level threshold at which the robot should redirect to the docking station, this is a difficult task due to the mobility of the robot, different methods are used for the calculation of this parameter among others the Kalman Filter (KF) algorithm [21], Risk and gain assessment method [22]. The mathematical formulation of the SOF can be given by [21]:

$$SOF = \begin{cases} 1, \ SOC \geq SOC_{threshold} \\ 0, \ SOC < SOC_{threshold} \end{cases} \tag{2.5}$$

2.2.2 Battery Modeling

Due to their physical and chemical process, the battery shows nonlinear characteristics, thus making the prediction of it's behaviour difficult. Two battery models are most often applied, the Electrochemistry model, which gives a good representation of the internal dynamics of the batteries, and the Electrical circuit model, which aim to reproduce the behaviour of the electrical quantities in the battery (SOC, Voltage and current) and allows them to be easily formulated into mathematical formula [14]. This model, as shown in Figure 2.6, use standard electrical components such as resistors, capacitors and voltage source. The values of this model are obtained from experimentation, where OCV tests are performed on successive charge/discharge process [15], [16], these tests are explained in more detail in chapter 4.

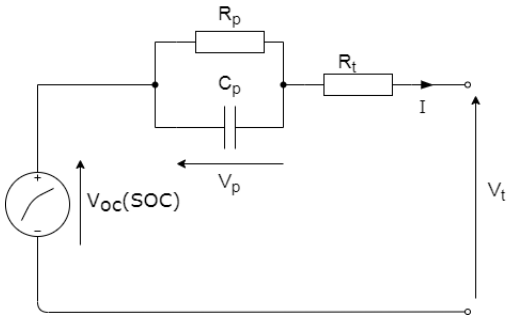

Figure 2.6: First order equivalent Lithium battery model

The voltage source denoted by V_{oc} represents the open circuit voltage and is in function with the SOC denoted (Equation 2.8 and 4.1), the series resistor R_t represents the voltage drops effect of the cell, the diffusion resistance is represented by the R_p resistor and C_p represents the polarization effect of the cell [1], [14]. The RC elements represent the relaxation effect of charging/discharging process of the battery and I is the current flowing through the model. The terminal voltage denoted as V_t, represents the output voltage of the cell, and is given by Equation 2.6.

$$V_t = V_{oc}(SOC) + I \cdot R_t + V_p \tag{2.6}$$

The mathematical relation of the SOC(t) is expressed as follow:

$$SOC(t) = SOC(t_{ref}) + \int_{t_{ref}}^{t} \frac{I}{C_{actual}}.dt \tag{2.7}$$

and,

$$V_{oc}(SOC) = a \cdot SOC + b \tag{2.8}$$

With, C_{actual} is the total energy storable in the battery in a reference time, and a and b are variables that fluctuate according to the SOC. The time derivative of equation 2.7 can be expressed as given by:

$$\dot{SOC} = \frac{I}{C_{actual}} \tag{2.9}$$

The polarization voltage is extracted as follow,

$$\begin{aligned} I &= I_R + I_c \\ I &= \frac{V_p}{R} + \frac{C \cdot dV_p}{dt} \\ \dot{V_p} &= -\frac{1}{R_p C_p} V_p + \frac{1}{C_p} I \end{aligned} \tag{2.10}$$

By substituting the equation 2.8 into equation 2.6 it is obtained:

$$V_t = a \cdot SOC + b + V_p + R_t I \tag{2.11}$$

The state equations describing the cell behaviour are expressed as the following system:

$$\begin{cases} \begin{bmatrix} \dot{SOC} \\ \dot{V_p} \end{bmatrix} = \begin{bmatrix} 0 & 0 \\ 0 & \frac{-1}{R_p C_p} \end{bmatrix} \cdot \begin{bmatrix} SOC \\ V_p \end{bmatrix} + \begin{bmatrix} \frac{1}{C_{actual}} \\ \frac{1}{C_p} \end{bmatrix} \cdot I \\ V_t = \begin{bmatrix} a & 1 \end{bmatrix} \cdot \begin{bmatrix} SOC \\ V_p \end{bmatrix} + R_t \cdot I + b \end{cases} \tag{2.12}$$

In general, a more complicated electrical model could be integrated with the addition of "n" successive RC elements and allows even more detailed monitoring of cell behaviour. Such system can be represented as in Figure 2.7.

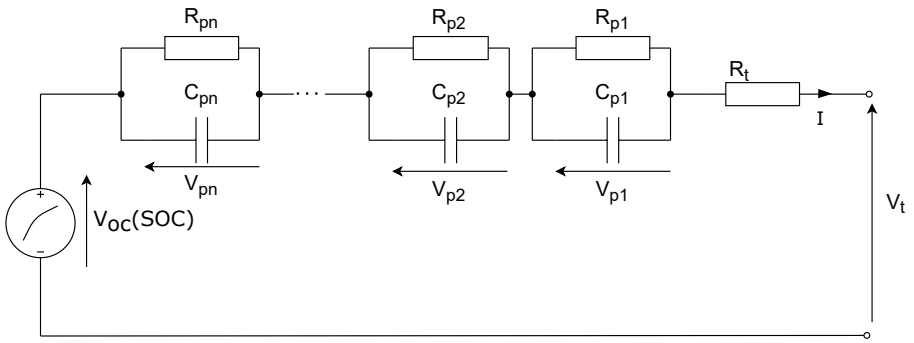

Figure 2.7: RC complex equivalent electrical model for lithium batteries

The state equation describing this electrical system is given as follow [1]:

$$\begin{cases} \begin{bmatrix} \dot{SOC} \\ \dot{V_{p1}} \\ \dot{V_{p2}} \\ \vdots \\ \dot{V_{pn}} \end{bmatrix} = \begin{bmatrix} 0 & 0 & 0 & \cdots & 0 \\ 0 & \frac{-1}{R_{p1}C_{p1}} & 0 & \cdots & 0 \\ 0 & 0 & \frac{-1}{R_{p2}C_{p2}} & \cdots & 0 \\ \vdots & \vdots & \vdots & \ddots & \vdots \\ 0 & 0 & 0 & \cdots & \frac{-1}{R_{pn}C_{pn}} \end{bmatrix} \cdot \begin{bmatrix} SOC \\ V_{p1} \\ V_{p2} \\ \vdots \\ V_{pn} \end{bmatrix} + \begin{bmatrix} \frac{1}{C_{actual}} \\ \frac{1}{C_{p1}} \\ \frac{1}{C_{p2}} \\ \vdots \\ \frac{1}{C_{pn}} \end{bmatrix} \cdot I \\ V_t = \begin{bmatrix} a & 1 & 1 & \cdots & 1 \end{bmatrix} \cdot \begin{bmatrix} SOC \\ V_{p1} \\ V_{p2} \\ \vdots \\ V_{pn} \end{bmatrix} + R_t \cdot I + b \end{cases} \tag{2.13}$$

In order to obtain the best performance, a first-order equivalent battery model is preferred, and represents the best compromise between accuracy and complexity, this study will focus on the equivalent circuit model with the equivalent mathematical model described in equation 2.14, this model offers sufficiently small matrices thus reducing the computational time and computational power [23]. As the system deducted in equation 2.12 is in continious time, it discretization results in the following form:

$$\begin{cases} \begin{bmatrix} \dot{SOC} \\ \dot{V_p} \end{bmatrix} = \begin{bmatrix} 1 & 0 \\ 0 & \exp\frac{-\Delta t}{R_pC_p} \end{bmatrix} \cdot \begin{bmatrix} SOC \\ V_p \end{bmatrix}_{k-1} + \begin{bmatrix} \frac{1}{C_{actual}} \\ \frac{1}{C_p} \end{bmatrix} \cdot I_{k-1} \\ V_t = \begin{bmatrix} a & 1 \end{bmatrix} \cdot \begin{bmatrix} SOC \\ V_p \end{bmatrix}_k + R_t \cdot I_k + b \end{cases} \tag{2.14}$$

Also, the effect of hysteresis on the battery is not modelled, as previous research has shown that including hysteresis effect for this model increases the accuracy of the model by approximately 5% [3].

2.2.3 States Determination Methods

Open Circuit Voltage Method

The open circuit voltage method is the most basic and economical method of easily identifying the SOC level. It can be used throughout the charging and discharging process, and is commonly used in most commercial devices (phones, laptops, drones...) and involves a direct measurement of the cell voltage at rest [9], [14]. The SOC is closely related to the OCV by a non-linear function ($V_{oc}(SOC)$) which is further defined in section 4.1.

This method mainly consists of grouping the SOC with its equivalent OCV for different temperature values and battery health states and storing them in a look-up table. The OCV measure certainly uses less time to calculate the state of charge, but does not produce the most accurate calculation and may give a misleading representation of it, it also requires a voltage measurement when the cell is at rest and stabilised, which may take more than an hour to reach. Continuous determination of the SOC can possibly be carried out even when the battery is in use, using the equivalent electrical model presented in the previous section.

Coulomb Counting Method

The Coulomb Counting method, also referred as *current integration* method, is one of the most used method for following the states of the battery and most accurate if correctly initialized. This method consist of a current measurement and integration in a specific period of time and link together the total actual capacity (C_{actual}) and the faradic efficiency (n_f). The state of charge evolution expression can be represented by the following expression:

$$SOC(t_n) = SOC(t_{n-1}) + \frac{n_f}{C_{actual}} \int_{t_n}^{t_{n-1}} i \cdot dt \tag{2.15}$$

But this method has several drawbacks that lead to errors in SOC determination. The variation in capacity and the inaccurate determination of faradic efficiency are important. For example, it is essential to exactly know the actual capacity of the battery, although

this parameter is difficult to determine, due to the variation in capacity with the change in temperature and SOC. In addition, the coulomb counting method is an open-loop method and its accuracy is therefore strongly influenced by the accumulated errors, these errors are produced by the erroneous initial determination of the faradic efficiency, the battery capacity, drift measurements and the SOC guess error [15]. Also, discretization frequency, according to Nyquist-Shannon's theorem, must be at least twice as high as the highest frequency of the signal. But considering that the actual signal is uneven and composed of an infinity of signals of different frequency, the shorter the time interval (the acquisition frequency is high), the better the accuracy of the BMS and therefore of our state of charge, the frequency is consequently, limited only by the capacity of the sensor and the microcontroller [1].

Fundamental of Kalman Filtering

In 1960, an article on a new method describing a recursive solution to the problem of linear filtering of discrete data was published by R.E. Kalman. Since then, and especially due to the advances in digital computing, the KF has been the subject of extensive research and applications, particularly in the field of navigation [24]. The Kalman filter is an algorithm that estimates the states of system from indirect and uncertain measurements of the system's input and output. KF algorithms are widely used for applications such as navigation and tracking, control systems, signal processing, computer vision, and econometric. The original Kalman filter is applied to linear systems, based on their linear model form, this system is add to it two Gaussian noise sources, corrupting the state of the system and the measurement. But, several extension enable it to be used in more various systems including the SOC estimation for batteries.

The state-space representation and the measurement equation are represented as :

$$\begin{cases} x_k &= A_{k-1} \cdot x_{k-1} + B_{k-1} \cdot u_{k-1} + \omega_k \\ y_k &= C_k \cdot x_k + D_k \cdot u_k + \upsilon_k \end{cases} \tag{2.16}$$

Where, $x_k \in R^{n\times 1}$ is the state vector, $A_k \in R^{nxn}$ is the system matrix in discrete time, $y_k \in Rm \times 1$ is the output, $u_k \in R^{m\times 1}$ is the input, $B_k \in R^{nxm}$ is the input matrix in discrete time, and $C_k \in R^{m\times n}$ is the output matrix in discrete time. ω *and* υ represents the Gaussian distributed noise of the process and measurement. The Kalman filter can be both formulated in continuous and discrete time, knowing that a microcontroller is to be used, the discrete time representation presented in Equations 2.16 was applied.

By overlaping the equation 2.14 and 2.16, it is possible to determine the $A_k,\ B_k,\ C_k$ *and* D_k matrices.

$$A_k = \begin{bmatrix} 1 & 0 \\ 0 & \exp\frac{-\Delta t}{R_p C_p} \end{bmatrix} \quad , \quad B_k = \begin{bmatrix} \frac{1}{C_{actual}} \\ \frac{1}{C_p} \end{bmatrix},$$

$$C_k = \begin{bmatrix} a & 1 \end{bmatrix} \quad , \quad D_k = R_t$$

The Kalman filter follow a precise step by step algorithm. First, the prediction step, also referred as "time update", predict the actual states and the different matrices describing the model ($A_k,\ B_k,\ C_k$ *and* D_k), using the previous estimation (or the initial guess for the first iteration), this step is summarized in the following equations:

$$\begin{aligned} \hat{x_k} &= A_{k-1} \,.\, x_{k-1} + B_{k-1} \,.\, u_{k-1} \\ \hat{P_k} &= A_{k-1} \,.\, P_{k-1} \,.\, A_{k-1}^t + Q \end{aligned} \tag{2.17}$$

Then, the Correction step, also referred as "measurement update", that achieve correction of the Kalman Gain K and the state prediction $\hat{x_k}$ and a prediction of the corresponding covariance matrix P, including the process noise Q [25]. One form of the correction step is given by equations 2.18.

$$\begin{aligned} \hat{y_k} &= C_k \,.\, \hat{x_k} + D_k \,.\, u_k \\ K_k &= \hat{P_k} \,.\, C_k^t \,.\, (C_k \,.\, \hat{P_k} \,.\, C_k^t \ + \ R)^{-1} \\ x_k &= \hat{x_k} \ + \ K \,.\, (U_k - \hat{y_k}) \\ P_k &= (I \ - \ K_k \,.\, C_k) \,.\, \hat{P_k} \end{aligned} \tag{2.18}$$

The equations starting from 2.17 and ending to 2.18 are then repeated at each iteration. It should be specified that Kalman filter equations can be algebraically manipulated into several forms, the chosen form is one of the most common.

The overall performance of the filters is set by the covariance matrix P, the process noise matrix Q and the measurement noise R. As stated in the literature [8], the determination of the parameters P and Q can directly be obtained through experience and empirical experiments, while the R represents the variance of a set of measurement samples, these parameters are given by:

$$Q = \begin{bmatrix} 0.25 & 0 \\ 0 & 0 \end{bmatrix}, \quad P = \begin{bmatrix} 1 & 0 \\ 0 & 1 \end{bmatrix} \quad and \quad R = 0.00001$$

The deliberate omission of an on-the-fly update formula of the measurement and process uncertainties in the algorithm, is due to the fact that it requires a huge computational power, things that can't be achieved with an 8-bits microcontrollers, thus, it is a very common technique to apply fixed values for these matrices in SOC estimation.

The Sliding Mode Observer

The sliding mode technique is best known for its robust control and was introduced in the Soviet Union in the 1960s. But nothing was discussed yet about observers, at that time the sliding mode focused only on the control paradigm. The observer associated with was developed much later and tries to find the state vector that works best for the system, like the Kalman filter, the dynamics of this system is translated into a model, the objective of this method is to drive the error between the observed output $\hat{y}$ and the real measured output y to zero. The state system considered by this observer is represented by the equation 2.19 [1].

$$\begin{cases} \dot{\hat{x}} = A \cdot \hat{x} + B \cdot u + L \cdot (y - \hat{y}) + M \cdot sign(y - \hat{y}) \\ \hat{y} = C \cdot \hat{x} + D \cdot u \end{cases} \tag{2.19}$$

The main advantage of this observer is the convergence ability to a correct result despite the presence of measurement uncertainty and non-linearities, the sliding mode observer is able to quickly extract the actual state vector in a finite time. This method could be similar to the Luenberger observer (shown in equation 2.20, but it is totally different because the Luenberger observer cannot cancel the error for the battery system due to the presence of non-linearity, this aspect is proved in chapter 5 [26].

$$\begin{cases} \dot{\hat{x}} &= A \cdot \hat{x} \ + \ B \cdot u \ + \ L \cdot (y - \hat{y}) \\ \hat{y} &= C \cdot \hat{x} \ + \ D \cdot u \end{cases} \tag{2.20}$$

2.3 Literature Review

Several research teams around the world have proposed different solutions to design an efficient BMS system for lithium-ion batteries. Taborelli *et al.* have proposed in [27], a design of an EKF and Ascending Extended Kalman Filter (AEKF) algorithms specifically developed for light vehicle categories, such as electric bicycles, in which a capacity prediction algorithm is also implemented tackling SOH estimation. The design has been validated by using simulation software and real data acquisition. In [28], Mouna *et al.* implemented two EKF and sliding mode algorithms in an Arduino board for SOC estimation, using an equivalent first-order battery as a model. Validation is performed by data acquisition from Matlab/Simulink. Sanguino *et al.* proposed in [29] an alternative design for battery system, where two batteries works alternatively, one of the batteries is charged through solar panels installed on the top of the VANTER mobile robot, while the other one provides the energy to the device. The battery SOC selection is performed following an OCV check only and the SOC monitoring is done by a coulomb counting method.

In addition, several devices are massively marketed, these products are used in different systems, from the smallest to the largest. The *Battery Management System 4 – 15S* is a BMS marketed by REC, it has the usual battery protections (temperature, overcurrent,

overvoltage) [30]. A cell internal DC resistance measurement technique is applied, suggesting the application of a simple resistor equivalent model and an open circuit voltage technique for SOC prediction, and an Coulomb counting technique for SOC monitoring. The device can be operated as a stand-alone unit and offers the possibility of being connected to a computer with an RS-485 for data export. This device is intended for use in solar system. *Roboteq's BMS10x0* is a BMS and protection system for robotic devices developed by Roboteq, it uses a 32-bit ARM Cortex processor and offers the typical features of a BMS, along with Bluetooth compatibility for wireless states checking. It can monitor from 6 to 15 batteries at the same time. Voltage and temperature thresholds are assigned based on the chemical composition of the battery. The SOC is calculated based on an OCV and CC techniques [31].

2.4 Conclusion

As the importance of energy storage has continued to grow in recent years, researchers around the world have been developing more powerful and efficient batteries, both in terms of energy density and resistance. But developing the most powerful battery without optimising its management remains an act of little value, hence the relevance of introducing a battery-related energy management system, which constantly monitors and controls various harmful parameters, in order to protect the battery and extract the maximum possible energy from it. A good BMS is one that accurately estimates the SOC and SOH, basic approaches such as OCV and CC techniques, or slightly more complicated ones such as sliding mode, artificial intelligence and Kalman filtering, are then used to try to estimate or predict the actual SOC of the battery.

As no specific accuracy requirement are defined, basic approaches are mostly used in smartphones and computers, they certainly use less time to calculate the state of charge, with a higher performance, but they do not produce an accurate calculation and generally give a misleading representation of it and lead to errors accumulation overtime. On the other hand, the complex methods, allow indeed to limit the error and the impact of uncertainties on the final result, but requires a computational power that is generally accomplished by the use of powerful controllers such as dSPACE. All research in the field of EKF-based BMS is based on bench-scale experiments using powerful software, such as MATLAB, for data processing. So far, the constraint of computational power limitation is not really addressed in the majority of scientific papers dealing with this subject.

Chapter 3

System Design and Technical study

The technical study of a project is a design expertise and represents a preliminary study for the realisation of a prototype to meet the defined expectations and the precise budget for its realisation. It consists mainly of presenting the information and technical characteristics of the prototype and includes all the choices made for the design, based on the defined specifications and the information obtained and summarised in the previous chapter. The design of a product is a complex activity that requires the mobilisation of multiple skills in different disciplines.

The ***Bbox*** project is the name of our product, and represents our proposed solution for a BMS in the robotics field. This chapter therefore aims firstly to describe the operating principle adopted for the battery management system, then to describe the various electronic components that make up the system, as well as the relationships between them. An economic and financial analysis is carried out at the end of this chapter.

3.1 Electronic Board Design

According to the specifications established at the beginning of the study, it is essential that the battery management system guarantees optimal operation of the battery with the possibility of isolating it electrically at any time, in order to increase its life and, consequently, that of the system in general. To achieve this, the electronic board to be

designed must meet these specifications. The Figure 3.1 attempts to show the different relationships between the components of the electronic system.

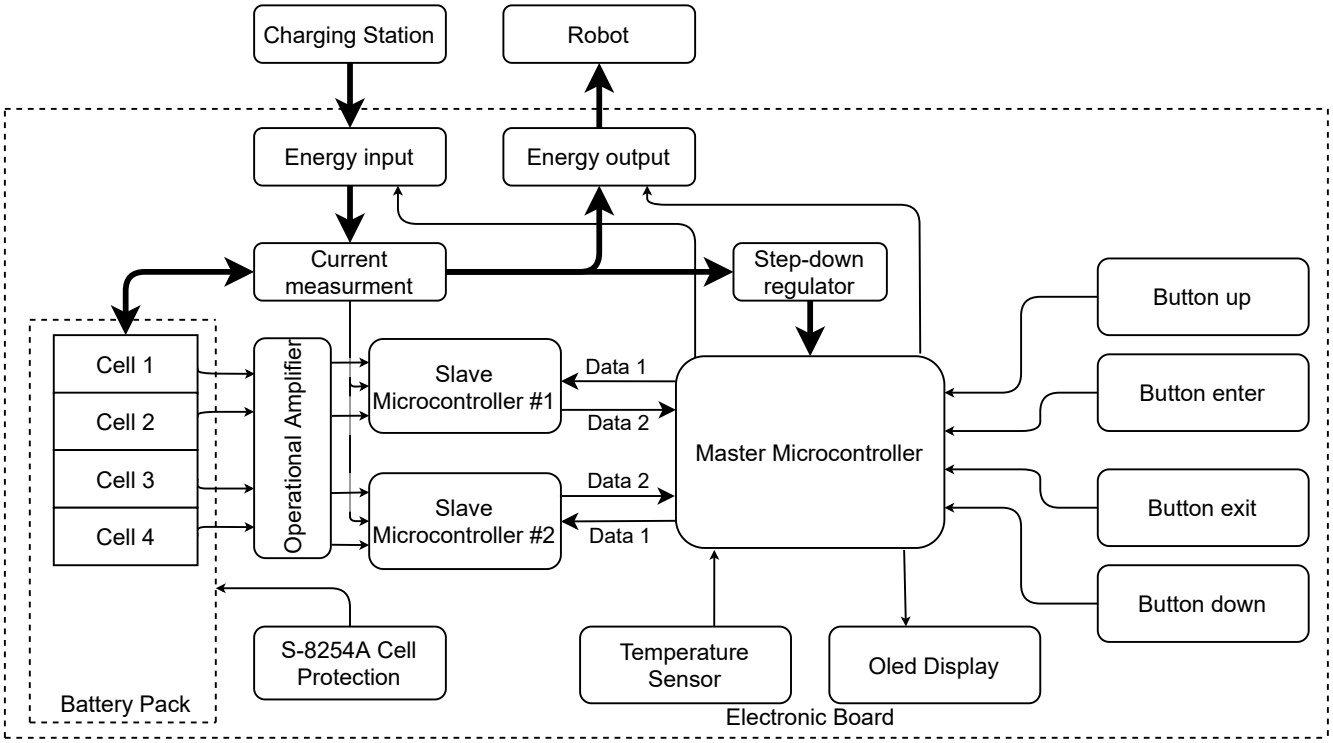

Figure 3.1: Block diagram of the system

The Master microcontroller is the central element of the system, it is based on the ATMEGA328P, it's choice is further discussed in section 3.1.1. It collect the State of Charge predicted by each ATMEGA328P slave microcontroller and control the energy flow according to the data collected. This microcontroller is connected to push buttons and an OLED screen to facilitate communication with the user. Power is supplied directly from the batteries, the voltage is stabilised and regulated for the BMS electronics by an LM7805 voltage regulator. The current flowing in and out the battery is measured with the use of an ACS-712 current measurment device. The voltage offered to the robot by the Bbox varies between 15 V and 11 V, no regulation is made keeping the regulation of the external voltage to the future users of the device.

3.1.1 ATMEGA328P Microcontroller

The ATMEGA328P is a 28-pin electronic component surrounded by an opaque plastic case. It is an 8-bits microcontroller, meaning that it can handle only 8 bits of data at a time, this type of microcontroller has a Flash memory type, in other words Electrically Erasable Programmable Read Only Memory (EEPROM), offering it the possibility of being electrically programmable and erasable, this feature is highly valuable, especially in the prototype development and test phases [32].

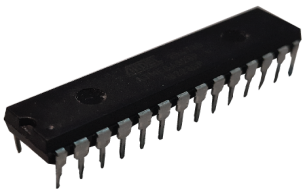

Figure 3.2: ATMEL ATMEGA328P - 28P3 Package Format

The choice of this microcontroller was not made randomly but following specific criteria; it need to meet the computing need, power consumption, availability of software and hardware development tools, wide product availability, reliability, documentation and being cost-effective. In addition to meeting these criteria, the ATMEGA328P has several advantages and characteristics that are listed as follow [33]:

- EEPROM Write/Erase cycle of approximately 100,000;
- Wide operating voltage range between 2.7V and 5.5V;
- Very low consumption, reaching approximatively 1.5 mA;
- Sufficient number of inputs and outputs for the device;
- Fast 10-bit Analogic to Digital Converter (A/DC);
- Master/Slave $I2C$ protocol;
- Industrial operating temperature range between -55°C to +125°C;

- Various packaging format;
- Extensive literature available;
- Low Cost per unit.

There are five major 8-bits microcontrollers manufacturer : Freescale, Intel's 8051, Atmel's AVR, Zilog's Z8 and Microchip's PIC. Another alternative considered was the PIC 18F4520, which outperforms ATMEGA328P in A/DC speed, power consumption, number of external interuption pins, operating frequency, and have a much higher write/erase cycle [34]. But the main advantages of ATMEGA over PICs are the ease of product development, the size and the widely available documentation. Also the programation of the ATMEGA328P through Arduino Uno, which is an open source electronic board that could accomplish various tasks easily, permit to ensure the vaibility of it in large quantities both now and in the future.
To create an executable assembly language, that can be used and read by the microcontroller, it is necessary to use the AVRStudio IDE, and write the algorithm in C language, and then burn the resulting "hex" file into the ATMEGA328P's program [32], or by using the Arduino IDE and using the Arduino developing board. This type of programming is preferred for its simplicity and flexibility to adapt to any change in the development process.

Calibrated Internal RC Oscillator

The microcontroller has a maximal 8.0 MHz internal clock, thus giving it the possibility to operate without any external components, but because the algorithm implemented need to have a low sampling time, it is necessary to use a external clock of 16.0 MHz. In addition using an internal oscillator greatly influence the voltage and temperature of the microcontroller, resulting in an error of up to 14 % [33]. The two pins of the external clock are XTAL1 & XTAL2.

External Reset

The MCU control register is reset when a low level is present on the $\overline{RESET}$ pin for longer than the minimum pulse length. It is necessary to add a series resistor, as shown in Figure 3.3, which can vary between 100 and 1000 Ω. Direct connection without a resistor is strongly discouraged by the manufacturer, as it can lead to unwanted resets or even destruction of the $\overline{RESET}$ pin.

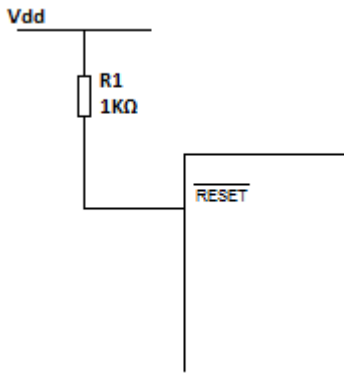

Figure 3.3: Reset pin wiring diagram

A Power on Reset (POR) pulse is also generated by an on-chip low voltage detector. The POR is activated whenever V_{dd} is below the detection level, and will trigger a start-up reset [33].

Input/Output Ports

In general, these are the most used resources in a microcontroller, depending on the device used, there are either five (05) or three (03) bi-directional ports, with a variable number of pins. Some of the pins are multiplexed with other features (interrupt, A/DC, I2C. . .). Each parallel port is controlled by three registers :

- DDRx : is the data direction register, it allows to define the operation of each pin as input or output. For example, setting a DDRB bit =1 is equivalent to defining all B Port it as output.
- PORTx : is the data register, it gives access to the physical state, it can be read and written depending on whether the pin is set as input or output.

- PINx : is the port input pins, it is a read and write register that receives data from the pins.

Where "x" is the numbering letter of the port which can be between B and D for the ATMEGA328P. It should be specified, by using the ARDUINO IDE as a compiler, it is not necessary to write individually each of these registers.

Interrupts

The ATMEGA328P is provided with two (02) pins that accept interrupts, they are triggered by the INT0 and INT1 pins in port D by a falling or rising edges. Since there are not enough external interrupt pins, they will be connected to the most heavily used buttons in both modes, namely the *ENTER* button and the *EXIT* button. Although, due to the high sampling time, the buttons operating without the interrupt features will function correctly.

Analog to Digital Converter

The ATMEGA328P consists of six (06) A/DC inputs, these input are shared between the PORT C and PORT D. The analogue-to-digital converter is based on a successive approximations model, it performs a sampling of the pin input voltage, and thus, enables the conversion of the analogue voltage into a corresponding 10-bit digital value. The AREF pin set the reference voltage, with the highest being Vdd (5V), it is preferred to keep the maximum value, as the voltage that can be delivered by the battery cells and the sensors is quite close to 5V (4.4 V).

I2C Communication

Also referred to as TWI in the manufacturer's datasheet, this protocol allows multiple microcontrollers to be interconnected using bidirectional bus lines Serial Clock Line (SCL) and Serial Data Line (SDA), multiplexed into the PC5 and PD4 pins respectively. The only external hardware required to implement the bus is a single pull-up resistor for each of the TWI bus lines. This microcontroller allows up to 128 devices to be interconnected with the bus, each with an individual address [33]. the I2C Protocol is further explained in section 4.3.3.

Electrical Caracteristics

The Table 3.1 represents the electrical characteristics for the ATMEGA328P based on the manufacturer recommendations [33]:

Characteristics	**Symbols**	**Typical**	**Units**
Supply Voltage	V_{cc}	2.7 to 5.5	V
Supply current[1]	I_{cc}	5.2 to 14	mA
Voltage on $\overline{RESET}$	N/A	-0.5 to 13.0	V
Voltage on the other pins	N/A	-0.5 to $V_{cc} + 0.5$	V
Maximum output current per port	N/A	40.0	mA
Maximum input current per port	N/A	40.0	mA
Maximum supply current	N/A	400.0	mA
Maximum Power Consumption	N/A	2	W
Start up time	t_{out}	4.1	ms
Operating temperature	T_A	-55 to 125	$°C$

Table 3.1: Operating and performance characteristics for the ATMEGA328P device

Not considering these specifications in the design can severely damage the ATMEGA328P, decreasing its long-term reliability and in the worst cases leading to its failure.

3.1.2 Current sensor ACS712T - 5A

In general terms, The sensors generate a continuous sequence of analogue values when powered. The *ACS712ELCTR-05B-T* is a low cost and precise solution for both alternative and direct current sensing. The device consists of a precise, low-offset, linear Hall sensor circuit with a copper conduction path located near the surface of the die. Applied current flowing through this copper conduction path generates a magnetic field which is sensed by the integrated Hall IC and converted into a proportional voltage, even if this device can measure until 5A The thickness of the copper conductor allows survival of the device at up to 5 times overcurrent conditions [35]. The accuracy, which represents the maximum deviation of the actual output from its ideal value, for this device is about 1.5% which give us an accurate result.

The following table (Table 3.2) resume the principal characteristics for this devices:

[1] 16.0 MHz and 5.0 V

Characteristics	**Symbols**	**Typical**	**Units**
Supply Voltage	V_{cc}	5.0	V
Supply current	I_{cc}	10	mA
Power on time	T_{PO}	35	μs
Operating temperature	T_A	-40 to 85	$°C$
Sensitivity	S	100	mV/A
Output Error (for 25$°C$)	E_{tot}	$\mp$1.5	%

Table 3.2: Operating and performance characteristics for the ACS712 5A device

3.1.3 0.91' Oled Display

This display is a monochrome graphic display module, 128 × 32 pixels high-resolution display, with embedded controller, communicating via I2C interface [36]. Due to its capability in displaying, even in dark environment, small size and low power consumption, this device was preffered over the typical 16 × 2 LCD. Figure 3.4 shows the oled 0.91' display.

Figure 3.4: 0.91' Oled Display

It simplifies the use of the product by displaying different messages, symbols or logos, it requires few external components and is very easy to program.

3.1.4 Temperature sensor LM35

The LM35 temperature sensor is an integrated circuit capable of determining the ambient temperature with an output error of more or less 0.25°C, this accuracy makes it extremely popular. The Texas Instrument analog sensor is very inexpensive, reliable and easy to use, and is capable of measuring temperatures from -55$°C$ to 155$°C$ with a sensitivity of 10$mV/°C$ at a supply voltage of 4V up to 30V. Figure 3.5 shows the LM35 device.

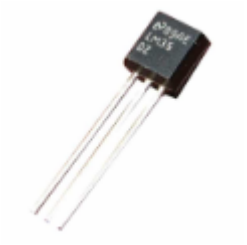

Figure 3.5: LM35 Temperature device [37]

3.1.5 Push Buttons

It represents a simple transient switch, offering a control possibility over the prototype. It is the main means of interaction between the user and the box. It allows the user to navigate the initialisation menu and display the battery information.

3.1.6 LM324N Operational Amplifier

These devices from Texas Instruments, consist of four independent high-gain operational amplifiers, specially designed to operate from a single supply over a wide voltage range. At least 1.5 V more positive V_{dd} than the input common mode voltage is required to obtain an accurate output [38]. Therfore, this device will be fed directly from the maximum voltage offered by the battery pack. This component will be used in a subtractor circuit to get the exact value of each cell. Figure 3.6 shows the LM324N component.

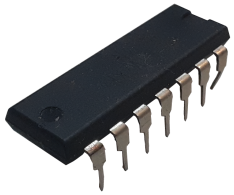

Figure 3.6: LM324N operational amplifier device

3.1.7 MOSFETs

The Metal-Oxide-Semiconductor-Field-Effect-Transistor (MOSFET), has three pins called: Source (S), Gate (G) and Drain (D). The voltage between the gate and the source (V_{GS}) determines whether or not a current flows between the drain and the source pin [39]. When choosing a MOSFET, it is important to take into consideration the losses due to the internal resistance of the MOSFET $R_{DS_{on}}$, for this reason some graphs in the datasheet are important mainly I_d (V_{DS}) which shows the relationship between the current flowing through the MOSFET and the voltage drop and I_d (V_{GS}) which shows the relationship between the gate voltage and the current flowing through the MOSFET [40], [41].

The two most common types of MOSFET are the N-channel MOSFET and the P-channel MOSFET, the main difference between the two is the voltage that V_{GS} must be subjected to in order to activate this component.

- *For the N-Channel,* a positive voltage must be applied (V_{GS} >0), the more positive the voltage V_{GS}, the more the current through the MOSFET increases, when discharging the IRF1405 has been chosen as the switch.

- *For the P-Channel,* the reverse is correct, a negative voltage must be applied (V_{GS} <0), the more negative the voltage V_{GS} the more the current through the MOSFET increases, for the charge application the IRF9610 was chosen as the switch.

3.2 Voltage Regulation

The power destribution and regulation is considered as the most important constraint to adress in embedded systems [42]. Three voltage levels are mainly present in the designed circuit, the first level is the input voltage, which is between *17 and 20* Volts (V_{input}), the second voltage level is of the various electronic components and microcontrollers used, which is 5V (V_{dd}), and finally, the last level is of the battery pack ($V_{battery}$), which has a variable value between 13.2 V and 17.2 V. The conversion from the V_{input} to $V_{battery}$ is achieved by the voltage drop between the drain and the source of the P-channel Mosfet

IRF9610 (V_{DS}) (Equation 3.1).

$$V_{battery} = V_{input} + V_{DS} \tag{3.1}$$

In order to achieve autonomy for the Bbox device, energy is taken directly from the installed battery, therefore it is essential to ensure perfect voltage regulation, with the additional challenge of a permanent variation of the input voltage ($V_{battery}$), this task is very tricky mainly due to the fact that the components used have to be powered in a fixed voltage range.

A voltage regulator is a circuit made up of different electronic components which allows the output voltage to be stabilised independently of the input voltage. This section groups together the different techniques considered to accomplish this task.

3.2.1 Zener Diode

The Zener regulator is the simplest to implement, it maintains a constant voltage at its terminals equal to its Zener voltage, despite variations in the input voltage.

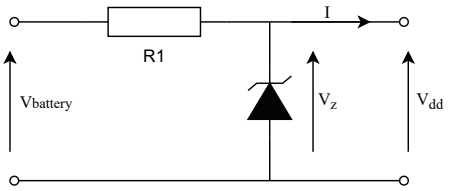

Figure 3.7: Zener based regulator

From Figure 3.7, it is clear that,

$$V_{dd} = V_z \tag{3.2}$$

By assuming that $\frac{dV_{battery}}{dt} = 0$, the I_s current is:

$$I_s = \frac{V_{battery} - V_{dd}}{R_1} \tag{3.3}$$

The Zener diode model *1N5231B* is an adequate diode tht could be implemented for this assembly, with a Zener voltage of 5.1 V and an Iz current of 20 mA. Unfortunately, the output voltage is dependant to the input one, also, this type of circuit causes significant voltage drops as the load current increases, since the current flowing through the zener diode modifies the output voltage significantly [39].

3.2.2 Serie Voltage Regulator

To keep a constant voltage at the output whatever the load, it is possible to add a transistor in series, if the output voltage tries to increase, this increase is applied to the base of the transistor through the Zener diode and the same thing for a voltage that tends to decrease. But this creates an additional voltage drop which is the Q1 transistor's voltage drop (V_{BE}). It is possible to integrate a current limitation in this regulator to increase the short-circuit protection. Figure 3.8 shows the scheme of a serie voltage diagram.

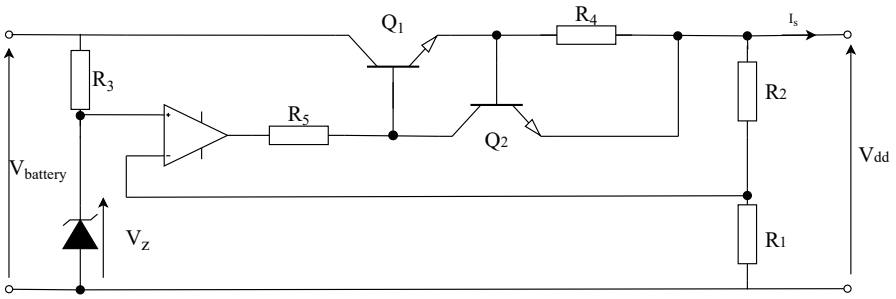

Figure 3.8: Serie voltage regulator scheme

The output voltage is to be calculated as follow:

$$V_{dd} = (\frac{R_1 + R_2}{R_1}) \times V_z \tag{3.4}$$

It is clear from equation 3.4, that the output voltage is totally independent from the input voltage. The maximal current flowing, can be calculated as given :

$$I_s = \frac{V_{BE}}{R_4} \tag{3.5}$$

Where, V_{BE} is the Q1 transistor's base-emitter voltage , and varies between 0.6 to 0.7 V. LM78xx series regulators is a fixed three terminal positive regulators. The 7805 regulator gives a voltage of 5V at its output, and a maximum output current of 1A [43]. All 78XX series regulators have an drop voltage of between 2 V and 3 V depending on the model. This implies an input voltage of at least 2 V to 3 V higher than the output voltage [39], therefore, this characteristic prohibits the use of this type of regulator in the design of an electronic circuit with one or two cells, since the minimum power supply offered by the battery is 3 V and 6 V respectively.

3.2.3 Buck Converter

Buck converters converts a higher input voltage into a stabilized lower output voltage, it can reach an efficiency of 97 % [44], which is very interesting. In an other hands, for this regulator, it is necessary to properly implement the controller, which is very difficult to parameterise. Incorrect control can lead to interference, radio frequency interference and harmonics which can affect the proper functioning of the electronic components or seriously reduce their service life. A simplified circuit diagram is shown in Figure 3.9.

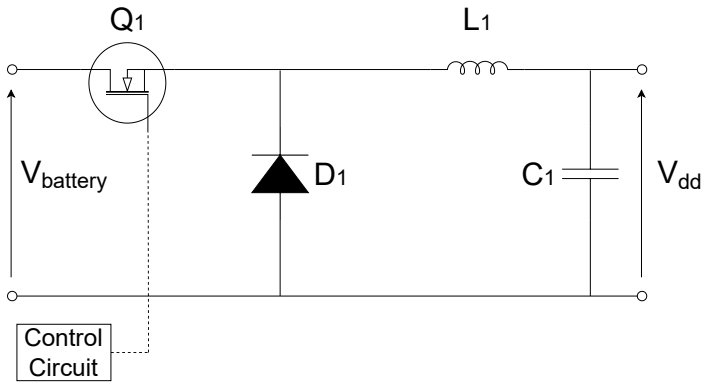

Figure 3.9: Buck converter scheme

The RECOM R-78xx series is a pin-compatible alternative to the linear 78xx series, discussed in the previous section (Section 3.2.2). The R-78xx is a complete buck regulator module that does not require any external components for normal operation. The input voltages can reach up to 72 V and quiescent consumption of 20 nA. One disadvantage of

a buck converter is that the PWM regulator feedback circuit requires a minimum output ripple to regulate properly, as the regulation is typically cycle-by-cycle [44].

3.2.4 LM317 Integrated Regulator

The LM317 is an adjustable 3–terminal positive voltage regulator capable of supplying in excess of 1.5 A over an output voltage range of 1.2 V to 37 V. This voltage regulator is exceptionally easy to use and requires only two external resistors to set the output voltage. Further, it employs internal current limiting, thermal shutdown and safe area compensation, making it essentially blow–out proof [45].

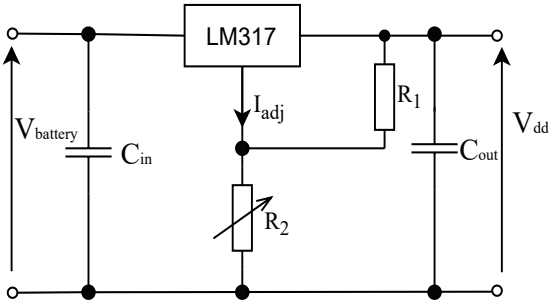

Figure 3.10: LM317 regulator scheme

The Output voltage is given as equation 3.6.

$$V_{out} = V_{ref} \times (1 + \frac{R_2}{R1}) + R_2 \times I_{adj} \tag{3.6}$$

V_{ref} is equal to 1.25 V, I_{adj} is the current in the middle pin and is about 50 μA, this low value of the current makes the second term insignificant compared to the first, thus, it is common to use for a first analysis the following expression [39]:

$$V_{out} = 1.25 \times (1 + \frac{R_2}{R_1}) \tag{3.7}$$

To obtain an output voltage value equal to 5 Volts, it is necessary to define the values of R1 and R2 as follows:

$$V_{out} = 1.25 \times (1 + \frac{660}{220}) = 5V \tag{3.8}$$

As *Bbox version 0.3.2* is designed to be used with 4 batteries connected in series, an LM7805 voltage regulator is applied directly as it is less space consuming. But it is important to note that for earlier versions, notably *version 0.3.0* of the *Bbox*, which was designed to be used with two batteries, the LM7805 was inadequate and the LM317 was chosen instead.

3.3 Power Consumption and Overall Efficiency

3.3.1 Battery Dimensioning

The total storable power offered by this model varies according to the capacity of the installed cells. It is clear that the use of 4 lithium cells of 2200 mAh, gives the system a battery capacity of 8800 mAh which is sufficient in the majority of small robots application, it should be noted that it is also possible to implement the 5500 mAh cell, giving the product developed great flexibility by offering the possibility of choosing the battery capacity to users. The maximum current that can be delivered is 2 A, and therefore allows to offer a power up to 32 W, which is sufficient to power the electronics of the robot, beyond this value and in order to offer an optimal safety to the battery, a shutdown protocol will stop the discharge of the battery. As for the charging process, the maximum current supplied by an external source is currently 0.5 A, in order to have a good protection when charging the batteries. With such a current, the charging process is slow, in fact it will take 8h and a half to reach the 80 % SOC advised for 4 $\times$ 2200 mAh batteries.

3.3.2 Bbox Power Consumption

The available components of the embedded systems (microcontrollers, sensors, mosfets...) require a specific electrical energy for their proper functioning and to prevent undesirable behaviour (POR, false measurements, wrong activation voltage...), this quantity of energy used is often called *consumed energy* and represents a decisive factor as well as the most important of the constraints [46]. The total power consumption of this device is calculated

by substituting the batteries with a power supply and then measuring the supply voltage $V_{battery}$ and the current $I_{battery}$, by applying the standard equation $P = V_{battery} \cdot I_{battery}$ it is possible to obtain the power consumed by the device. It should be noted that no charging or discharging was allowed during the tests.

The Bbox V0.3.2 electronics consume in average 1.15 W, giving it an efficiency of 96.15 %. Taking the same 4 × 2200 mAh reference, this device allows the battery to be monitored for a period of 88 *hours* or the equivalent of *3 days and 15 hours* continuously, after which the battery reaches 30 % of its capacity and no further discharge is allowed.

When charging the battery, and because a constant charging power is set, the Mosfet IRF9610 causes a constant power loss of 0.52 W, with a power delivery of 8,60 W. Thus, the charging process has an efficiency of 94 %. Taking into account both of the losses in the charging process and the components consumption, the total efficiency of the prototype reaches a value of 90.38 %.

3.3.3 Robot Power Consumption

While discharging the battery, as the regulation of the voltage supplied to the robot is left to the user and is done with a variable current, it is difficult to define with precision the general efficiency of this device. However, a relationship is defined between the current consumed by the robot $I_{battery}$ and the efficiency of the discharge process, this relation is shown in Figure 3.11. Thus, the maximal value of 2.5 %, will be considered for the discharge efficiency. In addition, by considering the components consumption, the efficiency reaches a value of 93.60 %.

3.3.4 Product Efficiency

The overall product efficiency is defined as the average efficiency between the component consumption efficiency, the charging process efficiency and the discharging process efficiency, respectively 96.15 %, 90.38 % and 93.60 %. The overall efficiency of the Bbox V0.3.2 prototype is therefore 94.38 %.

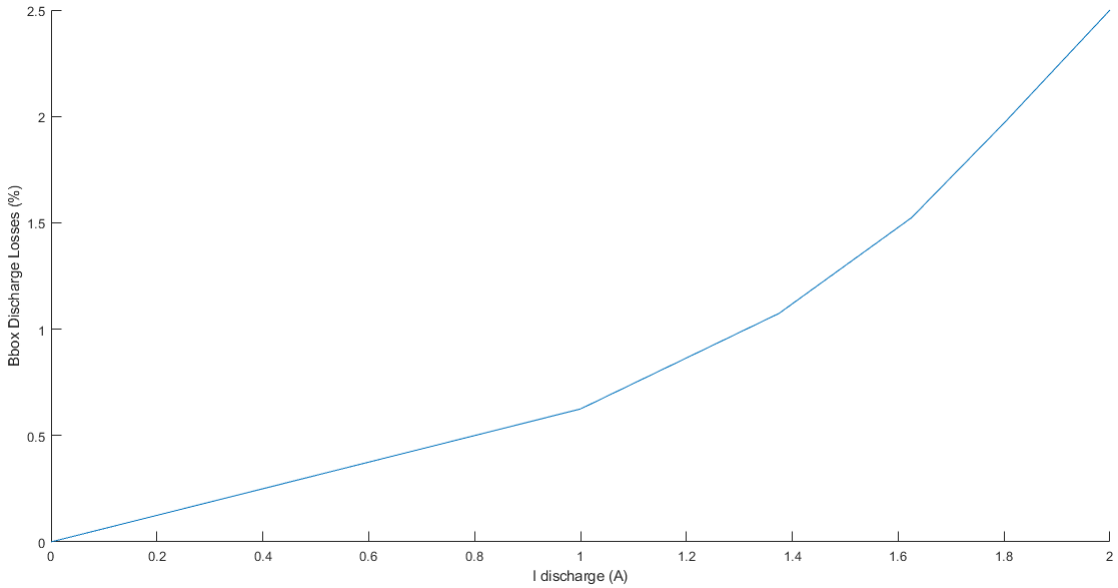

Figure 3.11: Bbox discharge characteristics

3.4 Cell balancing

Balancing is often referred as levelling the open circuit voltages of all cells. As this voltage is related to the SOC, it is a quick way to standardise the SOC so that all cells are placed in similar conditions, where their operating parameters are close. There are different techniques for achieving this, one called passive, where the excess energy is dissipated in resistors, and the other called active, where the energy is transferred between the cells. For this prototype, using a dissipative method would greatly decrease its efficiency, thus it was decided to use a circuit based on the S8254A, which is more of a cell protection than a balancer. Indeed, when charging the cells, if one of them reaches the SOC of 80 %, the cell will be disconnected and will not be charged anymore. When discharging, the cells will not be balanced, and when a cell reaches 30 % SOC, all cells will be deactivated.

3.5 Financial Study

This study offers an evaluation of the overall cost of the project. It takes into account the cost of purchasing the various electronic components, without taking into account

the cost of delivery. A good financial evaluation allows to know if the project is feasible and marketable, in addition, it can be presented to potential investors, who will bring additional capital, for the launching of an industrial production of the prototype. The table 3.3 summarises the cost of the different components used.

Components	Unity Cost (€/Unit)	Qty (Units)	Price (€)	Compo-nents	Unity Cost (€/Unit)	Qty (Units)	Price (€)
Electrolytic Capacitor	0.05	5	0,25	ACS712	1,92	1	1,92
Ceramic Capacitors	0,02	8	0,16	Resistors	0,02	27	0,54
PCB Manufacturing	2,80	1	2,80	IRF1405	2,12	1	2,12
ATMEGA328P	2,08	3	6,24	IRF9610	1,35	1	1,35
Push Buttons	0,15	4	0,60	LM324N	0,45	1	0,45
BC547C NPN	0,22	1	0,22	Crystal	0,19	3	0,57
Oled display	2,40	1	2,40	S8254A	4,23	1	4,23
Cell Holder	3,33	2	6,66	LM35	1,70	1	1,70
Total (€)							32,21

Table 3.3: Electronic components costs

The overall bill for electronic components is estimated to be 32.21 €, taking reference prices from Digikey.pt and Bot'n'roll.pt, this price is quite reasonable compared to the one proposed by similar products, that are less accurate, the prices of the products presented in section 2.3 are not available. It is important to note that the price presented corresponds for one single prototype; manufacturing a product on an industrial scale generally divides the price by 10.

3.6 Software and Programming Tools

Two software packages are mainly used for this project. MATLAB, where the algorithm was first developed and then applied to collect the information and record it in order to plot it as figures, and ARDUINO IDE to write and compile the algorithm via an Arduino board.

3.6.1 MATLAB

MATLAB is a powerful language that integrates computation, visualization, and an advanced programming environment. In addition, it is a modern programming language environment: it has sophisticated data structures, contains built-in editing and debugging tools, and supports object-oriented programming. These factors make MATLAB an excellent tool for teaching and research purposes [47].

3.6.2 ARDUINO IDE

The Arduino IDE is an open source software for Arduino, which uses an abbreviation of the C/C++ language, with many libraries already implemented or that can be implemented, it allows easy writing of codes and implementation [48]. This software can be used in any Arduino board, all that is required is to burn the algorithm and then remove the ATMEGA328P.

3.6.3 Schematic and PCB Design Software

Various software packages provide the possibility of designing electronic circuits, such as Fritzing, ISIS Proteuse, EASY EDA or Eagle, all of which have a large library containing hundreds or thousands of components. It is possible to make the equivalent circuit first, simulate it according to the software, and then make a PCB equivalent to the made circuit. Making a schematic is very useful because it allows you to detect possible problems in the design and to think more clearly about other alternatives. As the project progressed, a schematic was developed to meet the requirements of our project.

3.7 Conclusion

Each electronic component, when mounted in this electrical circuit, according to a defined installation principle, performs a specific function. The master microcontroller, which is the central element of the system, is one of the most important, but it depends on all the other components, meaning that if one of them fails, the whole system is at risk. Therefore, it is important to follow the instructions provided by the manufacturer for each of these components, which are summarised in this chapter.

Knowing the different characteristics of these electronic components allows, on the one hand, to know the voltage and current thresholds that it can support, but also essentially its consumption in terms of power, in fact knowing the overall consumption of the product is an important aspect when designing a prototype that should not be neglected, and allows to improve it later, for future versions, in order to achieve in terms a product with the lowest possible energy consumption. The Bbox V0.3.2 prototype can deliver a maximum of 32 watts at any given time and protects the battery from deep discharges or excessive energy demands from the robot, which then triggers a shutdown protocol. For this prototype, charging is done at a current of 0.5 A, which protects the battery but results in a slow charge rate.

The financial study determined a design price of 32 €, which is currently a very good price compared to similar products that cost 30 to 150 €. It is important to note that the 5 € boards commercialized do not represent a full BMS, but only overcharge protection, and do not provide SOC monitoring or discharge protection.

Chapter 4

State Determination

In order to design a BMS capable of predicting the SOC of a mobile robot's battery from an EKF, it is first necessary to establish a study on the possibility of implementing such an algorithm for estimating the SOC of a lithium battery in an ATMEGA328P microcontroller, which is one of the most widely used microcontrollers on small autonomous robots. The need for this study is due to the fact that no other study of this type has been reported, at the time this thesis was written, in the scientific literature. Therefore, this chapter first discusses the importance of manually determining the battery parameters (R_t, R_p and C_p), thus giving the EKF all the cards at its disposal to allow for optimal tracking. Secondly, the new approach of using a Dual Coulomb Counting Extended Kalman Filter, abbreviated by the authors as DCC-EKF, is described. This approach, according to the authors' knowledge and research, has also never been reported in the literature.

4.1 Cell Parameter Extraction

In order to enable optimal monitoring of the SOC by Bbox, it is essential to first identify the parameters of the equivalent first-order model described in section 2.2.2. These tests were performed on a Lithium 18650 battery to allow a quick and efficient comparison. The battery has a nominal capacity of 3040 mAh and a nominal voltage of 4.4 V.

4.1.1 Experimental Data Collect

The experimental data are obtained by performing at a room temperature a set of constant current discharge pulse of 1.6 A for 180 seconds, followed by a long resting period of 3600 seconds on a fully charged Lithium cell, the sampling time of the cell voltage and current is set at every seconds. This pulse curves help to provide a high-fidelity representation of the cell performance at multiple states of charge values [49]. The test results are shown in Figure 4.1.

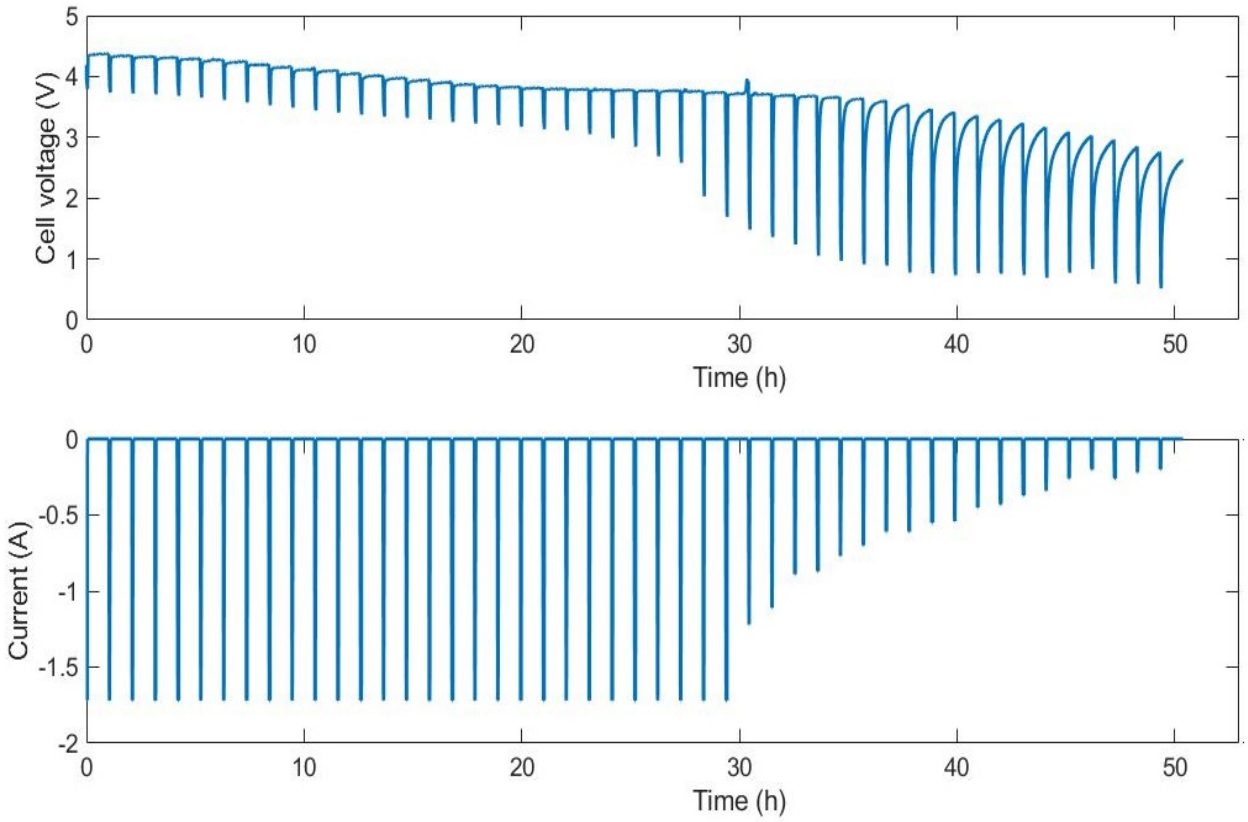

Figure 4.1: Voltage and Current for a constant current pulse discharge

This test also provides the relationship between OCV and SOC. In fact, the relationship that can be found in the manufacturers' datasheets is inaccurate, with a limited number of points and offers no useful information. Figure 4.2 shows a comparison of the acquired relationship between the SOC and the OCV, and a 7^{th} order polynomial approximation.

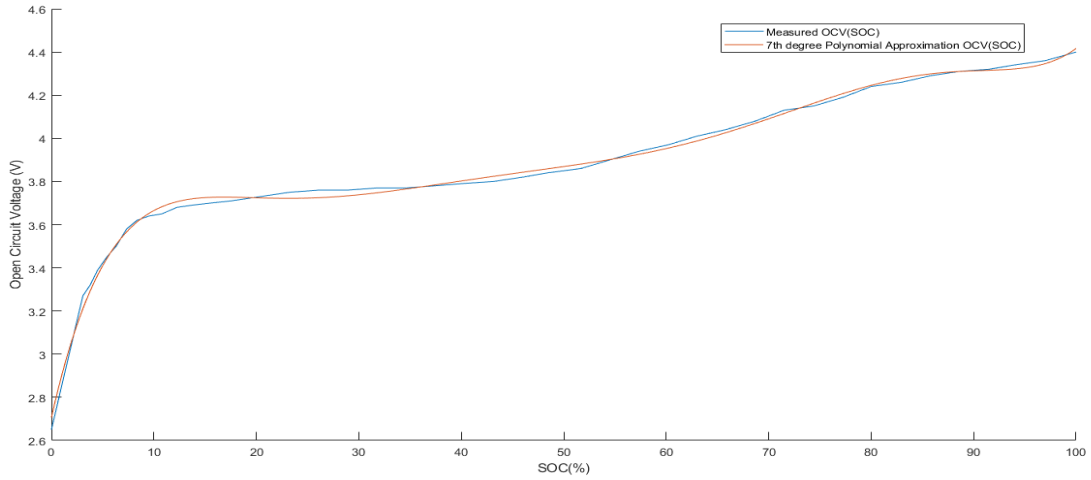

Figure 4.2: Open circuit voltage and State of Charge relation, for comparison between measured data and 7^{th} order polynomial approximation

The equation 2.8, expressed in the chapter 2, highlighting the relationship between OCV and SOC, can also be expressed as a 7^{th} order polynomial expression. This expression fits the global curve and is given as follows:

$$V_{oc}(SOC) = 3.4624e^{-12} \cdot SOC^7 - 1.3014e^{-9} \cdot SOC^6 + 1.9811e^{-7} \cdot SOC^5 - 1.5726e^{-5} \cdot SOC^4 + 6.9733e^{-4} \cdot SOC^3 - 0.017 \cdot SOC^2 + 0.21 \cdot SOC + 2.7066 \quad (4.1)$$

4.1.2 Parameter Estimation Technique

MATLAB offers a good tool to achieve the cell identification and estimation task, the Simulink design optimization, using optimization techniques to estimate model parameters, that computes and minimizes the error between the simulated and measured output can be used to achieve this task. To determine these parameters, a simulation of the previous real test was performed on a 1RC cell model in Simulink/MATLAB and run in a Least Squares curve-fitting algorithm, to solve for the optimal parameter settings, where each circuit elements (R_t, R_p and C_p) were represented by lookup tables [49].

Simulating the model for all the measurements acquired in 50 hours would take a

considerable amount of time and increase memory consumption, with the consequent risk of a non-convergent simulation result, thus, an overlapping technique was used, which consisted of breaking the resulting data into several pieces, taking care to include sufficient data and to overlap with the previous piece [49]. This method allows to reduce the problematic into something much smaller and simpler, than using the complete discharge data set. All the measured data are summarized in a tabular form, in Appendix A. The table 4.1 highlights the parameter data summarised for 10 separate points.

SOC	OCV (V)	a	b	R_0 (Ω)	R_p (Ω)	C_p (F)
1.000	4.40	0.800	3.60	0.4686	0.0968	715.600
0.800	4.24	0.800	3.60	0.4920	0.1138	1149.160
0.627	4.00	1.353	3.16	0.4614	0.1010	2718.350
0.517	3.86	1.320	3.17	0.4614	0.1010	604.480
0.431	3.80	0.700	3.50	0.4161	0.3922	283.736
0.346	3.77	0.350	3.64	0.4161	0.3922	563.120
0.232	3.75	0.176	3.71	0.4161	0.3922	19.550
0.122	3.68	0.636	3.60	4.2549	6.3909	85.600
0.037	3.27	4.260	3.16	4.9024	7.6956	91.623

Table 4.1: Summary of the result obtained by applying a Least Square curve-fitting algorithm

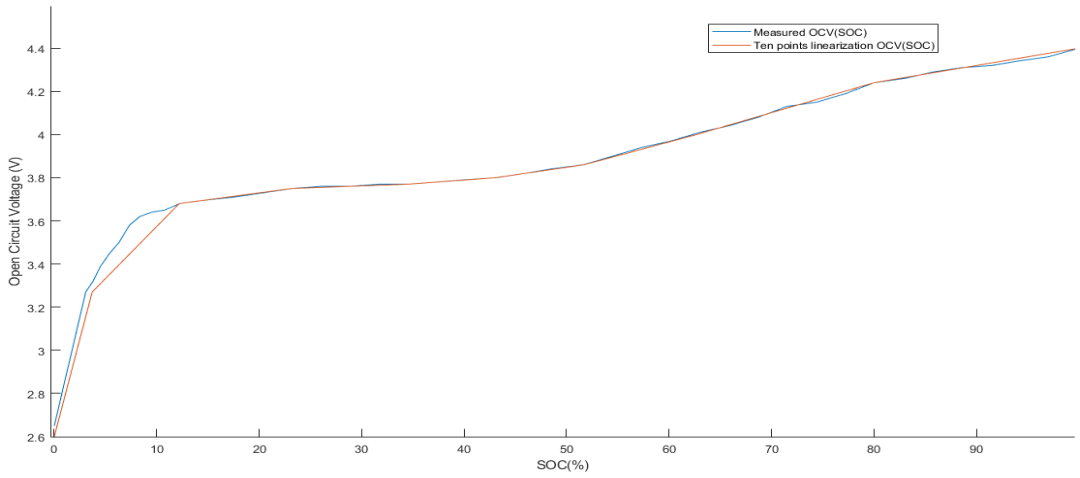

Figure 4.3: Open circuit voltage and state of charge relation, for comparison between measured data and 10 points linearization

Nevertheless, to achieve a low sampling time for the prediction algorithm implemented in each slave ATMEGA328P microcontroller, it is essential to limit the computing power, thus, the linearization of these curves is done in only 10 points. These 10 points are shown in the previous Table and in Figure 4.3 where the a 10-point linearisation approximation and a comparison of the acquired relationship between the SOC and the OCV are highlighted.

4.1.3 Parameter Estimation Circuit

The Voltage and Current flowing through the battery are the two parameters needed to extract the behaviour of the battery cell, these parameters are gathered through out an Arduino Uno board, following the electronic circuit shown in Figures 4.4 and 4.5.

The circuit applied to extract these parameters is composed of different electronic components. A 16x2 LCD is connected to the microcontroller via the digital pins (PORT4 to PORT9), this LCD is used to display the voltage, current and SOC at the exact time "t". Current and voltage are collected through ports A0 and A3 respectively from two LM358P DUAL-Amplifiers (U2:A and U1:A). The IRF1405 Mosfet (Q1) keeps the voltage across the resistor and thus the current constant, and is controlled by a comparator (U1:B), which compares the current resistor voltage with another reference voltage, the reference voltage is set manually by the user. Because the Mosfet is switched at its maximum, capacitors and resistors (R0, C1, C2 & C3) are added to limit the interferences [43][39]. This circuit makes it possible to keep the current drawn by the battery constant without any external human intervention, regardless of the gradual voltage drop seen in Figures 4.2 and 4.3, as the SOC decreases. The collected data are sent directly to the computer via an USB connection and are grouped by MATLAB.

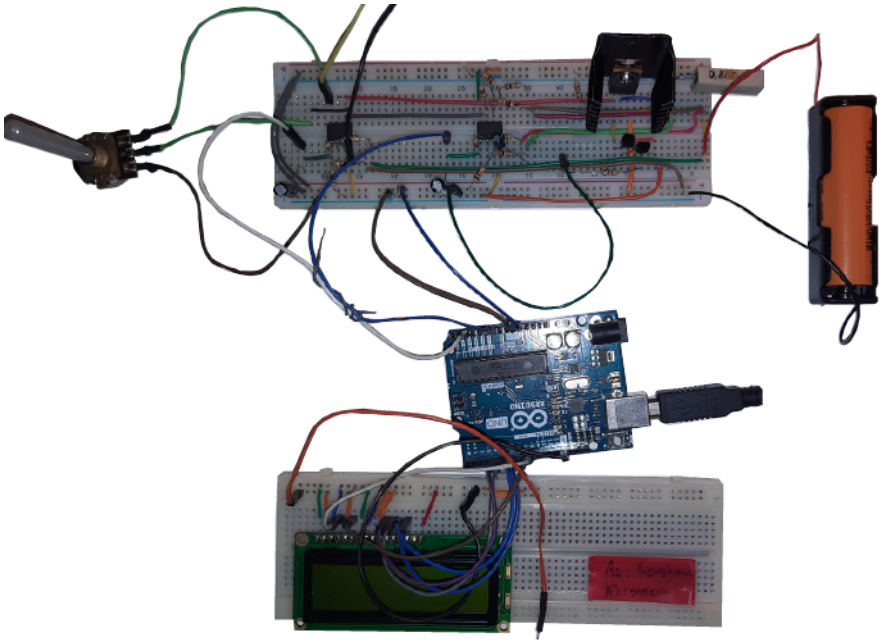

Figure 4.4: Electronic circuit for current and voltage measurements

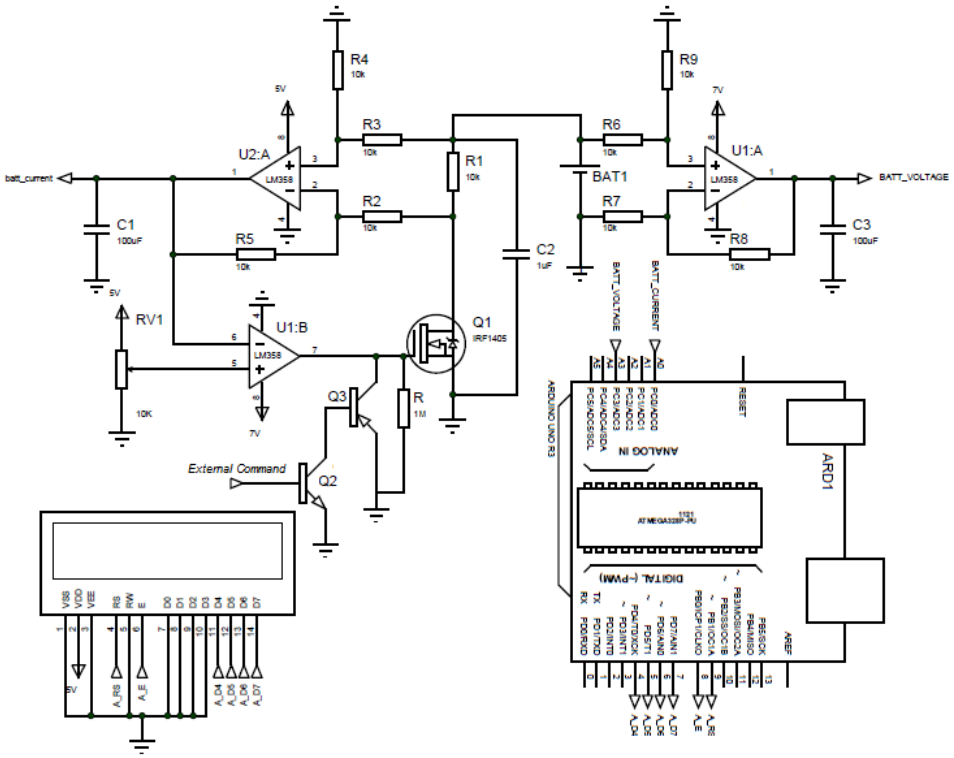

Figure 4.5: Schematic diagram of the electronic circuit for current and voltage measurements

4.2 Proposed Algorithm

The algorithm is written in such a way as to allow calculation with the smallest possible time interval in order to have the most accurate and fast results. In version 0.3.2 of Bbox, the master microcontroller monitors the SOC, and takes appropriate action to avoid damaging the battery. This system is mainly characterised by two modes, the *initialization mode* and the *on-mode*, both of which are highly dependent on each other and can be switched between modes at any time using a single button. This section summarises the algorithms used and gives a more in-depth explanation of the DCC-EKF approach.

4.2.1 Extended Kalman Filter Algorithm

It is well known that the Kalman filter, in general, provides an optimal estimate for linear system with not directly measurable states. However, in the case of nonlinear systems such as batteries, the equation 2.16 can not provide an accurate estimation of the states of the battery (SOC and V_p), in this case, the Extended Kalman Filter (EKF) is used to include the non-linear behaviour and to determine the states of the system [8], [14], the EKF equation have the following form:

$$\begin{cases} x_{k+1} &= f(x_k, uk) &+ \omega_k \\ y_k &= h(x_k, uk) &+ \upsilon_k \end{cases} \tag{4.2}$$

Where, the matrices A_k and C_k from equation 2.16 are redefined as:

$$A_k = \frac{\partial f(x_k, u_k)}{\partial x_k}, \quad C_k = \frac{\partial h(x_k, u_k)}{\partial x_k} \tag{4.3}$$

Equations 4.3 are refered as Jacobian matrices. Taking these variations into account, the algorithm of the EKF works analogously to the KF described in Section 2.2.3 and is summarized in Figure 4.6.

The algorithm is written in a way that allows calculation with the smallest possible

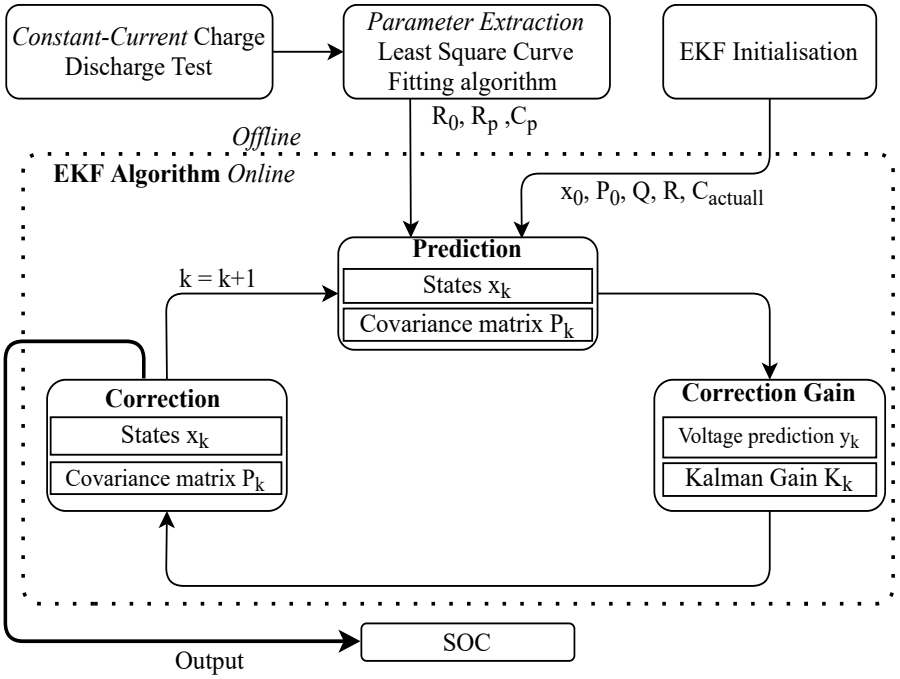

Figure 4.6: Flow chart of the EKF algorithm implemented in the Arduino

time interval in order to have the most accurate result, the sampling time is set at rate of 0.04 seconds. In addition to Figure 4.6, the working principal of the KF Algorithm implemented in each ATMEGA328P slaves microcontroller is shown in Algorithm 1.

4.2.2 Coulomb Counting Algorithm

The Coulomb counting method involves measuring and integrating the current flowing into and out of the battery over a specific time period. Although this method is one of the most widely used methods for monitoring the condition of batteries, as discussed in section 2.2.3, it has several drawbacks that lead to errors. In the case where this method is applied alone, it is strongly recommended to start the calculation from a fully charged or discharged battery so that the state of charge is known (1 or 0). However, as it is defined for the system to have a high flexibility of use, and to offer the possibility to start the SOC monitoring at any time, the EKF algorithm is integrated in the ATMEGA328P for an on-the-fly prediction.

Algorithm 1: Extended Kalman Filter Function

initialise $A_0, B_0, C_0, D_0, P_0, I_0, x_0, Q$ *and* R ;
while *EKF Called* **do**
  I_k measurements;
  V_{t_k} measurements;
  $\hat{x_k} = A_{k-1} \,.\, x_{k-1} + B_{k-1} \,.\, I_{k-1}$;
  $\hat{P_k} = A_{k-1} \,.\, P_{k-1} \,.\, A_{k-1}^t + Q$;
  $\hat{P_k}$ *not diagonal* $= 0$;
  if $S\hat{O}C_k \in$*[SOC interval]* **then**
    R_t, R_p and C_p updated;
  end
  $C_k = Voc(S\hat{O}C_k) + \hat{V}_{P_k}$;
  $D_k = R_t$;
  $\hat{V}_{t_k} = C_k + D_k \cdot I_k$;
  $L = C_k \cdot \hat{P}_k \cdot C_k^t + R$;
  if $L \neq 0$ **then**
    $K_k = \hat{P}_k \cdot C_k^t \,/\, L$;
  end
  $x_k = \hat{x_k} + K_k \cdot (V_{t_k} - \hat{V}_{t_k})$;
  $P_k = (I - K_k \cdot C_k) \cdot \hat{P}_k$;
  P_k *not diagonal* $= 0$;
  $k = k + 1$;
  Result: Send x_k
end

For the CC algorithm, it is noted that the sampling time is critical and should be kept as low as possible in order to achieve the most accurate result, making applications where the current varies rapidly inadvisable with this method. The evolution of the state of charge for this method, can be described by the following expression:

$$SOC(t_n) = SOC(t_{n-1}) + \frac{n_f}{C_{actual}} \int_{t_n}^{t_{n-1}} i \cdot dt \tag{4.4}$$

$$with \quad \begin{cases} n_f = 0.9 \quad for \quad i > 0 \\ n_f = 1 \quad for \quad i < 0 \end{cases}$$

4.3 Operating Principle

The algorithm of this system consists mainly of two modes, the *initialisation mode* and the *on-mode*, both of which are highly dependent on each other. The use of an *initialisation mode* may seem strange at first sight for this type of product, but it is important to remember that the characteristics between cells are not uniform, neglecting this aspect can significantly reduce accuracy, therefore to allow flexibility of operation the *initialisation mode* is important. It is possible to switch from one mode to the other at any time by pressing a button. In the following section a closer look will be took at each mode, mainly indicating the principle of operation of each, the relationship between them and their advantages.

4.3.1 Initialisation Mode

Because the characteristics between the batteries are not uniform, and can vary greatly, and in order to achieve high accuracy of SOC prediction, the *initialization mode* is introduced into the system, it is possible to skip this mode and ignore it, but at the cost of reduced accuracy.

This mode is activated by default when the board is switched on, or after pressing the *exit* button when the program is in the *on-mode*. As the name suggests, this part of the algorithm is responsible for the initialization of the main variable that governs the mode, namely the battery capacity. As for the battery parameters (R_t, R_p and C_p), despite their importance during active use of the cell, the effect of a bad initialization of these parameters can be neglected when the cell is at rest or when a low current (in our case 70 mA) is flowing through it, this aspect is proven in chapter 5.

In addition, it is possible to activate some specific functionalities of this board, mainly, The state of charge Prediction through the Extended Kalman Filter Algorithm and using the DCC-EKF approach, the activation of deep discharge protection, and the state of health. It is also possible, if the SOC is known, to introduce the value manually to ensure a more accurate result. This mode takes the form of a Menu, it is possible to navigate,

with the help of four buttons, between the different sections and sub-sections as it is shown in the (a) flowchart of Figure 4.7.

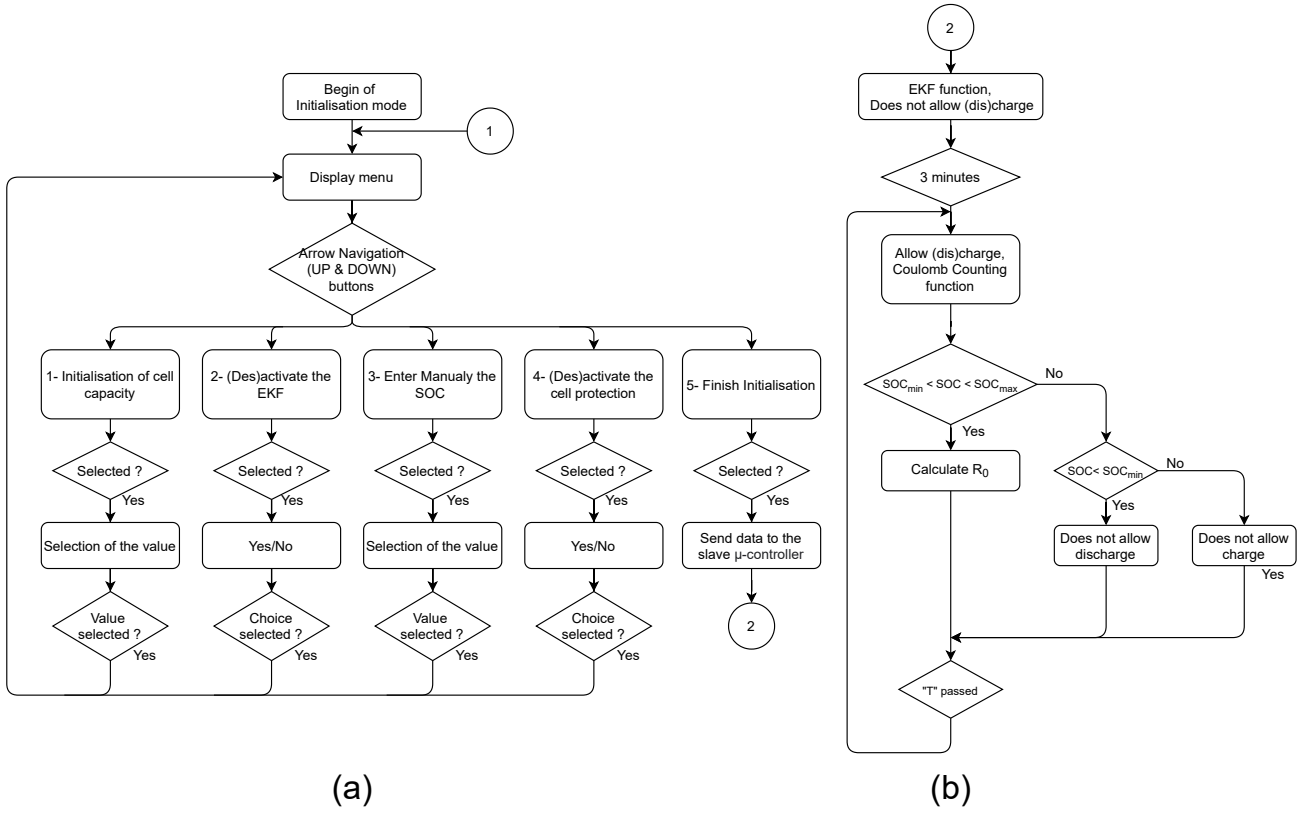

Figure 4.7: Flow chart of the system algorithm. (a) Initialisation mode flow chart. (b) On-mode flow chart with EKF algorithm activated.

4.3.2 On Mode

According to what was initialized, the Battery Management System begins by carrying out the assigned tasks for each battery cell.

- If the EKF prediction was set on during the initialization mode, the device shall begin the prediction of the actual SOC value for each cell, and prohibits the passage of current to the robot for a period of approximately 3 minutes, the BMS electronics are still powered with a 70 mA current. The equivalent flowchart is shown in the (b) flowchart of Figure 4.7.

- If the EKF prediction was set off during the initialization mode, and an SOC Value was introduced, the device permit the current to flow directly, and start the SOC monitoring according to the chosen value using the couloçb counting function only.
- If the Protection was set off, the battery will be discharged and charged even deeper, taking the risk of shorten the life span of the batteries.

4.3.3 I2C Communication Protocol

The Inter-Integrated Circuit (I2C) is a bus interface connection incorporated into many devices such as sensors, RTC, and EEPROM. It is also referred to as IIC, I^2C or TWI in many technical literature . I2C is ideal for attaching low-speed peripherals to a motherboard or embedded system over a short distance, it provides a connection-oriented communication with acknowledge [32]. Figure 4.8 shows the interconnection principal.

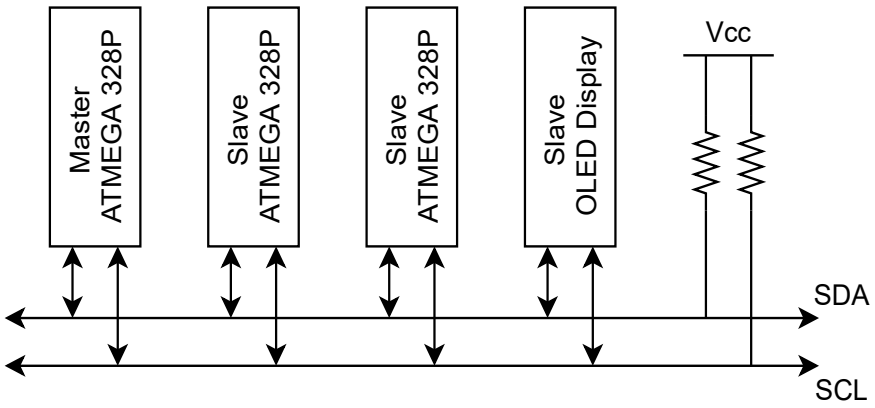

Figure 4.8: I2C bus connection principle

I2C devices use only two (02) pins for data transfer, called SCL, which synchronize the data transfer between two chips, and SDA, each data to be transmitted must be framed in a 9 bit long packet, the first 8 bits are data while the 9th bit is the acknowledgement. This reduction of communication pins reduces the package size and the power consumption drastically (30 μW) [33], making it ideal for many applications in which space is a major concern. Only a 4.7 kΩ pull-up resistor is needed for each of bus lines. Each device can operate as either a master or a slave. The master is a device that generates the clock

to which the other devices obey, as well as initiating and terminating any transmission. The slave is the device that receives the clock. Both the master and the slave can receive or transmit data. Therefore, there are four modes of operation: **Master transmitter**, **Master receiver**, **Slave transmitter** and **Slave receiver**.

The battery states are determined for each cell independently of the others by a specific microcontroller assigned to it, and works with the principle of Master/Slave communication by the means of I^2C. One microcontroller defined as a Master regroup the information and characteristic gathered from each other slaves microcontroller, analyses them and takes the main precautions to avoid any deep charge or discharge of the batteries, In order to keep a low sampling time, one slave microcontroller is assigned to two batteries, reaching a sampling time of the implemented algorithm of 0.085 seconds.

Master to Slave Communication

Designated as data 1 in Figure 3.1, this exchange occurs mainly during the transition from initialization mode to on-mode, where the initialization parameters are sent to the slave microcontrollers, in order to be updated. The parameters sent take the form of a successive signal bus and are shown in Figure 4.9.

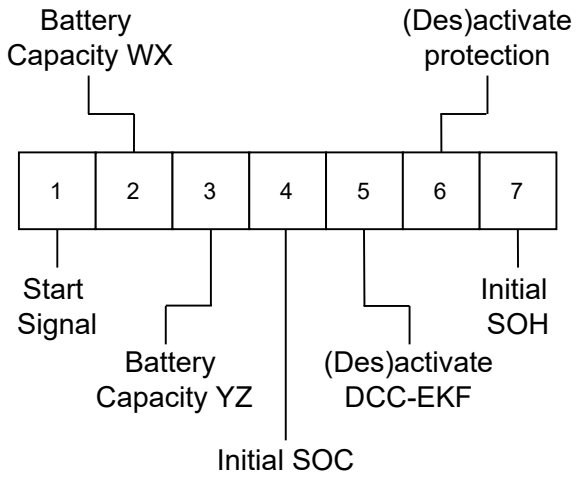

Figure 4.9: Master to slave microcontrollers bus signal

The bus signal begins with a start signal, equivalent to a value of 255, this start signal is implemented to ensure that the slave microcontroller receives the values in the correct

order and that these values do not get mixed up. It is followed by sending the battery capacity ($C = WXYZ\ mAh$) in two packet. Then, by sending the initial SOC value, the activation or deactivation of the DCC-EKF approach as well as the battery protection. And Finally with the initial SOH value.

Slave to Master Communication

Designated as data 2 in Figure 3.1, This communication is done during the on-mode. Figure 4.10 is a representation of the parameters continuously sent.

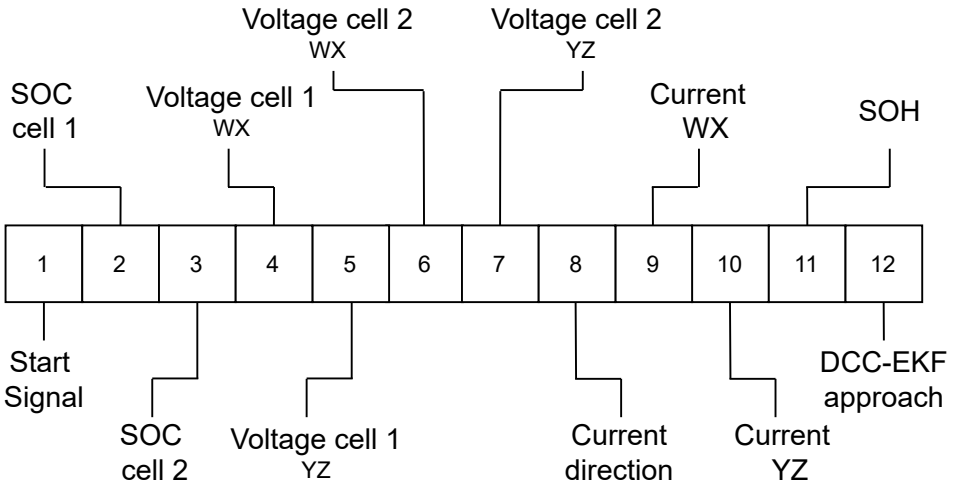

Figure 4.10: Slave to master microcontroller bus signal

As in the case of communication in the reverse direction, a start signal is also used and has the same value of 255. This is followed by sending the calculated state of charge values for the first cell and the second cell in two different packets. Next, the voltage values are sent for each cell in two packets (packet 4, packet 5 and packet 6, packet 7), with the voltage taking the form of $V = W.XYZ\ V$. Then the direction of the current (charge or discharge) is sent, where $Current\ direction = 10$ means discharge, and $Current\ direction = 254$ means charge. Then the current value is sent in two packet (packet 9 and packet 10) with $Current = W.XYZ\ A$. And finally in the last two packets the state of health value is sent and the slave microcontroller confirms the use or not of the DCC-EKF approach.

4.4 Conclusion

In order for the EKF to accurately track the SOC of each cell independently, it is essential that it has knowledge of the equivalent electrical parameters of each cell. Indeed, using an EKF alone in the battery domain is unthinkable, as the equivalent parameters evolve over time, and it is therefore necessary to update them after a certain period of time, otherwise the EKF may make a mistake in its prediction and reach an error of 20%, this aspect is discussed in the next chapter. Therefore, it is essential to link it with another algorithm.

For this purpose, two main types of methodology are applied for the prediction of the parameters, the so-called offline method, which extracts the parameters following a constant current discharge test of a few seconds followed by a period of rest of the cell, such as explained in section 4.1, and the so-called online methods, which allow an on-the-fly estimation, by applying algorithms such as the double extended Kalman filter or an online parameter estimator. Unfortunately, the application of an online technique will further reduce the sampling time, resulting in a divergence for the parameter predicted by the algorithm and a decrease in the accuracy for the implemented EKF. In the case of the offline technique, this is achievable but after some period of operation of the cells, it will be necessary for the users to perform this time-consuming test, and will lose the flexibility aspect intended for this product.

The proposed DCC-EKF approach, takes advantage of the EKF's ability to predict quickly and accurately when the cell is at rest or has a small current flowing through it. Unlike the OCV, which requires a fully rested battery and 1 hour to obtain an accurate result, the EKF allows the SOC to be determined within 3 minutes with an accuracy of 5% even with a low current flowing through the battery and a non-accurate setting of R_p C_p and R_t.

Chapter 5

Results and Discussion

Implementation and realisation is the most important phase of project design. This phase consists of the concretisation of the conceptual model created and allows a confirmation of the model on the one hand, but also to find different issues that have not been detected.

Also, this chapter offers a validatation of the proposed approach. Validation is the process that consists in checking if the designed model is appropriate or not for the defined objective, often validation and design are considered as two totally independent activities, while they should be intertwined and implemented during the different phases of the project development [46]. In the following chapter, it will be presented the different results acquired for the EKF algorithm, as well as the different schematics and pictures of the Bbox prototype.

5.1 Simulation Results

Simulation is a very common technique for evaluating and validating approaches and allows for rapid prototyping [46]; these simulations are based on models that are approximations of reality. MATLAB is a modeling and simulation tool based on mathematical models, including matrices, partial differential equations, and provided with various tools and libraries. In this thesis, the simulation is considered as an aid to find flaws in the proposed algorithms and not as a validation of the prototype.

5.1.1 Simulink Battery Model

The graphical representation of MATLAB/Simulink using graphical blocks to represent mathematical and logical constructs and process flow is intuitive and provides a clear focus on control and observation functions. Although Simulink has been the tool of choice for much of the control industry for many years [50], it is best to use Simulink only for modelling battery behaviour and not for the prediction algorithm. The battery model presented in section 2.2.2 is used as a base model, the complex model described in the same section will give a precision hardly more perceptible than the 1RC model and will in addition increase the time needed for the compilation. Figure 5.1 represents the battery simulation used in MATLAB/Simulink

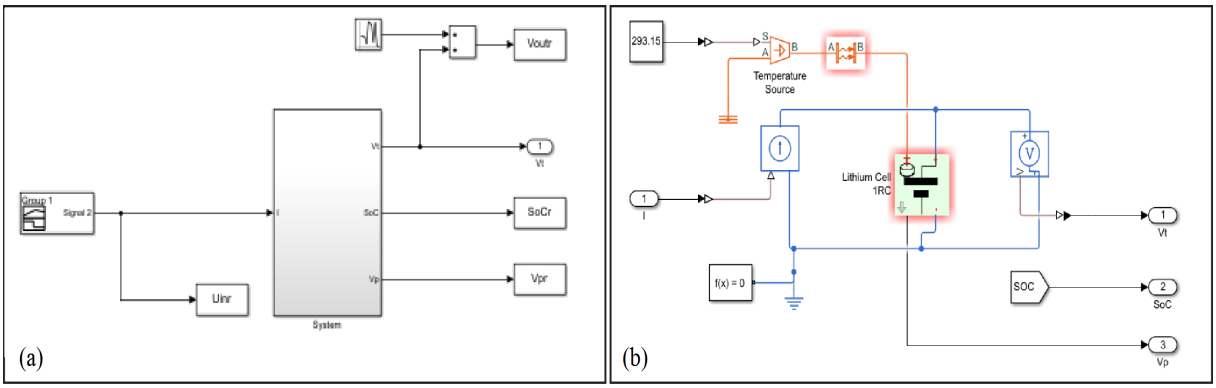

Figure 5.1: (a) overall Simulink model highlighting the Input/Output of the simulation (b) Battery sub-system model

In order to confirm the simulated model, the test carried out in section 4.1 to extract the battery's parameter is simulated through this model. The measured and collected real current is supplied to the model at the input, then the voltage at the model output is collected and compared to the real one. It is clearly evident from a quick comparison between the Figure 5.2 and Figure 4.1 that the simulated battery model follows almost perfectly the behaviour of a real battery, confirming the statements made in the previous chapters according to which the equivalent first order model offers high enough accuracy to be used by the Kalman filter. Figure 5.2 shows the battery simulation voltage and the input current.

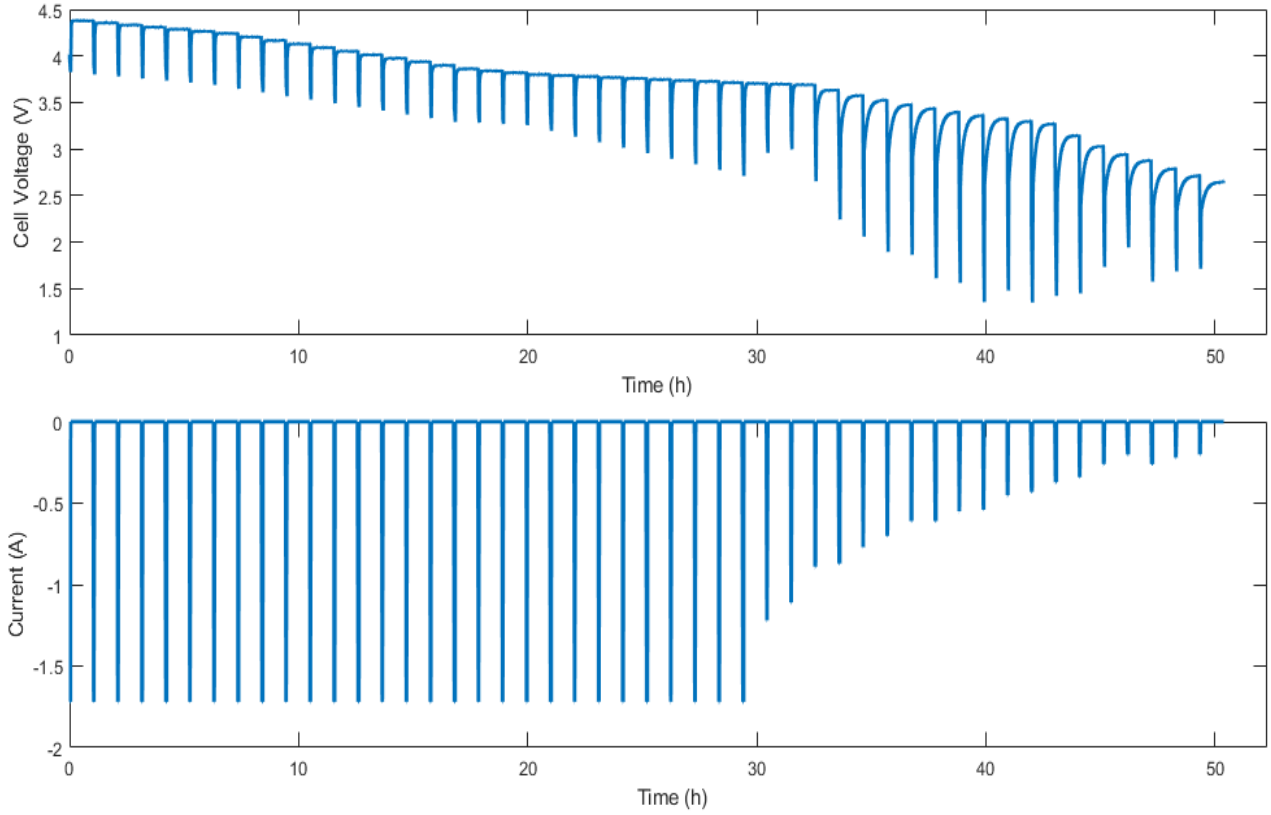

Figure 5.2: Voltage & Current for a constant current pulse discharge simulation

5.1.2 Simulation Results

After implementing and confirming the battery model to be used, various algorithms reported in the literature and described in chapter 2 are developed on Matlab. It should be noted that these tests are carried out in an ideal environment (i.e. without external disturbance), in order to show the maximum that these methods are able to offer in terms of prediction accuracy.

Luenberger Observer

The main objective of this observer is to cancel out the error between the estimate and the measurement, and thus to propose the most suitable observed state. Figure 5.3 shows the Luenberger observer's model simulated implemented in Matlab/Simulink software.

In Figure 5.4, the initial state is assumed to be unknown, and is initialized to a value

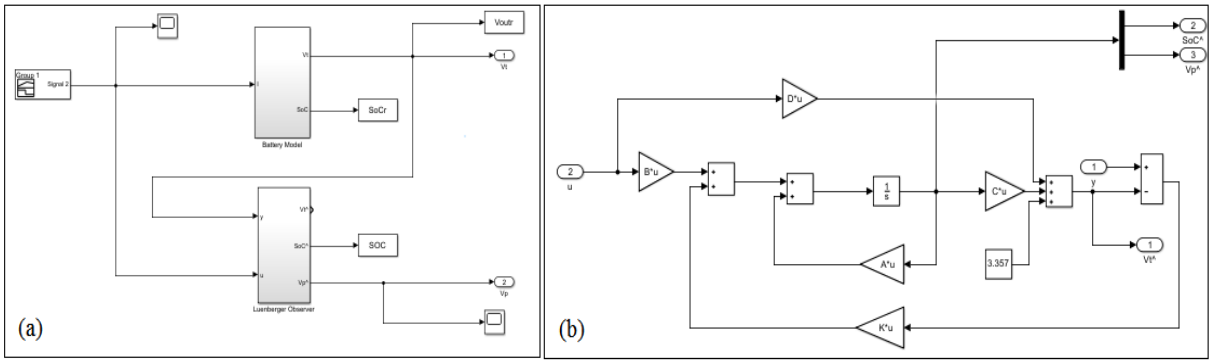

Figure 5.3: (a) overall Simulink model highlighting the Input/Output of the battery model simulation and Link with the Luenberger Observer (b) Luenberger observer sub-system model

of 50 % SOC, since the values of the equivalent model may be subject to changes due to ageing or temperature, these values are deliberately approximated to see the effectiveness of this observer over the long term.

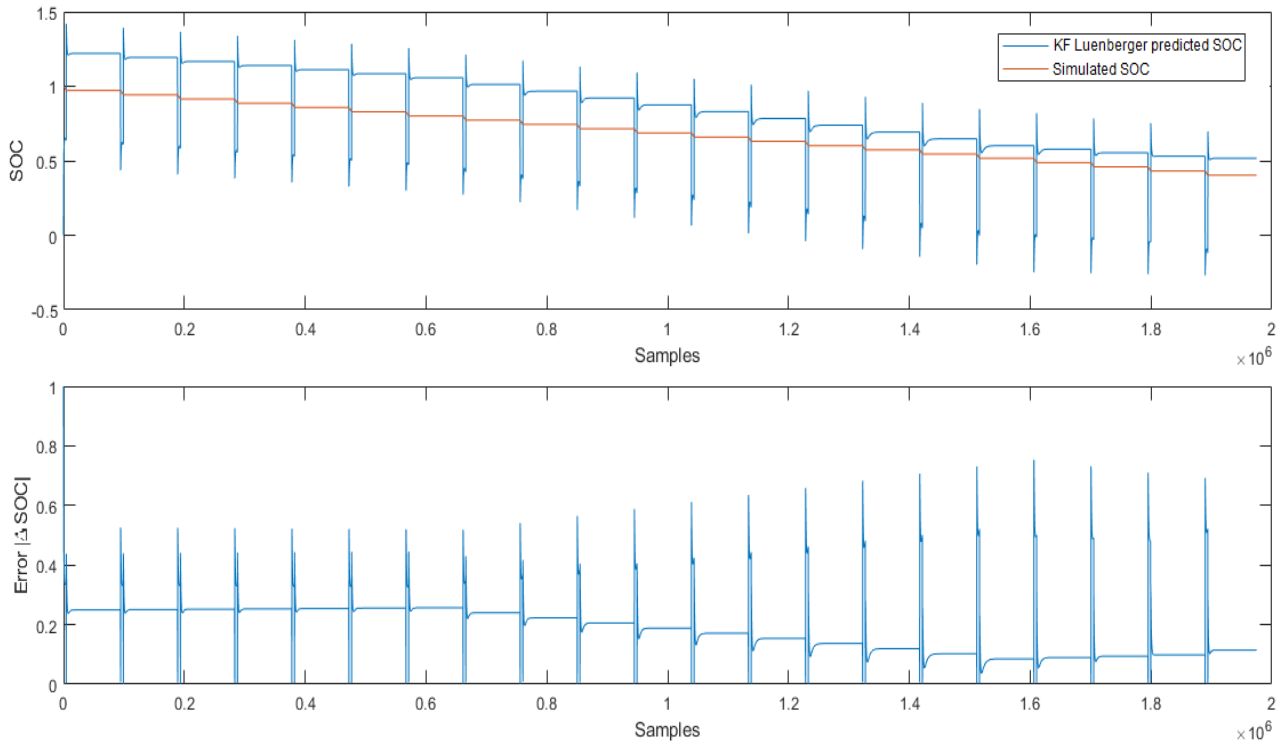

Figure 5.4: Estimated and reference SOC comparison with the absolute error of the SOC for Luenberger Observer

In the previous figure, it is clear that for a continuous state estimation, without updating the battery characteristics, this observer is divergent, indeed it is seen that the observer reach an error higher then 20 %, which is unacceptable and therefore rules out using this observer. As an additional information, it is quite possible to integrate the algorithms directly in the form of block diagrams on Simulink (As showed previously in Figure 5.3), but it was preferred for the other algorithm, to develop them on Matlab - Editor, in order to facilitate their future implementation on a microcontroller.

Kalman Filter

The Kalman filter is an observer that applies to linear systems. Even if it is known that the battery has a non-linear behavior, it is still interesting to see the behavior of this filter when applied to batteries. Figure 5.5 shows a comparison of the battery state of charge after simulation for the Kalman Filter provided with the absolute error comparison between the real state of charge value and the predicted one.

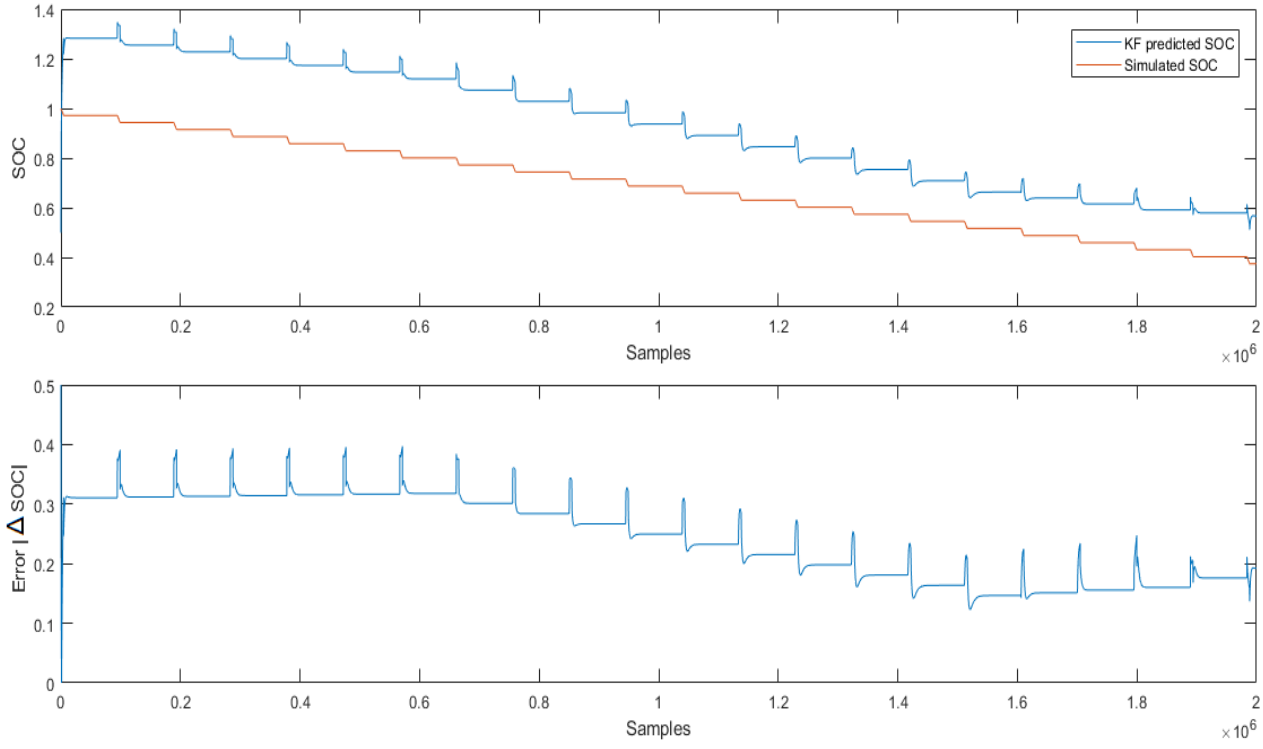

Figure 5.5: Estimated and reference SOC comparison for Kalman Filter

As the Kalman filter and the Luenberger observer are linear observers and the cells follow a non-linear behaviour, described in the previous sections, the estimator converges to an incorrect SOC value, the error depends on the initialized parameters, for these tests the average value of each parameter presented in Table 4.1 is implemented. Although it does not reach a correct value, it is clear from the previous figure that this filter offer a small prediction peak. Considering this performance and the proposal made in various researches to implement an extended Kalman filter to overcome the nonlinearity of the systems [18], [25], the EKF simulation is performed in the following of this section.

Extended Kalman Filter

Following the same initial data, EKF was also simulated, again, the operating range is defined as 80-40 %, so the majority of linearisation points are included in this range. Figure 5.6 shows a comparison of the SOC of the battery with simulation for the Extended Kalman filter, and a plot of the error with the real and the predicted one.

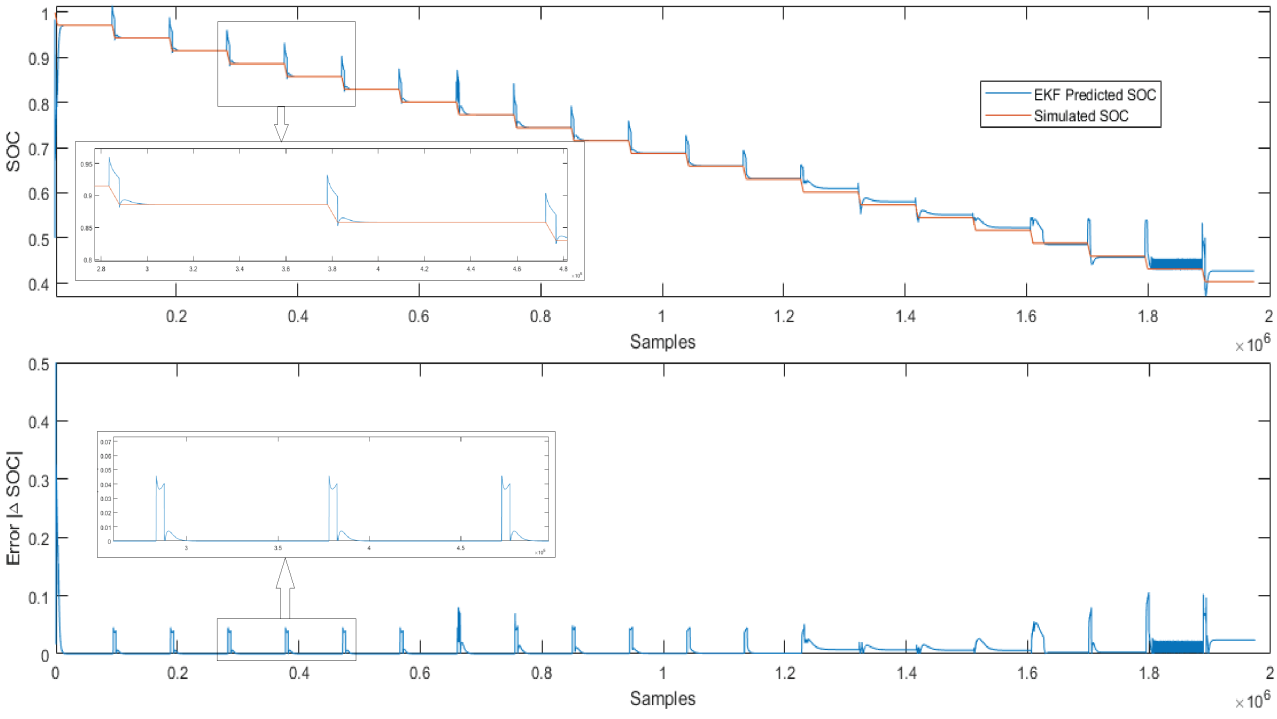

Figure 5.6: Estimated and reference SOC comparison with the absolute error of the SOC for Extended Kalman Filter with a constant discharge test and a rest period.

The continuous update of the correction gain (K), which is due to the continuous re-transcription of the error covariance matrices and the continuous correction of the parameters and the SOC(OCV) function, makes the predicted state of charge to converge to the actual state of charge value. The response of the Extended Kalman Filter estimator to the determination of the SOC can be very fast. Also, from the previous figure it is clear that, for known parameters, the state of charge can be tracked accurately with less than 5 % of error, and record a perfect prediction for when the battery is at rest. This response has made the EKF filter to be chosen for further testing. Figure 5.7 shows a comparison of the SOC of the battery with simulation results of a constant current discharge test, a plot of the error is also shown in the figure.

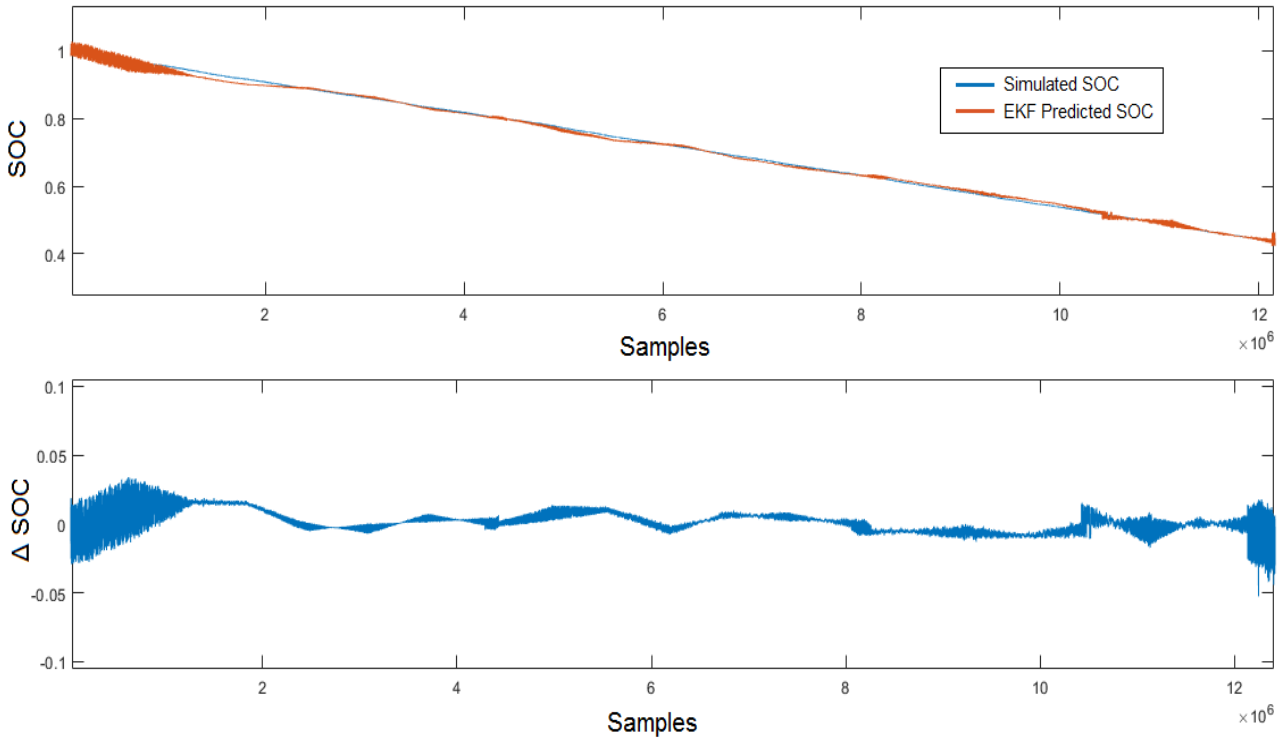

Figure 5.7: Estimated and reference SOC comparison with the absolute error of the SOC for Extended Kalman Filter with a constant discharge test.

5.2 Hardware Validation

In order to confirm the good implementation of the estimator and its performance, a cell is tested under room temperature, using the electronic circuit shown in Figures 4.4 and 4.5. The cell start fully charged (100 % SOC) with an initial guess of the estimator set at 50 %, which will show the robustness of this estimator on an ATMEGA328P. Also, in an effort to get as close as possible to a real environment, the discharge test is not done with a constant current, since the mobile robot can ask the battery to supply it with variable power (therefore variable current), the test will therefore be done with a constant current for a variable period of time and will change afterwards. The tests of the EKF algorithm are performed for correct and incorrect values of the cell equivalent electrical parameters and are summarized in this section.

5.2.1 Correct Cell Parameters Implementation

The battery data, shown in Table 4.1, is fed in the algorithm, the real SOC used for comparison is calculated with a coulomb counting method with known initial conditions. The predicted voltage by the on-board estimator is compared with the real voltage of the Lithium-ion cell measured and is shown in Figure 5.8.

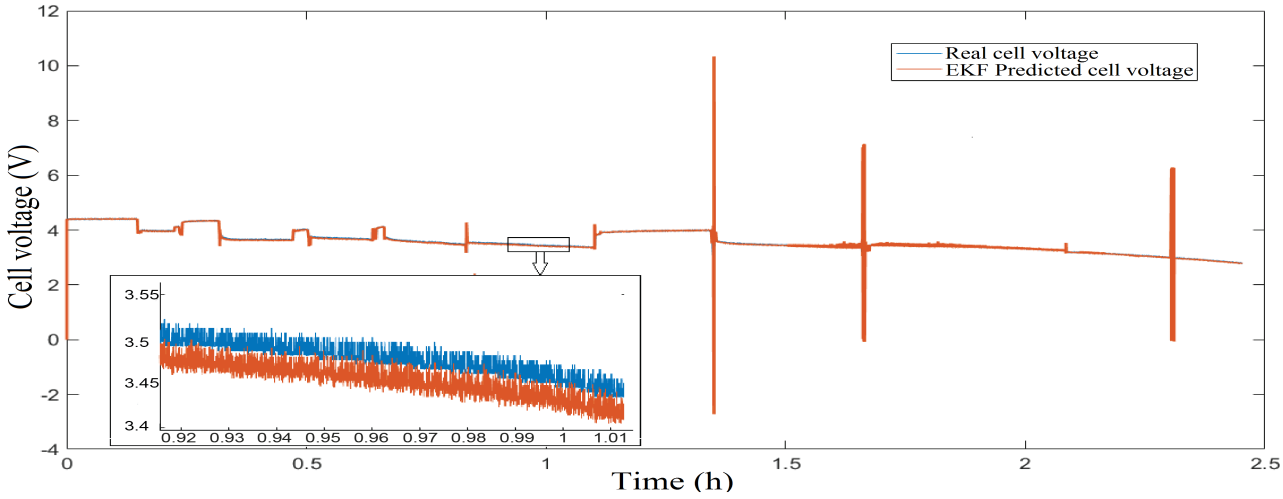

Figure 5.8: The measured battery terminal voltage compared with the estimated voltage by the proposed Extended Kalman Filter algorithm

The result of the SOC estimation of the EKF compared with the real SOC, are shown in Figure 5.9.

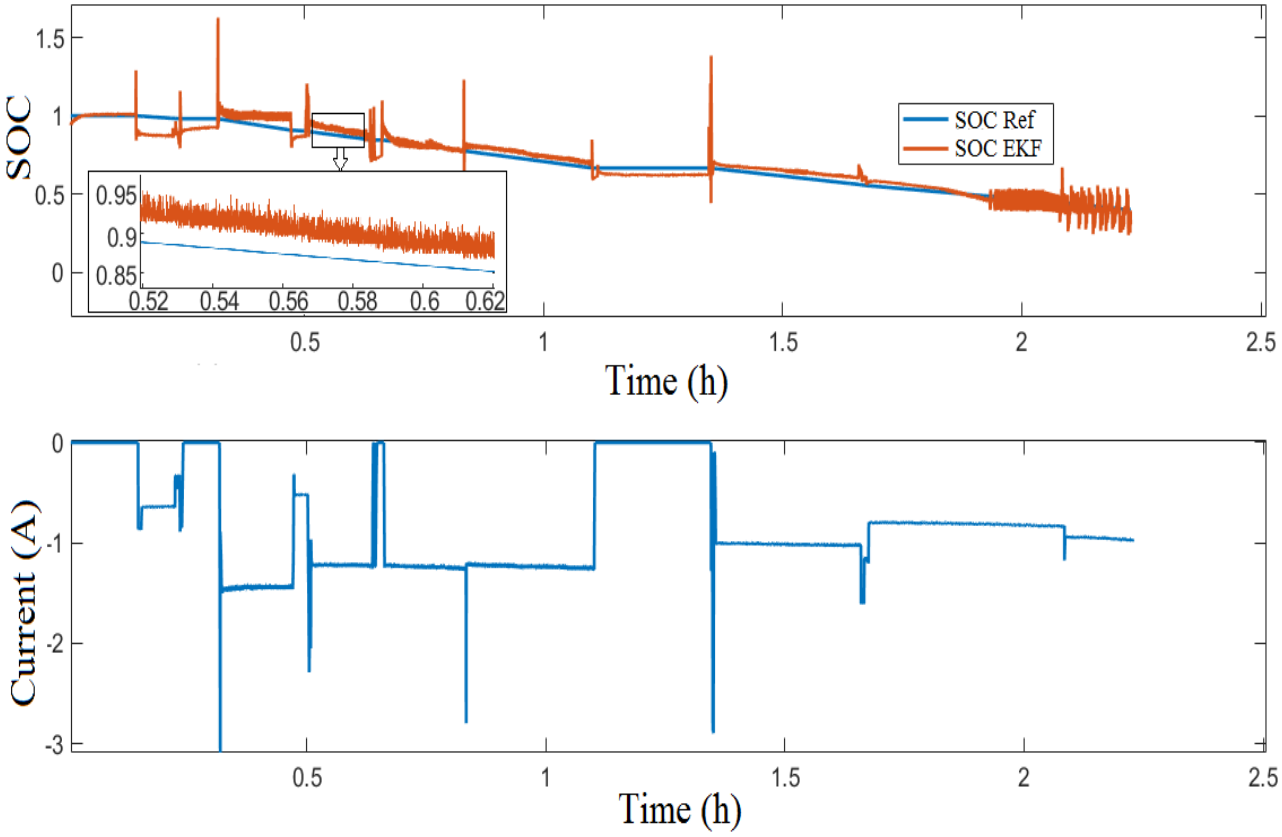

Figure 5.9: The reference SOC compared with the SOC estimated by the Extended Kalman Filter and the current measured

It is clearly seen from Figure 5.8 that apart from a few exceptions due mainly to current measurement error (Figure 5.9), the EKF implemented in the Arduino follows the battery voltage perfectly, minimizing the error as much as possible. In Figure 5.9 the estimated SOC track the true SOC value during all the test but more especially between 80 % and 34 % of SOC of the battery, because, between these two values, the battery follows more or less a linear behavior and this can be proved from Table 4.1, Figure 4.2 and Figure 4.3. In order to limit the computational power, the linearization of these curves is preferred to the 7^{th}-order polynomial approximation. As this curve is approximated on only 10 points and concentrated in the linear region between 80 % and 40 % of SOC, it does not offer

the most accurate results and explains the poor prediction outside this region. Figure 5.10 shows the error ($|\Delta SOC|$) between the predicted SOC and the real SOC.

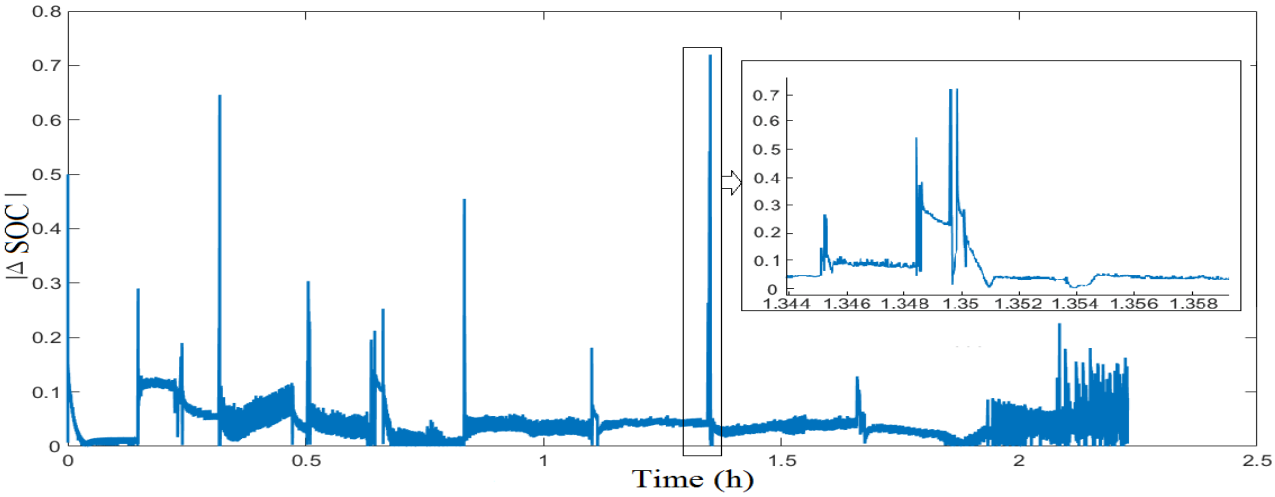

Figure 5.10: Absolute Error

It is worth highlighting that the MATLAB environment is only used for the purpose of collecting the results at each iteration (Voltage, Current, SOC), and it should be specified that no calculation is made through it. During the rough passage from one current to the other, the Mosfet generates interference that affect the correct reading of the current, this results in a false current peak measure that can be seen in the figure 5.9, this peak causes the divergence of the estimate during 5 iterations, this interference are kept and not filtered in order to allows the validation of the robustness of this estimator, indeed after only 200 iterations (equivalent to 8 seconds) the prediction of the SOC converges again. If this brief divergence is not taken into account, the majority of the error for each SOC sample is less than the 10 % value, indeed an average error of 3.81 % in over more than 2 hours of use is recorded. Figure 5.11 represent the begining period of Fig 5.9 (The first three minutes), even if this algorithm can be qualified as robust, it still takes for it 2 minutes to reach the reference.

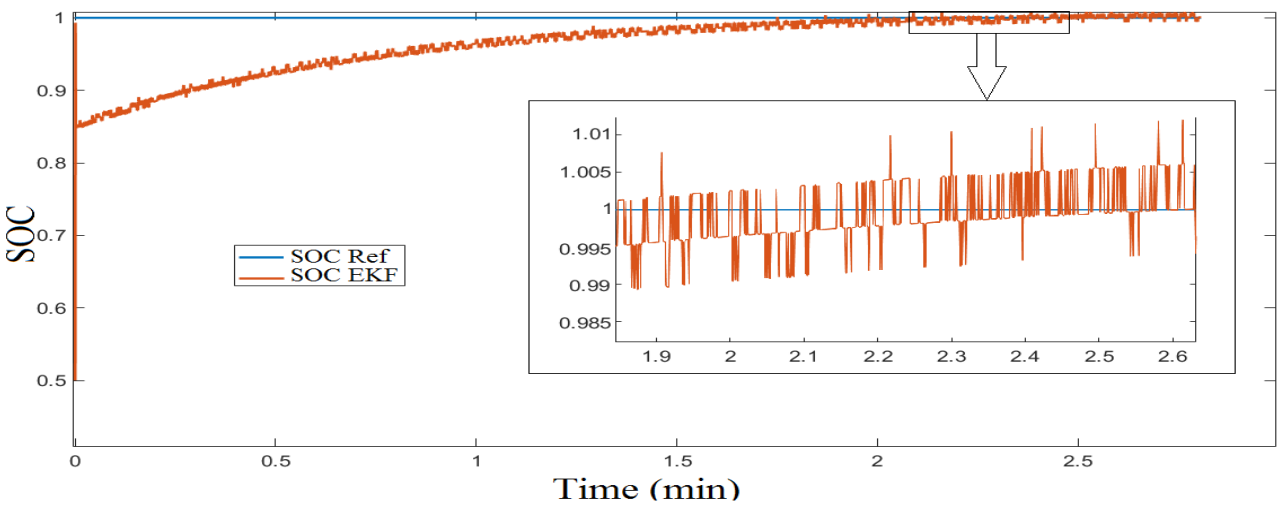

Figure 5.11: The reference SOC compared with the SOC estimated within the first 3 minutes of estimation

5.2.2 Incorrect Cell Parameters Implementation

Even with the use of a Kalman filter for SOC prediction based on the use of MATLAB, its behaviour with incorrect parameterization is poorly reported in the literature and research work in this area. For this reason, the parameters summarised in Table 4.1 have been deliberately alternated, a value of 0.2 Ω has been added for each of the resistors R_p and R_t and 200 F for C_p. It goes without saying that this result were obtained by using the same circuit and algorithm as in the previous subsection.

The implemented EKF reached an error of 30 % during the whole period when the discharge takes place. When the current stopped, the EKF converged rapidly, reaching a preliminary error of 10 % within a few sampling times, and then slowly converged to the reference SOC, after about 3 minutes it reached an error of less than 5 %. Although the error reached a value of 30 % while the cell was in use, the EKF converged rapidly for the battery at rest, with an error of 5 %. This feature represents an asset that can be used to advantage, as the use of an EKF instead of the OCV, which is currently widely used for SOC updating, represents a faster and more accurate alternative. Figure 5.12 shows the result of the SOC prediction after a full charged cell has been discharged at constant current for a defined period of time and then stop all the current flow.

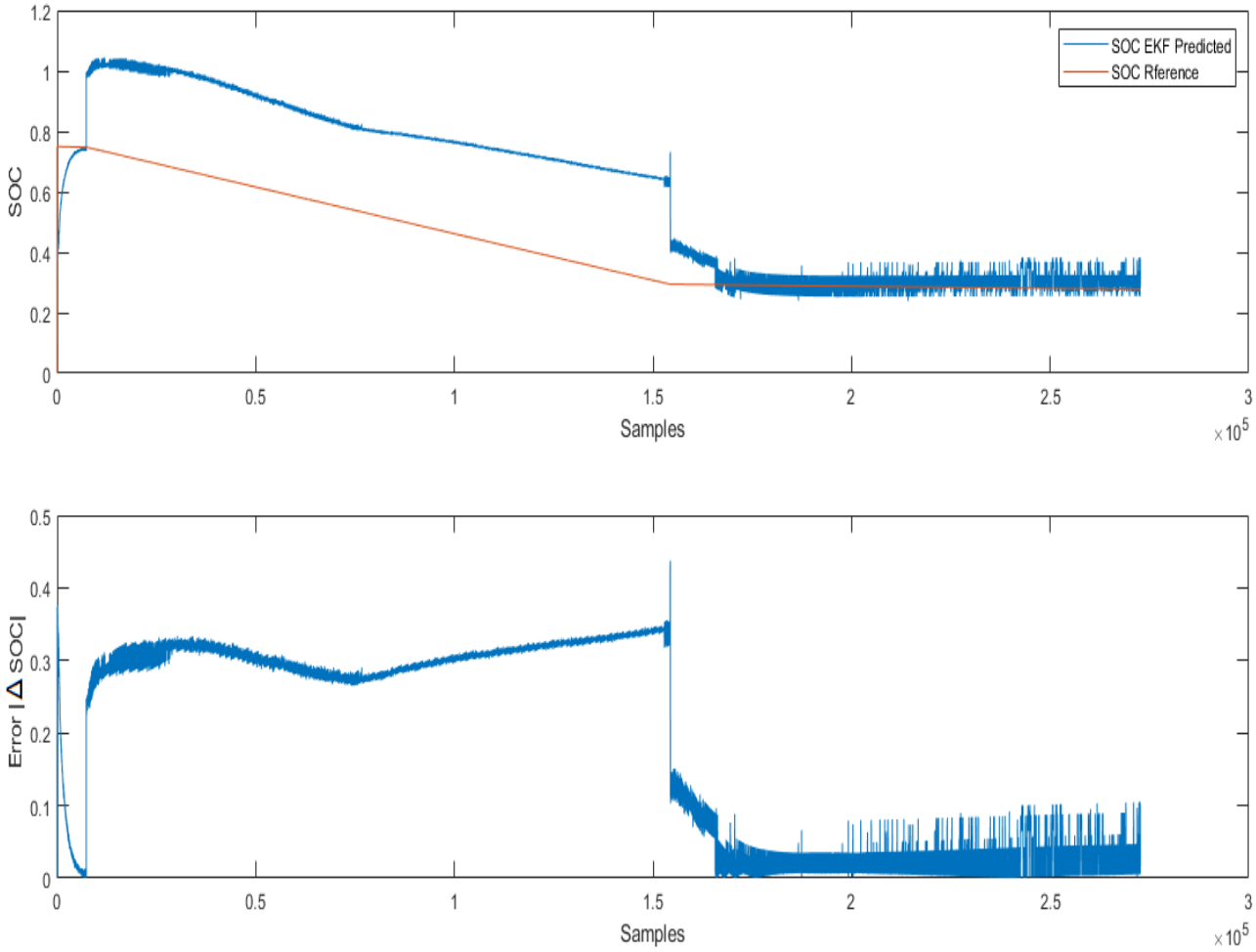

Figure 5.12: Results of the EKF prediction with wrong parameters

5.3 Electronic Circuit

The Electronic circuit presented by Figures 4.4 and 4.5 is able perform the monitoring of one battery without problems, but the use of a resistor based current measurment doesn't represent the most efficient way to perform current reading. In fact the current passing through this 0.82 $\Omega/7\ W$ resistor will create power losses, for a 2 A current, a power losses of 3.28 W is to be waited. In this section, the *Bbox V0.3.2* is presented, this prototype use the DCC-EKF algorithm described and is able to perform monitoring for 4 batteries mounted in series simultaneously.

5.3.1 Circuit Diagram

Through experimentation and testing, several versions have been developed, each incorporating a new feature, the most advanced being versions 0.3.0 and 0.3.2. Version 0.3.2 allows the management of four batteries simultaneously, while version 0.3.0 only handles two. In this section, the focus will be on version 0.3.2.

The development of the circuit in software is an important aspect, even if it is not 100% reliable, it allows debugging the circuit and finding quick solutions to problems. The *Bbox V0.3.2* scheme is designed to meet the requirements of our specifications, namely flexibility of use, precise definition of the SOC and ease of use. The components are selected and linked together. The figure B.1 in appendix B represents the complete schematic of the electronic board. The wiring link is as follows, the 18650 Lithium cells are placed in the two cell holder (1BH, 2BH). The Oled display (OLED1) is connected via I2C by SCL and SDA respectively, the ATMEGA328P microcontroller (MASTER, SLAVE1, SLAVE2) are connected to the I2C wire through pins PC5 and PD4. The current is measured from the ACS712 (U1) and gathered by the slave microcontrollers (SLAVE1, SLAVE2) from the analog pin PC0. A quadruple precision amplifier LM324 (U5) is used to measure the voltage at each cell terminal, with the use of a simple voltage divider. The push buttons are linked to the master microcontroller via the digital pins (PD2, PD3, PB4, PB5), an IRF1405 N-Channel Mosfet is used as a power switch to the load (mobile robot) while an IRF9610 P-Channel Mosfet is used as a power switch from the power supply, they are controlled from master ATMEGA328P pins PB3 and PB2 respectively. A step down voltage regulator is applied to regulate the voltage supplied to the electronics to 5V, this power is either gathered from the battery pack or the power supply.

5.3.2 Breadboard Circuit

The test plate is an insulated plastic plate perforated with numerous of holes. These holes are spaced 2.54 mm apart, which is the standard spacing for the electronic components useed in the assemblies. This is a very good way to test a solderless assembly, to adjust

what needs to be adjusted, and to correct various errors related to the design and sizing phase. Figure 5.13 shows the Breadboard circuit.

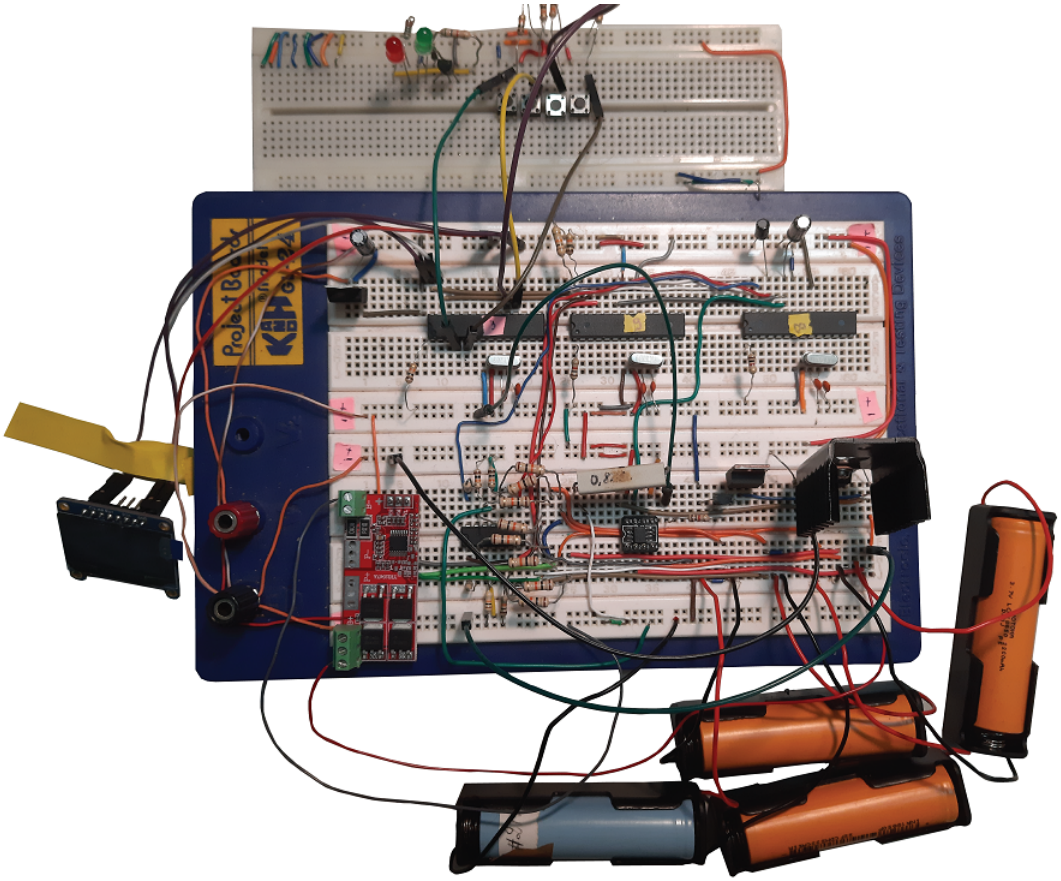

Figure 5.13: Breadboard circuit

When powered on, the Oled displays the IPB and ESSAT logos successively for few seconds as it can be seen from Figure 5.14.

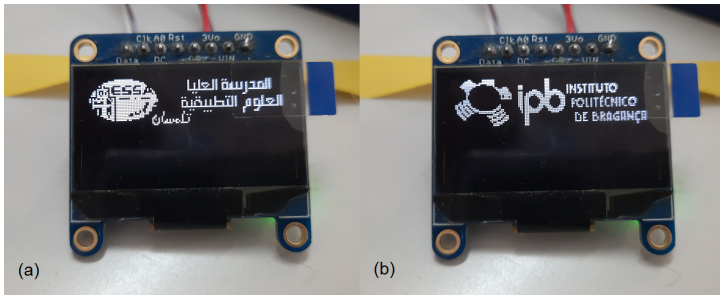

Figure 5.14: Logo display. (a) ESSAT. (b) IPB

Afterwards, the menu of the initialisation mode is displayed as it can be seen in Figure 5.15. It is possible to navigate on the menu, by using the Up, Down, Enter Exit buttons.

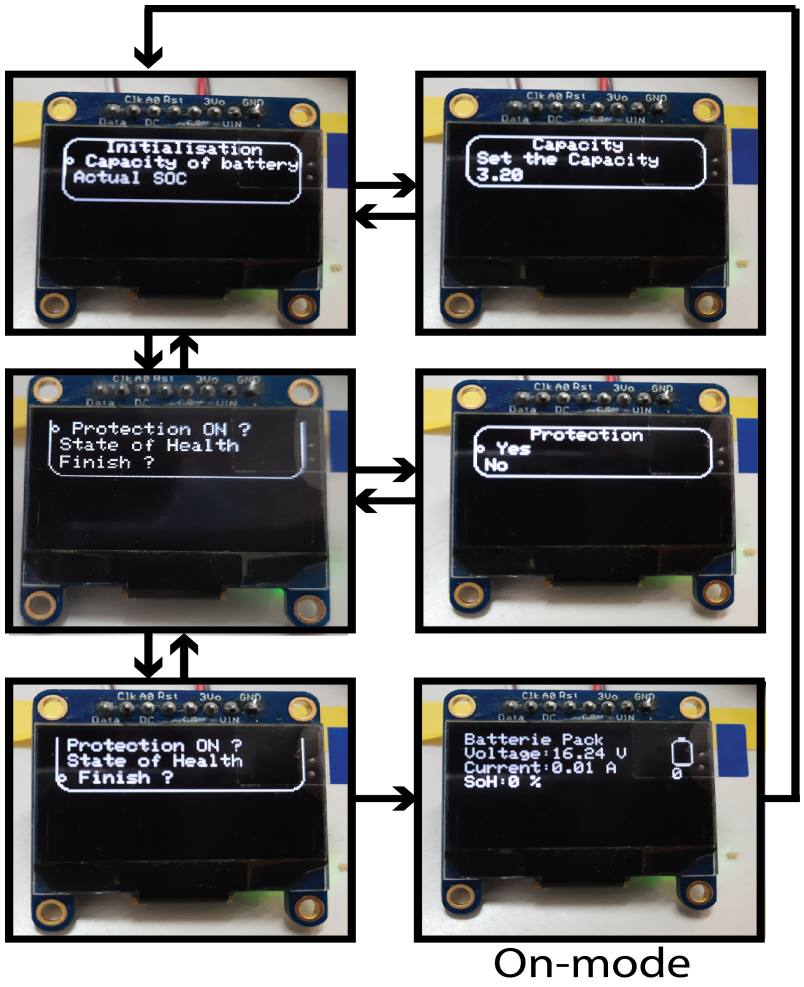

Figure 5.15: Menu display

The SOC values, voltage and current are displayed directly on the Oled screen. It is possible to display the overall battery status, or cell by cell for a more detailed view. Figure 5.16 shows the on-mode display for the 4 cells. In the normal operating area, the EKF prediction reaches an error of 5 % in the worst case, for SOC cells above 80 % the accuracy drops to 8 %, while for SOC below 30 % the algorithm diverges completely. Taking into account that this approach and the algorithm are constantly being improved, not all features such as the SOH and temperature are fully integrated.

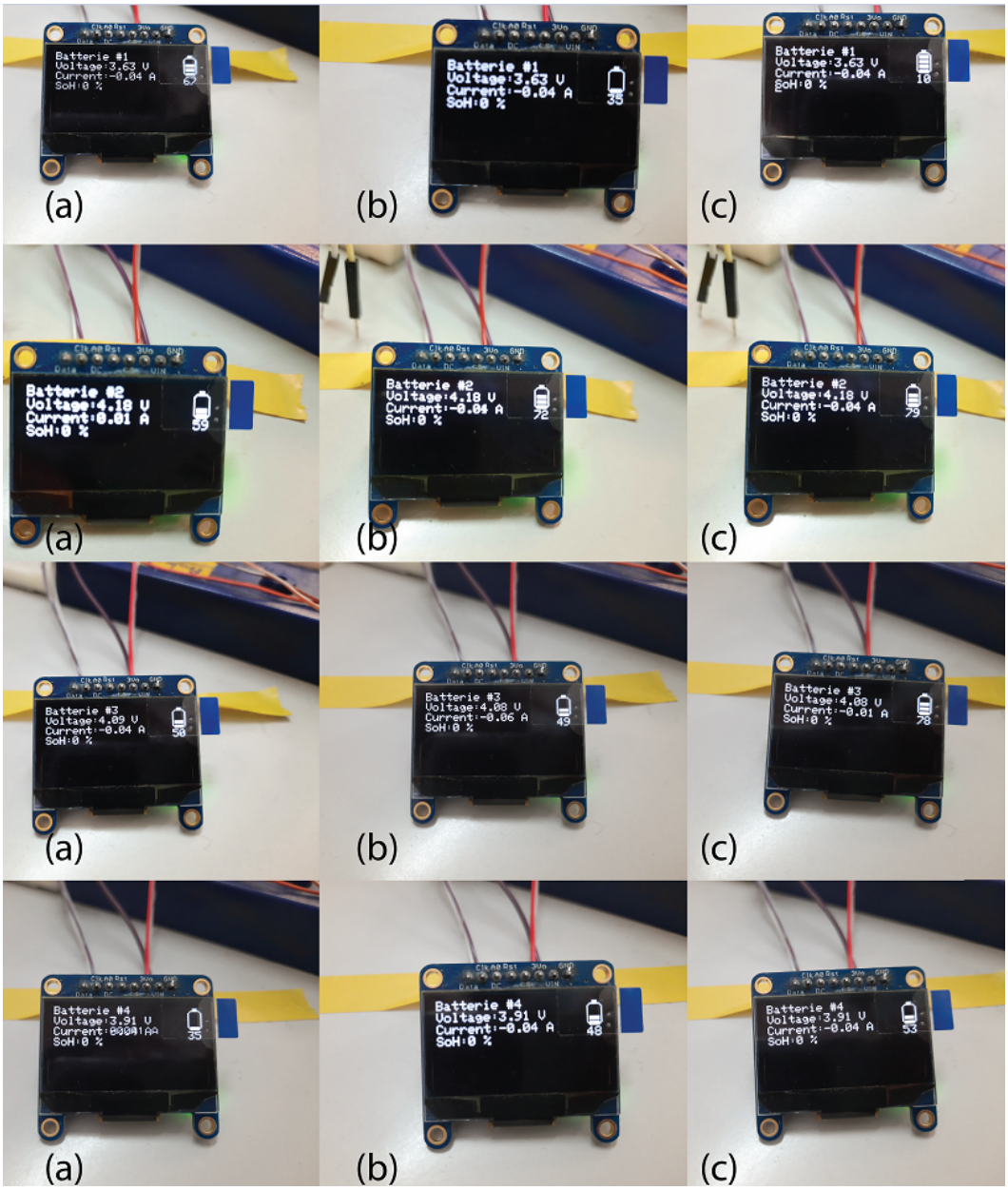

Figure 5.16: On-mode display of cells 1, 2, 3 and 4 with a SOC value of 9.51 %, 77.25 %, 71.10 % and 55.02 % respectively. (a) Average SOC of the first 50 iteration. (b) Few seconds after. (c) approximately 1 minute after.

It is constated that for cell 1, the algorithm diverges for the SOC estimate. For cell 2, the estimate has reached the SOC value with an error of 1.75 %. For cell 3, after 1 minute, the prediction has not yet reached the estimated value with an error of 6.90 %. For cell 4, the estimate has reached the estimated value with an error of 2.02 %.

5.3.3 Printed Circuit Design

Various software packages such as Eagle, EasyEDA, ARES provide access to a PCB development interface, It is important that the various components are positioned so as to minimise the occupied space. Some software offer the possibility automatic routing feature that allows the different components to be connected in a few seconds, but it is much more efficient to do it manually, which is what was chosen. The Figures B.2 and B.3 in Appendix B show the electrical circuit diagrams of the bottom layers, also refereed in this thesis as components view, and top view used to print the PCB. Figure 5.17 is a picture of the PCB taken by the company.

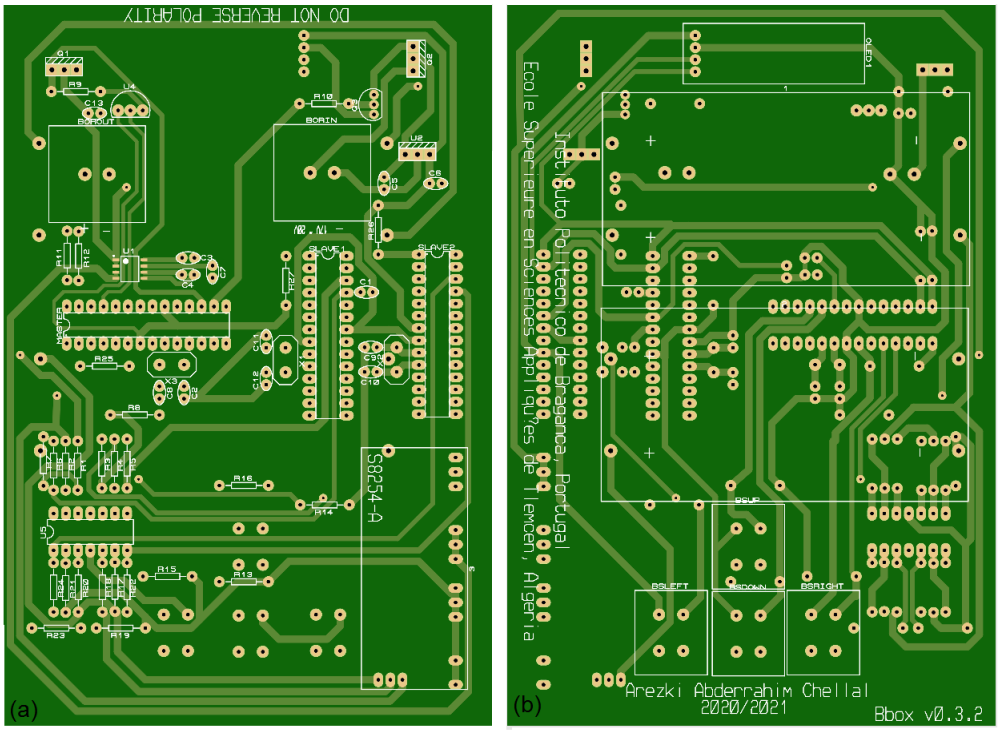

Figure 5.17: Printed Circuit Board. (a) components view. (b) top view

Printed Circuit Board (PCB) is a plate that holds and interconnects the different electronic components of the Bbox by means of copper tracks. In our case, this plate consists of two copper layers separated by an insulator (double-sided plate). The copper layers are etched using a precise chemical process and different steps (Drilling, Copper Deposition, Image the outer layers, Pattern Plating, Automatic Optical Inspection, Silkscreen, Hot

Air Solder Leveling, Profiling,V-cut scoring). A PCB was ordered from the Hong Kong-based company *JLCPCB*. This company prints professional quality circuits at low cost. Figure 5.18 shows the printed PCB with the soldered components on it.

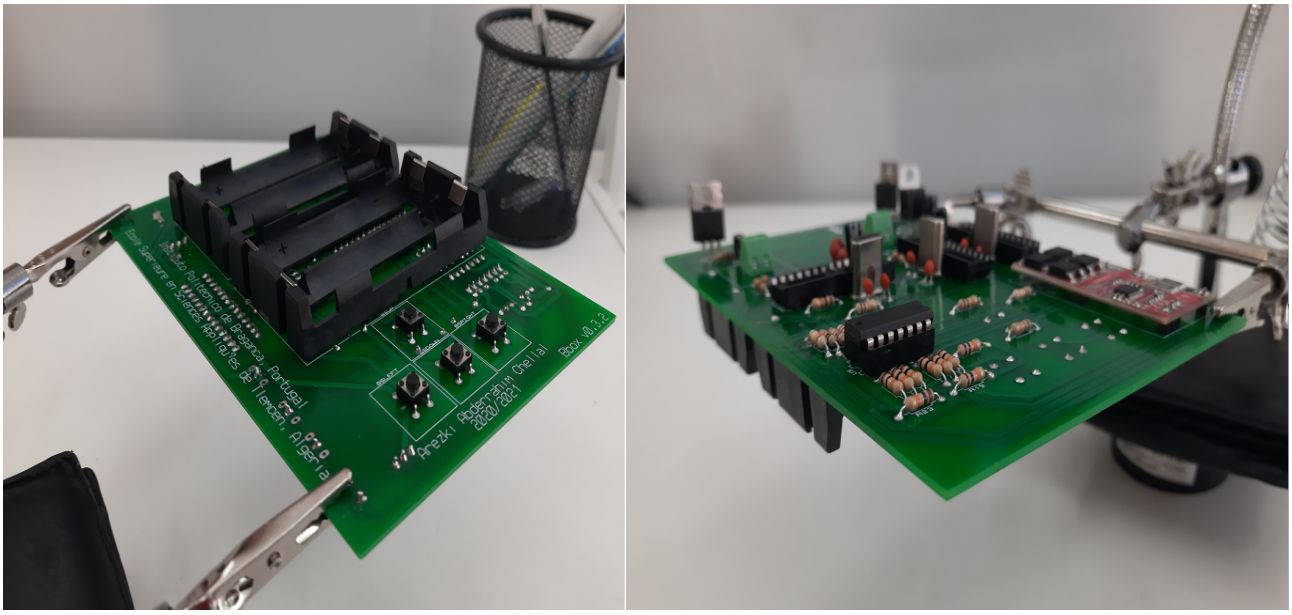

Figure 5.18: Printed Circuit Board with soldered components

5.4 Product Incorporation Principal

The product is designed to be "Plug & Play", which means that the user can simply position it anywhere on the robot and allow tracking. Figure 5.19 shows an application illustration, based on a radioactive spatial mapping robot developed by Luis Fernando Piardi [51].

As it can be seen, the printed circuit board can be just placed and plugged to the overall system. This prototype can also be connected to small solar powered systems, for robots and other systems. An example is a solar watering system, called Arden, for which a power supply of 20.75 W is required for the product to operate in all conditions. However, voltage regulation (MPPT-based or not [52]) is required at the input of the Bbox prototype to ensure safer charging of the batteries [37], [53].

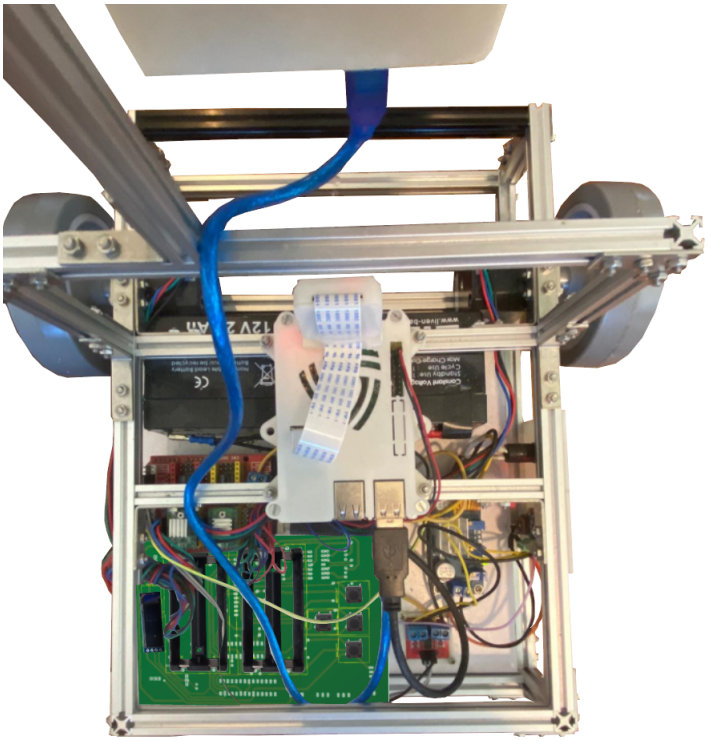

Figure 5.19: Bbox incorportation principale

5.5 Conclusion

The results of this thesis are multiple, first of all it is presented the result of a study on the feasibility of implementing an EKF for the prediction of the state of charge of a battery in an 8-bit microcontroller, this study had until now never been proposed and realized in previous scientific studies. This confirmed the possibility of implementing such an algorithm, which is extensively reported in the literature as being among the best, but which had never before found its way out of the research laboratory and powerful softwares such as MATLAB.

The findings of this study led to the design of the new DCC-EKF approach, representing the second result obtained, this approach, which has also never been reported in the literature, allows to take advantage of the excellent behaviour of the Kalman filter when the batteries are at rest, the filter converges directly after a few minutes for an accuracy of less than 5%. This replaces the CC-OCV methodology that is generally used in commercial products and offers increased prediction accuracy.

The last result is the design and development of a BMS from scratch that allows the monitoring of 4 batteries in series, this BMS takes into consideration the main constraints that need to be addressed and proposes the aspect of flexibility and ease of use in addition. The DCC-EKF approach is implemented and tested also from the prototype designed called Bbox V0.3.2. and showed convincing results of its ability to monitor accurately each cell independently.

Chapter 6

Conclusion and Future Work

The aspect of energy management has always been an important aspect in electrical and energetic systems. In mobile systems, whether they are large systems such as hybrid vehicles or small systems such as mobile robots and smartphones, the battery is the only reliable source of energy they can rely on. It is therefore very important to optimise the use of this stored energy, which can be done by knowing the precise state of charge of each cell in the battery pack. For this reason, the Battery Management System is introduced in all battery-based systems, allowing real-time management of the energy supplied by the cells while protecting them from possible short circuits and anomalies. As no specification has been made concerning the accuracy that these devices needs to reach, commercialized BMS generally use a combination of two methods, referred to as basic in this study, which are Open Circuit Voltage measurement and Coulomb Counting, which provide a prediction that may be unsatisfactory but works very well for batteries with low ageing rates. Algorithms that accurately predict and optimally monitor the SOC exist and have been reported in the literature in over 200 scientific papers worldwide, including Kalman Filter, Sliding Mode and Neural Network. However, these algorithms have hardly ever left the laboratory development stage and, according to the research, no paper to date, has proposed the implementation of an EKF in an 8-bit microcontroller, in order to provide autonomous state of charge prediction for batteries.

The EKF requires an equivalent model of the battery to allow the prediction of the SOC, different models have been proposed, from the simplest to the most complicated, in previous studies. In this study, the first order equivalent model has been chosen as the reference to be followed by the EKF, this choice is clearly justified, mainly due to the low computational power offered by this type of microcontroller. This model requires the knowledge of the parameters R_p, C_p and R_t, these parameters are extracted by applying a constant current discharge test for a short period of time followed by a one hour relaxation. Then, using a Least Square Curve-Fitting algorithm, these parameters are extracted for different SOC values.

In order to prove the possibility of implementing such an algorithm in a PIC18F4520 or an ATMEGA328P, a first circuit based on the components described in chapter 2 has been realized. A test of the proposed algorithm was performed for correct and incorrect parameters in order to know its exact behaviour. For correct parameters, the EKF algorithm converges quickly and accurately to the SOC, an average of 3.81 % was recorded, in addition, this estimator is robust and resistant to external noise, a very important aspect for a BMS. But for inaccurate parameters, the algorithm converges to an incorrect value, the error increases as the difference between the actual value and the value of the implemented parameter increases. This result was problematic during the study because the parameters evolve over time, so it was inconceivable to implement an EKF alone in a BMS. From this observation came the idea to replace the traditional OCV-CC method with the proposed DCC-EKF approach, given the excellent result of the EKF, with a prediction accuracy in record time for batteries at rest, whether or not correct parameter are implemented, the prediction task that is traditionally done by the OCV is accomplished by the EKF. This approach is also new and according to the best of the author knowledge has not been reported in the literature.

Following these satisfactory results, a BMS was designed from scratch, which will implement the new approach. The prototype, named Bbox *V0.3.2*, is the most advanced prototype designed so far, it can measure voltage with an accuracy of 100 mV and current with an accuracy of 40 mA and has an average efficiency of 94.38 %. The S8254A provides

deep charge and short circuit protection, while deep discharge protection are provided by the algorithm itself, the overall algorithm is implemented in three ATMEGA328P microcontrollers operating on the master/slave principle and communicating via I2C. After breadboard testing, the designed PCB is sent for manufacturing to the specialist company JLCPCB, based in Hong Kong. The total manufacturing cost of one single prototype is estimated at 32.21 €, which is a very good price compared to other BMSs on the market.

This prototype and the results obtained are just the beginning, in fact, both on the software and hardware side, future improvements are planned to make this product more efficient.

Software and algorithm improvements:

- The DCC-EKF approach represents only one way to improve the online SOC prediction and monitoring task, but it is preferable to enable the SOC monitoring and prediction by the full EKF. To this end, it is planned to validate the implementation of different approaches to determine and update the online equivalent battery parameters using different methods proposed in the literature, mainly the double extended Kalman filter by using microcontrollers of 8 bits or more. The ESP32 is a very good candidate that is already being considered for use in future releases.

- The effect of temperature should be addressed in future versions, it is an important aspect, the Bbox V0.3.2 will be used as an interface for the development and improvement of the algorithm, indeed the possibility to measure temperature is implemented in this version for this purpose.

- The SOH is a very important parameter, and in great demand, this parameter is also very lacking in accuracy. By using the DEKF, it will be possible to accurately predict the SOH of the cells.

Hardware improvements:

- The efficiency currently achieved is good and has been improved from version to version, but it can be even better, so particular attention will be given to this characteristic in future versions.
- Product minimisation is an aspect that is defined as essential according to the aspiration of the product specification, the screen interaction of the product is easy for the user, but consumes power and is space consuming, adding to this the push buttons. It will therefore be eliminated in favour of other modes of communication.
- Enabling communication via I2C with the robot is one aspect considered, by offering the SOC data to the robot, it will be possible to establish the third state for a BMS which is the operating state. This system will be based on an architecture with two microcontrollers working as a master.
- A diversification of communication modes is envisaged for future versions, in particular the use of IOT, the ESP32, which is a 32-bit microcontroller, or the ESP12e are envisaged not only for their processing speed, but also because they offer the possibility of communicating by WiFi or even Bleutooth which is an undeniable advantage.

Bibliography

[1] A. Lievre, "Dévloppement d'un système de gestion de batterie lithium-ion à destination de véhicule "mild-hybrid"", PhD thesis, Université Claude Bernard - Lyon 1, 2015.

[2] T. B.Reddy, *Linden's handbook of Batteries*, 4th.

[3] X. Hu, S. Li, and H. Peng, "A comparative study of equivalent circuit models for li-ion batteries", *Journal of Power Sources*, vol. 198, pp. 359–367, 2012.

[4] S.Muench, A.Wild, C.Friebe, T. B.Häupler, and U. S. Schubert, "Polymer based organic batteries", *Chem. Rev*, 2016.

[5] L.Long, S.Wang, M.Xiao, and Y.Meng, "Polymer electrolytes for lithium polymer batteries", *Journal of Materials Chemistry A*, Jan. 2016.

[6] V. Etacheri, R. Marom, R. Elazari, G. Salitra, and D. Aurbach, "Challenges in the development of advanced li-ion batteries: A review", *Energy and environmental sciences*, May 2011.

[7] F. Jordan, "Electrical power system (eps), report of diploma", PhD thesis, Haute ecole d'ingénierie et de gestion du Canton de Vaud- Yverdon, Switzerland, 2006.

[8] *Lithium-ion battery datasheet,battery model lir18650 2600 mah*, EEMB, 2010.

[9] V. Pop, H.J.Bergveld, P. H.L.Notten, and P. Regtien, "State of the art of battery state of charge determination", *Measurement Science and Technology*, Dec. 2005.

[10] T. Bruen and J. Marco, "Modelling and experimental evaluation of parallel connected lithium ion cells for an electric vehicle battery system", *Journal of Power Sources*, vol. 310, pp. 91–101, 2016.

[11] L. H. Saw, Y. Ye, and A. A. Tay, "Integration issues of lithium-ion battery into electric vehicles battery pack", *Journal of Cleaner Production*, vol. 113, pp. 1032–1045, 2016.

[12] F. Leng, C. M. Tan, and M. Pecht, "Effect of temperature on the aging rate of li ion battery operating above room temperature", *Nature*, 2015.

[13] A. Delaille, "Développement de méthodes d'évaluation de l'état de charge et de l'état de santé des batteries utilisées dans les systèmes photovoltaıques.", PhD thesis, Université Paris VI, 2006.

[14] I.-S. Kim, "A technique for estimating the state of health of lithium batteries through a dual-sliding-mode observer", *IEEE*, Apr. 2010.

[15] I.-S. Kim, "Nonlinear state of charge estimator for hybrid electric vehicle battery", *IEEE TRANSACTIONS ON POWER ELECTRONICS*, Jul. 2008.

[16] J. Du, Z. Liu, Y. Wang, and C. Wen, "An adaptive sliding mode observer for lithium-ion battery state of charge and state of health estimation in electric vehicles", *Elsevier*, May 2016.

[17] Y. Xu, M. Hu, A. Zhou, Y. Li, S. Li, C. Fu, and C. Gong, "State of charge estimation for lithium-ion batteries based on adaptive dual kalman filter", *Applied Mathematical Modelling*, vol. 77, pp. 1255–1272, 2020.

[18] B. Xia, Z. Lao, R. Zhang, Y. Tian, G. Chen, Z. Sun, W. Wang, W. Sun, Y. Lai, M. Wang, *et al.*, "Online parameter identification and state of charge estimation of lithium-ion batteries based on forgetting factor recursive least squares and nonlinear kalman filter", *Energies*, vol. 11, no. 1, p. 3, 2018.

[19] S. Jiang, "A parameter identification method for a battery equivalent circuit model", SAE Technical Paper, Tech. Rep., 2011.

[20] T. Hu, B. Zanchi, and J. Zhao, "Determining battery parameters by simple algebraic method", in *Proceedings of the 2011 American Control Conference*, IEEE, 2011, pp. 3090–3095.

[21] L. W. Juang, P. J. Kollmeyer, T. Jahns, and R. Lorenz, "Implementation of online battery state-of-power and state-of-function estimation in electric vehicle applications", in *2012 IEEE Energy Conversion Congress and Exposition (ECCE)*, IEEE, 2012, pp. 1819–1826.

[22] V. Berenz, F. Tanaka, and K. Suzuki, "Autonomous battery management for mobile robots based on risk and gain assessment", *Artificial Intelligence Review*, vol. 37, no. 3, pp. 217–237, 2012.

[23] F.-X. R. Frédéric Magoulès, *Calcul scientifique parallèle - Cours, exercices corrigés, exemples avec MPI et openMP*. Dunod, 2017, ISBN: 978-2-10-077223-0.

[24] K. E. Roaldsnes, "Exploration of nonlinearities in a lithium ion battery cell model and their impact on particle filters and nonlinear kalman filters for state of charge estimation", PhD thesis, Norwegian University of Sciences and Technology, 2017.

[25] C. Campestrini, "Practical feasibility of kalman filters for the state estimation of lithium-ion batteries", PhD thesis, Technische Universität München, 2017.

[26] F. Zhong, H. Li, S. Zhong, Q. Zhong, and C. Yin, "An soc estimation approach based on adaptive sliding mode observer and fractional order equivalent circuit model for lithium-ion batteries", *Communications in Nonlinear Science and Numerical Simulation*, vol. 24, no. 1-3, pp. 127–144, 2015.

[27] C. Taborelli, S. Onori, S. Maes, P. Sveum, S. Al-Hallaj, and N. Al-Khayat, "Advanced battery management system design for soc/soh estimation for e-bikes applications", *International Journal of Powertrains*, vol. 5, no. 4, pp. 325–357, 2016.

[28] A. Mouna, B. Abdelilah, N. M'Sirdi, *et al.*, "Estimation of the state of charge of the battery using ekf and sliding mode observer in matlab-arduino/labview", in *2018 4th*

International Conference on Optimization and Applications (ICOA), IEEE, 2018, pp. 1–6.

[29] T. d. J. M. Sanguino and J. E. G. Ramos, "Smart host microcontroller for optimal battery charging in a solar-powered robotic vehicle", *IEEE/ASME transactions on mechatronics*, vol. 18, no. 3, pp. 1039–1049, 2012.

[30] *Battery management system 4 – 15s. rec*, REC, Control your power, 2017.

[31] *Bms10x0: B40/60v, 100 amps management system for lithium ion batteries*, RoboteQ, 2018.

[32] M. A. MAZIDI, S. NAIMI, and S. NAIMI, *The AVR Microcontroller and Embedded System using Assembly and C*. PEARSON, 2017.

[33] *Atmega328p, 8-bit microcontroller with 32k bytes in-system programmable flash*, ATMEL, 2008.

[34] *Pic 18fxx2 data sheet high-performance,enhanced flash microcontrollers with 10-bit a/d*, MICROSHIP, 2006.

[35] *Acs712 - fully integrated, hall-effect-based linear current sensor ic with 2.1 kvrms isolation and a low-resistance current conductor*, Allegro MicroSystms, inc., 2020.

[36] *0.91inch oled module user manual*, WaveShare, 2016.

[37] H. Megnafi, A. A. Chellal, and A. Benhanifia, "Flexible and automated watering system using solar energy", in *International Conference in Artificial Intelligence in Renewable Energetic Systems*, Springer, 2020, pp. 747–755.

[38] *Lm124, lm124a, lm224, lm224a, lm324, lm324a, lm2902, lm2902v, lm224k, lm224ka, lm324ka, lm2902k, lm2902kv, lm2902kav quadruple operational amplifier*, Texas Instruments, 2005.

[39] P. M. Albert and B. David, *Principe d'électronique*. DUNOD, 2016.

[40] *Datasheet: Automotive mosfet irf1405*, International Rectifier (IR), 2005.

[41] *Mosfet irf9610*, International Rectifier (IR), 2005.

[42] L. D. Eggermont, "Embedded systems roadmap 2002", *Vision on Technology for the Future of PROGRESS*, vol. 30, 2002.

[43] *Mc78xx/lm78xx/mc78xxa 3-terminal 1a positive voltage regulator*, Fairchild semiconductor, 2001.

[44] S. Roberts, *DC/DC Book of Knowledge*. RECOM, 2015.

[45] *Lm317 three–terminal adjustable positive voltage regulator*, ON Semiconductor, 2002.

[46] P. Marwedel, *Embedded system design: embedded systems foundations of cyber-physical systems, and the internet of things*. Springer Nature, 2021.

[47] D. Houcque *et al.*, "Introduction to matlab for engineering students", *Northwestern University*, p. 74, 2005.

[48] H. W. Together and N. Dunbar, "Alternatives to the arduino ide in : Arduino software internals", 2020.

[49] R. Jackey, M. Saginaw, P. Sanghvi, J. Gazzarri, T. Huria, and M. Ceraolo, "Battery model parameter estimation using a layered technique: An example using a lithium iron phosphate cell", *SAE Technical Paper*, vol. 2, pp. 1–14, 2013.

[50] N. Marian and Y. Ma, "Translation of simulink models to component-based software models", in *8th International Workshop on Research and Education in Mechatronics (REM'2007, Proceedings)*, Citeseer, 2007, pp. 262–267.

[51] L. Piardi, J. Lima, and P. Costa, "Development of a ground truth localization system for wheeled mobile robots in indoor environments based on laser range-finder for low-cost systems.", in *ICINCO (2)*, 2018, pp. 351–358.

[52] M. Chellal, T. F. Guimarães, and V. Leite, "Experimental evaluation of mppt algorithms: A comparative study", *International Journal of Renewable Energy Research (IJRER)*, vol. 11, no. 1, pp. 486–494, 2021.

[53] A. A. Chellal and A. Benhanifia, "Conception et réalisation d'un système d'arrosage automatique et autonome", *Engineering degree dissertation, Ecole Supèrieure en Sciences Appliquées de Tlemcen, Algérie*, 2020.

Appendix A

Least Square Curve-fitting results

SOC (%)	OCV (V)	R_0 (Ω)	R_p (Ω)	C_p (F)	SOC (%)	OCV (V)	R_0 (Ω)	R_p (Ω)	C_p (F)
100.00	4.40	0.3049	0.06948	274.21	40.00	3.79	0.4314	0.0979	254.05
97.00	4.36	0.4238	0.1126	370.92	37.45	3.78	0.4682	0.0974	254.05
94.00	4.34	0.4238	0.1023	556.66	34.61	3.77	0.4277	0.1227	189.38
91.50	4.319	0.4096	0.1022	618.56	31.76	3.77	0.3520	0.0635	1042.30
88.60	4.31	0.4471	0.0942	1285.00	28.92	3.76	0.3199	0.1875	223.50
85.80	4.29	0.4096	0.1022	618.56	26.08	3.76	0.45617	0.1038	797.31
83.00	4.26	0.4471	0.09426	1285.30	23.23	3.75	0.4583	0.3292	30.42
80.00	4.24	0.4096	0.1022	618.56	20.40	3.73	0.0918	0.9443	6.02
77.25	4.19	0.44716	0.094264	1285.30	17.55	3.71	0.3029	1.0097	12.98
74.41	4.15	0.4349	0.0992	1013.20	15.53	3.70	0.7174	1.2651	24.17
71.50	4.13	0.2798	0.1073	1738.20	13.70	3.69	0.9036	2.0115	24.176
68.70	4.08	0.4324	0.1044	765.44	12.23	3.68	0.7174	2.0115	24.176
65.80	4.04	0.48413	0.0863	1474.3	10.80	3.65	1.8817	2.4600	60.8
63.00	4.01	0.4577	0.0745	2451.40	09.51	3.64	2.0767	3.5881	78.31
60.20	3.97	0.5022	0.1553	2491.60	08.35	3.62	3.0234	2.6081	97.5
57.35	3.94	0.4636	0.0753	3052.30	07.34	3.58	2.8081	5.7402	105.95
54.51	3.90	0.5018	0.1110	2878.10	06.32	3.50	3.3279	17.629	85.00
51.67	3.86	0.4088	0.1030	309.29	05.41	3.45	2.8744	7.4693	95.97
48.42	3.84	0.4773	0.0540	1182.80	04.52	3.39	3.6807	14	76.50
45.98	3.82	0.4143	0.0923	321.35	03.78	3.32	3.1604	8.6721	89.08
43.14	3.80	0.4510	0.0933	274.72	3.07	3.27	3.0445	6.7191	94.16

Table A.1: Least Square curve-fitting algorithm results

Appendix B

Wiring Scheme

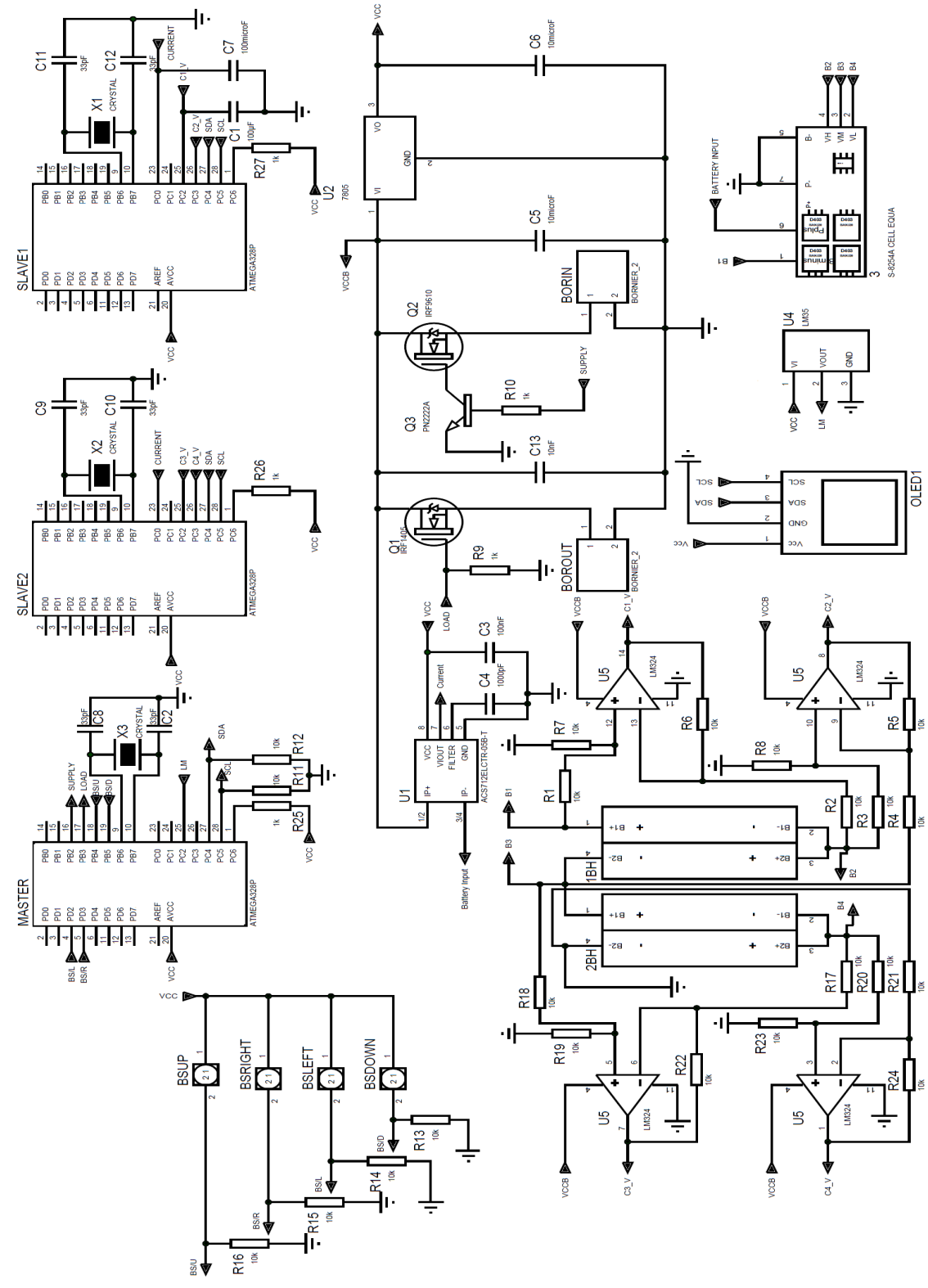

Figure B.1: Schematic diagram of the electronic circuit

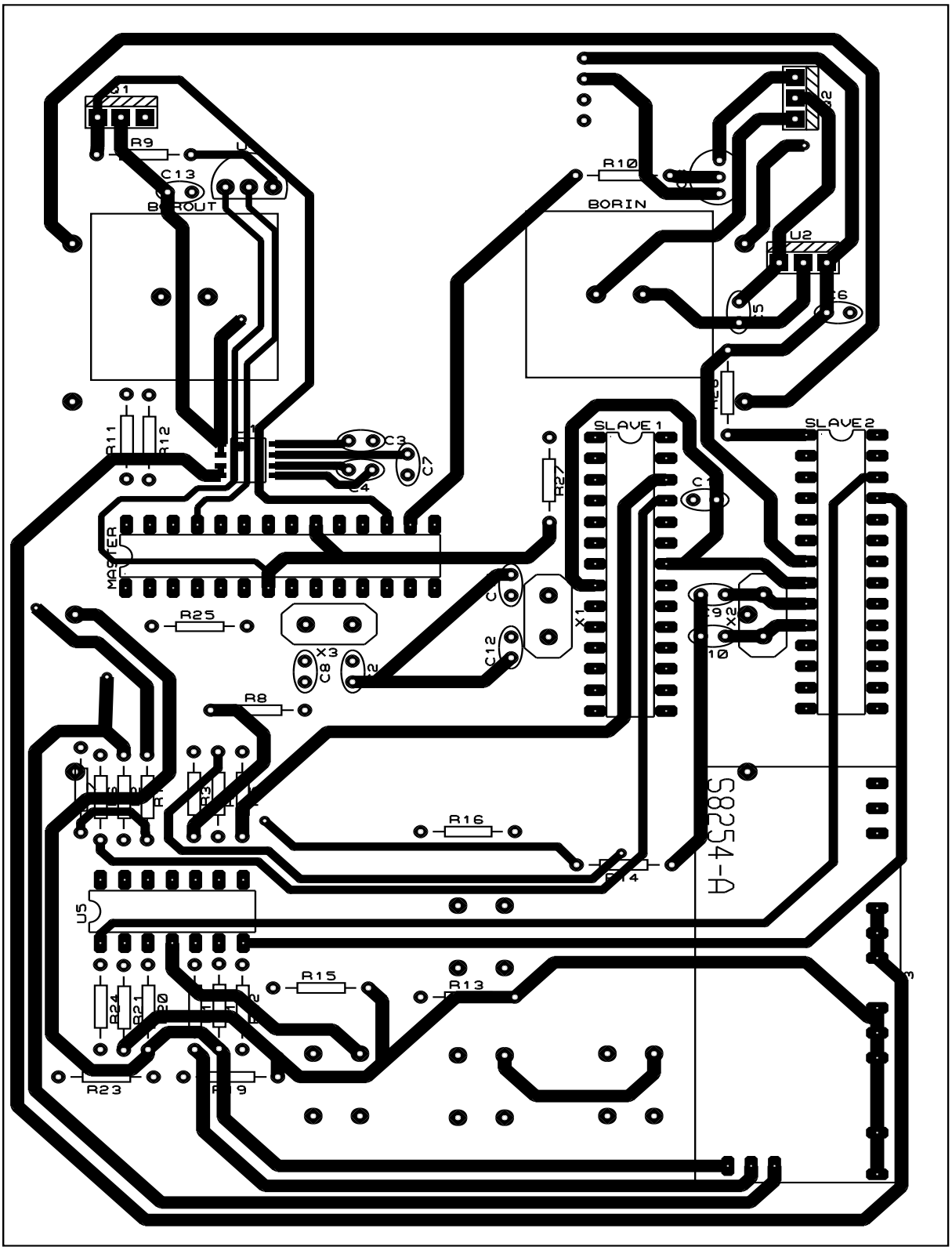

Figure B.2: PCB Design Diagram - Top Layer

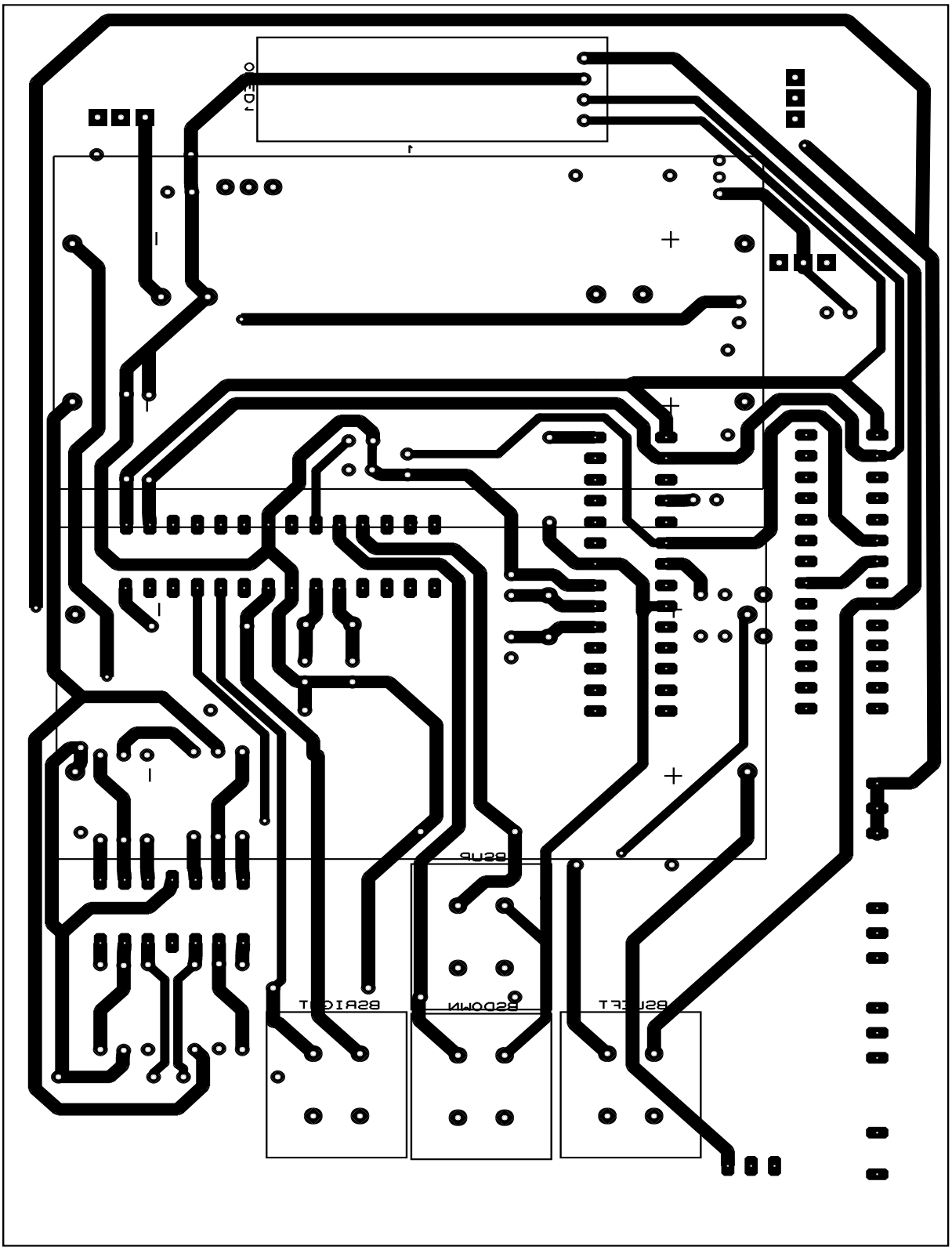

Figure B.3: PCB Design Diagram - Bottom Layer